A DISTRIBUTIVE APPROACH TO TACTILE SENSING FOR APPLICATION TO HUMAN MOVEMENT

Nikolay Mikov

Brunel Institute for Bioengineering

Brunel University

A thesis submitted for the degree of

Doctor of Philosophy

April 2015

To my brother and mother, Todor and Veselina Mikov
for always loving and standing by me.

To my father's memory.

Declaration of Authenticity

I hereby declare that I am the sole author of this thesis.

Nikolay Mikov

Abstract

This thesis investigates on clinical applicability of a novel sensing technology in the areas of postural steadiness and stroke assessment. The mechanically simple Distributive Tactile Sensing approach is applied to extract motion information from flexible surfaces to identify parameters and disorders of human movement in real time. The thesis reports on the design, implementation and testing of smart platform devices which are developed for discrimination applications through the use of linear and non-linear data interpretation techniques and neural networks for pattern recognition.

In the thesis mathematical models of elastic plates, based on finite element and finite difference methods, are developed and described. The models are used to identify constructive parameters of sensing devices by investigating sensitivity and accuracy of Distributive Tactile Sensing surfaces.

Two experimental devices have been constructed for the investigation. These are a sensing floor platform for standing applications and a sensing chair for sitting applications. Using a linear approach, the sensing floor platform is developed to detect centre of pressure, an important parameter widely used in the assessment of postural steadiness. It is demonstrated that the locus of centre of pressure can be determined with an average deviation of 1.05mm from that of a commercialised force platform in a balance application test conducted with five healthy volunteers. This amounts to 0.4% of the sensor range.

The sensing chair used neural networks for pattern recognition, to identify the level of motor impairment in people with stroke through performing functional reaching task while sitting. The clinical studies with six real stroke survivors have shown the robustness of the sensing technique to deal with a range of possible motion in the reaching task investigated.

The work of this thesis demonstrates that the novel Distributive Tactile Sensing approach is suited to clinical and home applications as screening and rehabilitation systems. Mechanical simplicity is a merit of the approach and has potential to lead to versatile low-cost units.

Acknowledgements

I would like to express my special appreciation and thanks to my supervisors Professor Peter Brett, Dr. Xinli Du, Dr. Amir Mohagheghi and Dr. Thomas Korff.

Grateful acknowledgement is made to Dr. Cherry Kilbride and Dr. Meriel Norris for their help and support on clinical matters.

Special thanks to Dr. Masoud Zoka Assadi, Jenny Kume, Roger Patton and all participants and support members of this project.

I would like to thank my family, friends and colleagues for all their encouragement and support during this project.

Contents

List of Figures

List of tables

Glossary and Abbreviation

3D: Three-Dimensional
AAMV: Average Absolute Maximal Velocity
AD: Anterior Deltoid
BI: Biceps
Cerebral lesions: areas of tissue in the cerebellum (part of the brain responsible for coordination of movement, attention, speech, and the regulation of certain emotions) that have been damaged by a traumatic brain injury or a disease.
COP: Centre of Pressure
DAQ: Data Acquisition
DTS: Distributive Tactile Sensing
EMG: Electromyography
FDM: Finite Difference Method
FEM: Finite Element Method
FP: Force Platform
Hemiparesis: physiological impairment associated with muscular weakness of the entire left or right side of the body
IR: Infra-red
LES: Left Erector Spinae
NI: National Instruments
NN: Neural Network
PC: Personal Computer
PCA: Principal Component Analysis
PD: Posterior Deltoid
RES: Right Erector Spinae
RIS: Reach Initiation Stage
RMS: Root Mean Square
RMSE: Root Mean Square Error
Stroke: clinical condition associated with poor blood flow to the brain resulting in death of brain cells.
TR: Triceps
USB: Universal Serial Bus

Nomenclature

a – Coefficient in polynomial equations

D – Plate flexural rigidity

E – Young's modulus

g – Gravitational acceleration ($g = 9.8\ m/s^2$)

h – Plate thickness

i, j – Indexes

K – Kinetic energy

l – Length

L – Lagrangian component

m – Mass

m_x, m_y – Two-dimensional components of force moments

n – Number of mesh elements, Index

p_z – Distributed force applied transversely to the elastic plate

p_{zT} – Total force applied transversely to the elastic plate

P_z – Concentrated force applied transversely to the elastic plate

P – Potential energy

q – Joint angle vector

$\dot{q}$ – Joint angular velocity vector

Q – Joint angles

$\dot{Q}$ – Joint angular velocity

$\ddot{Q}$ – Joint angular acceleration

t – Time

T – Period of time

x, y, z – Cartesian coordinates in three dimensions

$\dot{x}$ – Velocity in x direction

$\dot{y}$ – Velocity in y direction

ε – Error term describing discrepancy of the FDM plate model

μ – Error order of the biharmonic operator

λ – Length of a single mesh element in both x and y directions

π – Mathematical constant ($\pi = 3.14$)

τ –Torque

u – in-plane rotation

v – Poisson ration

ϑ - Velocity

w – Displacement of elastic plates

∇^2 – Biharmonic operator

Chapter 1

Introduction

1.1 Principal Aim and Outcome

This thesis describes a novel sensing technology for discriminating human motion based on the mechanically simple Distributive Tactile Sensing (DTS) approach. The work presented in this thesis is dedicated to verifying the clinical applicability of the technology in the assessment of postural steadiness and arm movements in stroke survivors. Two demonstration devices have been developed to discriminate movement related parameters in human participants. The performance of the technology has been verified using mathematical models and readily available commercial measuring systems.

1.2 Background

Human motion analysis has been applied to a wide variety of clinical applications to diagnose a range of disorders associated with posture, gait, and individual body parts movement (Aggarwal & Cai, 1999; Lu & Chang, 2012). The analysis of human motion involves different types of measurements, including measurements of reaction forces, body coordinates, centres of mass and pressure. In recent years much attention is focused on labelling the human motion, which is associated with the interest of identifying the motion itself, rather than its causes (Lim et al., 2014). A common way of labelling the type of motion is by applying

different pattern recognition techniques. The technology presented in this thesis is based on a novel approach to tactile sensing which discriminates human motion by type and behaviour. The method has been used to discriminate describing parameters from movement in both healthy and clinical populations to discriminate certain disorders in real time.

In current practice, different instrumentation is used for evaluation of the human movement including Force platforms (FP), pressure mats and full motion analysis systems which are commercially available. These systems provide precise measurement of the force, patterns of force distribution and movement kinematics, however they have the disadvantages of high cost, time consuming set up and calibration, and requirement of the analysis of the data by an experienced operator. An advantage of these systems is that they can be used to measure and analyse movements in order to identify, describe and quantify impairments which are unknown to the science. In contrast the proposed DTS technology is suitable for identifying certain or already established describing parameters associated with human motion.

The term 'tactile sensing' refers to a processes in the biological somatosensory systems, which is associated with the sense of touch (Tiwana et al., 2012). In engineering, tactile sensing refers to extracting information from the contact between a surface and a contacting object (Lee & Nicholls, 1999). Typically this information is extracted in the form of measurement of parameters such as force and pressure. Figure 1.1 illustrates two typical examples of tactile sensing devices used in human motion analysis corresponding to the mechanical principles of commercialized force platform and pressure mat. Force platforms consist of rigid platform of limited sizes (typically 400 x 600mm) with force transducers integrated into the platform at its corners while the pressure mats have a large number of small size pressure sensors set into arrays. The force platform is a device which presents the resultant ground

reaction force in three dimensions when a person walks/runs/jumps on it and the pressure mat measures the pressure distribution underneath the foot (Linthorne, 2001; Razak et al., 2012).

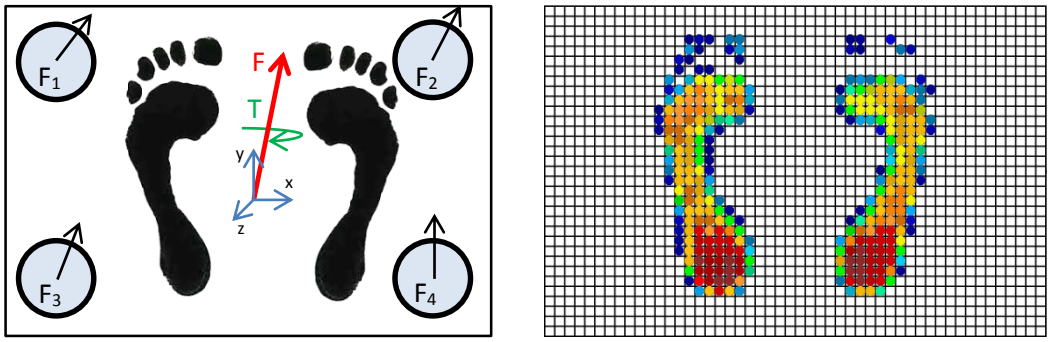

A **B**

Figure 1.1 – Mechanical principle of typical Tactile Sensing Devices: Force platform – Force sensors located at the corners of a rigid plate (A); Pressure Mat – Large amount of sensing elements set into arrays (B).

In the proposed Distributive Tactile Sensing approach the distributive response of a surface is detected by the use of few low-cost coupled sensors placed at strategic points underneath a flexible surface medium, corresponding to specific surface deformation subject to various force stimuli. The contact with the surface causing the surface deformations is based on force stimuli provoked by the human body. Figure 1.2 illustrates a generalized concept of Distributive Tactile Sensing.

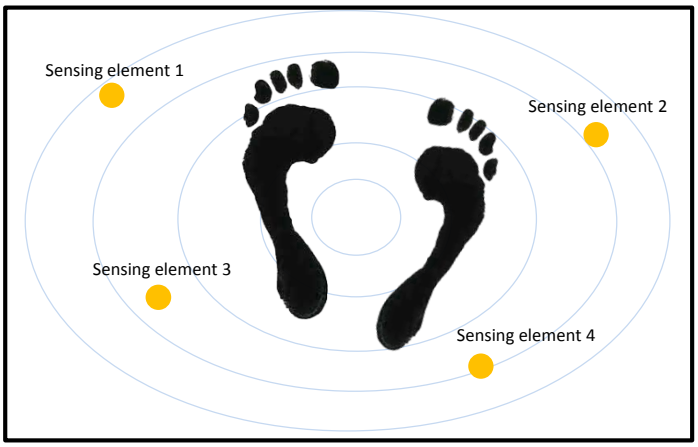

Figure 1.2 – Generalised mechanical concept of Distributive Tactile Sensing - Small amount of sensing elements stimulated by surface deformation in response to static and inertial forces of the moving human body.

DTS approach is used to discriminate different deformation profiles of surfaces associated with specific types of motion. The method engages artificial neural networks to accomplish automated discrimination process via specialized system training. The main advantages of the method are its mechanical simplicity, low-cost implementation, and minimizing the need of post-examination data processing. It has been successfully used to discriminate multiple conditions including types of gait and different personnel (Elliott et al., 2009a).

This work describes the development of novel DTS devices, sensing floor platform and sensing chair, and their clinical applicability in postural steadiness and stroke assessment.

1.3 The prime application considered in this thesis

Stroke is the third largest cause of death in UK which affects more than 150 thousand people every year (“Stroke Association", UK, 2015). Stroke

leads to brain damage and is the largest cause of adult disability affecting approximately 80% of patients acutely and 40% chronically (Alt Murphy et al., 2011). The damage of the brain in a large number of stroke survivors results in a wide variety of the motor system dysfunctions. This includes weakness of the muscles, inability to move one or more limbs, poor coordination of the movements of the whole body or individual limbs (Gresham et al., 1995). This leads to inability of stroke survivors to perform simple daily activities, including eating, having a shower, dressing, writing, self-care, walking, etc. (Cirstea & Levin, 2007).

The main challenge in stroke rehabilitation is the recovery of upper-limb motor function. Recent studies show significant gain in rehabilitation interventions that improve the performance of the arm in stroke survivors with hemiparesis (Langhorne et al. 2009). The process involves identification of movement deficits by assessing the dynamic performance of the impaired arm. In particular, reaching task performance tests are used in assessing the ability of the central nervous system to integrate multiple degrees of freedom during the movement. This can be done by determining the contributions of different body segments (e.g. arm-trunk contribution) to the task. For example determination of arm-trunk contribution in the reaching task might have a prognostic value. Therefore arm-trunk contribution might be used to monitor the stroke survivors in regaining coordination (Cirstea & Levin, 2000).

In current practice usually expensive and time consuming motion analysis systems are used to evaluate the arm-trunk movements during reaching. In present study, the proposed DTS technology provides low cost and time efficient alternative in evaluating arm-trunk contribution to a reaching task in stroke survivors. This is achieved by the development and use of a DTS chair which is able to discriminate different degrees of trunk bending in the reaching task. Approximation of the arm-trunk contribution allows determination of the level of motor impairment in stroke survivors.

1.4 Aims and Objectives

The main aim of this project is to verify the clinical applicability of Distributive Tactile Sensing technology in the assessment of postural steadiness and reaching task in stroke survivors.

To accomplish the aim of this work the following objectives had to be fulfilled:

- Development of mathematical models of elastic plate for defining constructive parameters of the DTS devices and theoretical validation of the DTS technology.
- Construction of a DTS floor platform for applications associated with the measurement of posture.
- Verification of the performance of DTS floor platform by comparing its outcome with that of commercially available force platform.
- Development of DTS chair which was able to discriminate between different levels of trunk bending in performing a reaching task during sitting.
- Development of a mathematical model of the biomechanical system to simulate the performance of a complete DTS system in performing the reaching task and generating simulation data to train neural networks.
- Collecting normative and clinical data with the DTS chair, gold standard 3D motion capture and electromyography systems to verify the performance of the DTS chair in reaching task application.

1.5 Contributions

In previous investigations the work by Brett and Stone (1997) demonstrated a technique for measuring contact force distribution in minimally invasive surgical procedures. Tongpadungrod et al. (2003) optimized the performance of the distributive method by using genetic algorithms to find the finest sensor positions in one-dimensional distributive sensing surface. Further to this Elliott et al. (2009a) applied the distributive method to discriminate and classify between different gait patterns. The main contributions of this research leading to the further development of the technology can be summarised as the following:

- The DTS technology has been improved by the development of mathematical models of a plate which helped to investigate and better understand the performance of the distributive surfaces under different loading conditions. The sensitivity and accuracy of the DTS devices were increased by investigating different plate surfaces and supports.
- For the first time the performance of a DTS device was compared with that of a commercial force platform in determining the locus of centre of pressure (COP) in real time. The results showed that the DTS technology can determine the locus of centre of pressure with minor deviation from that of a force platform.
- The DTS technology has been extended by applying it to a new application to discriminate motion in people. A DTS chair was constructed via modification of a regular chair integrated with a sensing system. The usage of the DTS technology was expanded to sitting applications.
- Extending the applicability of the DTS technology by developing applications with clinical usage in stroke assessment and rehabilitation. An application for assessing the arm-trunk contribution in reaching task was developed and verified by

collecting referent data from gold standard 3D motion capture and electromyography systems.

1.6 Structure of thesis

This thesis consists of seven chapters.

Chapter 2 – Literature review – This chapter provides recent review of the literature in the relevant areas. This includes review of previous applications of the Distributive Tactile Sensing approach, and its clinical applications in human movement science.

Chapter 3 – Mathematical Model – This chapter explains the development of mathematical models of elastic plate used to identify specific design characteristics (plate materials, supports, and thicknesses) for the development of the DTS experimental setups.

Chapter 4 – DTS approach applied to detect the locus of centre of pressure – This chapter explains the development of DTS floor platform for standing applications. Methodology for detecting and tracking centre of pressure is described and implemented theoretically and practically. In this chapter the DTS technology has been contrasted with that of a commercialized force platform in real time application for detecting and tracking the locus of centre of pressure.

Chapter 5 – DTS approach for discrimination of trunk movement in a reaching task – This chapter explains the development of DTS chair for sitting applications. A clinical application for determining the level of trunk contribution in performing reaching task is described and theoretically verified by further developed mathematical model.

Chapter 6 – Clinical Evaluation – In this chapter the performance of the DTS chair is tested in a cross-sectional study with groups of healthy and stroke volunteers. Motion capture and EMG systems were used to verify the results.

Chapter 7 – Conclusion

Chapter 2

Literature Review

2.1 Introduction

The work in this thesis describes the development of two clinical applications of the Distributive Tactile Sensing approach applied in the assessment of postural steadiness and upper limb motor impairment in stroke. The first clinical application is for detecting of an important parameter in the assessment of postural steadiness called centre of pressure, while the second one is for identifying the level of upper-limb motor impairment in stroke survivors through performing a functional reaching task. To support the need for such applications, this chapter reports on the clinical use of COP measure and reaching task functional test in the assessment of postural steadiness and functional motor impairments after stroke, respectively. The literature review of this chapter is organised as shown in Table 2.1.

Table 2.1 – Literature Review content.

In order to introduce the reader to the scope of the DTS technology, the first section of this chapter reviews some of the previous work of the Distributive Tactile Sensing approach showing the wide range of applications of this technology in industrial and clinical settings. Section 2.3.1 reviews some early research papers which have reported on the use of centre of pressure in the assessment of postural steadiness. A few recent research papers are also reviewed indicating the COP based assessment is still widely used. In support of the second clinical application developed, section 2.3.2 reviews recent papers in which reaching tasks have been applied to assess motor impairments gained after stroke.

As the work of the thesis covers relatively wide area of research, engaging mathematical modelling and artificial neural networks, Sections 2.4 and 2.5 review on common numerical methods used in the analysis of elastic plates, and applications of neural networks applied in the science of human movement, respectively.

2.2 Distributive Tactile Sensing

Work conducted in this thesis is based on applying the principles of Distributive Tactile Sensing in order to obtain motion information from people performing functional tasks on top of a flexible surface. The DTS approach represents a type of tactile sensing in which a small number of coupled sensing elements are used to detect flexible surface deformations caused by static or dynamic objects contacting with the surface. Obtained deformation data in the form of sensing transients is then associated with types, conditions or properties of the contacting object. In this project contacts caused by the moving human body have been investigated. In previous work the principles of the Distributive Tactile Sensing approach have been applied in several applications including, industrial grippers

(Stone et al. 1998), surgical robotics (Tam et al., 2010), and human motion analysis (Molloy, 2006; Elliott et al., 2009a,b).

Stone et al. (1998) applied Distributive Tactile Sensing to a system for automatic handling of dough-like materials. In this application the distributive method was used to determine material behavioural properties that describe deformation during handling. The system developed by Stone et al. was used to predict the effect of different handling strategies on materials with low stiffness and variation in material properties. The mechanical construction of the system was defined as a manipulator integrated gripping device in which the distributive method was implemented through aluminium tactile surface with integrated strain gages. The system operated using software algorithm which was developed to interpret the collected sensing data and estimate the properties of handling material through discrimination.

In another study Tam et al. (2010) applied the distributive approach to an embedded sensing system as an actuated flexible digit for use as a surgical tool in minimal access therapy. The digit system represented a steerable tip element of devices such as endoscopes and laparoscopes. It consisted of a flexible tube with diameter of 12mm and length of 120mm, made from clear Perspex material for visibility. The distributive method was implemented by the use of strain-gage sensing elements positioned at 20mm, 60mm and 85mm from the fixed root of the digit. The system was tested experimentally in retrieving tactile parameters to aid guidance of tool tips and interpretation of contact relating to palpation and navigation in lumen. In this work artificial neural networks were used to accomplish automated discrimination in types of surface contact and tissue interaction. Obtained information was used by the system to automatically change the shape of the flexible digit according the profile of the lumen.

Molloy (2006) applied the DTS approach for analysing human motion in sports. In this work the Distributive Tactile Sensing was implemented in a sensing golf mat for classification of specific dynamic movements associated with possible flaws during golf backswing. In his experimental rig, Molloy used an aluminium square plate (850 x 600 x 6mm) and eight non-linear reflective optical sensing elements to sense the plate deformations. Neural network classification techniques such as linear inverse regression and regressive single and multi-layer layered perception methods were investigated. In this application of the distributive approach successful discrimination was demonstrated between poor or good posture of the legs during golf backswing, correct movement of the left foot off the surface during backswing, and poor or good orbit angle takeaway of the club during backswing.

Elliot et al. (2009b) used Distributive Tactile Sensing in an experiment for quantifying balance and sway through surface deflection patterns. In this experiment, Elliot et al. simulated sway conditions using a pendulum positioned on a supported flexible steel plate. Three infrared displacement sensors were used to capture dynamic surface deformation corresponding to the moving pendulum. It was demonstrated that by using a multilayer perception back-propagation neural network, the 3D location of the moving pendulum can be detected. The outcome of this work suggested that the distributive method can be applied to clinical applications that involve the measurement of balance and sway in patients.

In another experiment Elliot et al. (2009a) applied the distributive method to a walking platform for discriminating between people through their gait patterns. Using similar neural network classification algorithms as in the balance application, Elliot et al. demonstrated successful discrimination in a group of five randomly selected healthy volunteers. Further to this, discrimination of small changes in gait patterns associated with normal

and abnormal walking was demonstrated. For that purpose gait patterns were simulated by instructing a participant to walk with and without a backpack style bag containing a 10kg mass. Classification accuracy of just under 90% based on 46 trials (23 natural walking and 23 walking with a backpack) was obtained. Work conducted by Elliot et al. suggested that the DTS approach has the potential to be successfully developed to clinical applications for identifying certain pathological or neurological gait disorders.

2.2.1 Conclusion

In this section some of the previous work which used the DTS approach was reviewed showing examples of some practical application of this method. The review showed that the approach provides mechanically simple implementation and has the potential to be developed to a variety of applications with real usage. Examples of industrial, sports and clinical applications were shown including industrial grippers for soft material handling, surgical penetration tools and smart platforms for human motion analysis.

In this thesis two novel applications of the Distributive Tactile Sensing are presented. Chapter 4 will explain an application with use in the assessment of postural steadiness. In Chapters 5 and 6 the Distributive Tactile Sensing will be applied in an application for assessing motor impairments gained after stroke.

2.3 Examples of tactile sensing applications in the human movement science

2.3.1 COP based assessment of postural steadiness

In the past 45 years a large number of parameters which are based on the behaviour of the centre of pressure (COP)[1] have been proposed and validated for the quantitative assessment of postural steadiness (van der Kooij et al., 2005). Postural steadiness is the ability of the human postural control system to maintain balance during quiet standing (Prieto et al., 1996). Postural control deficits are usually associated with problems of the somatosensory system leading to increased risk of fall related injuries. Predicting the risk of future falling is necessary to prevent potential injury (and in elderly population, fear of falling), which may cause limitations in everyday activities and disability (Lord et al., 2007).

Interest in quantifying postural steadiness by the use of COP based measures was triggered by the appearance of the first commercially available force platform devices in 1970s (Sutherland, 2001; Kapteyn et al., 1983; Murray et al., 1975; Terekhov, 1976). During the years force platforms become the standard equipment for the measurement of postural steadiness (Goldie et al., 1989; Mizrahi et al., 1989; Prieto et al., 1996; Soutas-Little et al., 1992), and COP-based parameters become the most widely accepted parameters for characterising postural steadiness (Lafond et al., 2004; Piirtola & Era, 2006; Prieto et al., 1996). Despite the fact that several limitations of COP-based assessments have been reported (e.g. no information on the underlying pathophysiology of the impaired posture and balance can be provided via these measures)(Mancini &

[1] Centre of pressure is defined as the point of application of the resultant ground reaction force vector acting under the feet.

Horak, 2010; Pasma et al., 2014), new parameters are still being developed (Cavanaugh et al., 2005; N. Stergiou & Decker, 2011).

A major barrier to the use of force platform data for the objective assessment of balance impairments is its relatively high cost (Linthorne, 2001). Moreover, although nowadays portable devices are available, the specific installation requirements for the ground mounted devices further limit their application in the clinic and sports grounds. In the following paragraphs, some of the early work on the use of COP in postural steadiness which are reflecting the era of commercialisation of the force platform devices, and few recent works showing the contemporary measurements of balance based on the COP data are reviewed. The conducted review is in support of the experimental work presented in Chapter 4 in which the Distributive Tactile Sensing approach has been used to detect the locus of COP, and overcome some of the limitations of the traditional force platforms.

Husfschmidt et al. (1980) introduced few new parameters for the quantification of body sway in healthy individuals and people with cerebellar and labyrinthine lesions. By using a "Kistler" force platform, they obtained COP data which was used to calculate parameters such as COP mean amplitude, sway path, mean frequency, and lateral and sagittal components of the three afore-mentioned parameters. Husfschmidt et al, discussed the clinical significance of these parameters for documentation and follow-up studies, and making differential diagnosis. They reported that in patients with cerebellar lesions, COP sway path and mean amplitude were up to ten times larger with a pronounced anterior-posterior instability compared to the healthy people.

Maki et at. (1987) developed a posture control model and balance testing methodology for predicting relative postural stability. They investigated

the balance test responses in healthy young and elderly people, and showed that the test can be used to identify balance impairments. The proposed balance test was based on the posture control model which defined the relative stability of a person by quantifying a COP based parameter named 'saturation amplitude'. Saturation amplitude was calculated as the proportion between the average anterior-posterior length of the feet and the derived peak of COP displacement. Results showed significant age-related differences in the balance test response, but they provided only preliminary indication of the ability of the balance test to identify balance impairments.

Prieto et al. (1996) were the first to conduct a comprehensive analysis of the COP-based measures for the assessment of changes in postural steadiness related to age. Prior to this study, COP-based measures had only been discussed and evaluated by Hufschmidt et al. (1980) in a comparison between healthy people and patients with cerebellar and labyrinthine lesions to test the diagnostic significance of a group of measures. In their study, Prieto et al. described and compared a representative set of previously used COP-based measures which had been proven useful for the evaluation of postural steadiness. It was suggested that the adequate assessment of postural steadiness in age related studies required using multiple measures. A number of COP-based measures was recommended for use which included COP mean velocity, root mean square (RMS) distance, area measures, and time and frequency domain measures (centroidal and mean frequencies, respectively).

Prieto et al. work is an example of classical papers which shows differences in balance control between young and old people. Importantly, Prieto et al. described mathematics and procedures for measuring COP based measures of balance. These have been used in many studies since the publication of their paper. In the remaining text of this section few

papers are reviewed to show that since the time of Prieto et al., COP based parameters are still largely in use (Pasma et al., 2014; Wang & Newell, 2014).

Recently Rhea et al. (Rhea et al., 2014) have presented a novel COP-based measure that describes the rate of change in the direction of COP displacement in two dimensions. This new measure named *COP heading change* was applied to distinguish in COP behaviour between a healthy and clinical population with an anterior cruciate ligament rupture prior to surgical intervention. Rhea et al. indicated that previously developed measures that described the movement of COP trajectory were mainly used to examine characteristics associated with the magnitude of displacement. They suggested that postural instability can be examined more accurately when considering both the magnitude with the direction components of the resultant COP trajectory. The novelty and utility of this new COP-based measure allows for a description of directional changes in the COP that may reflect postural adaptability. Rhea et al. also suggests that for more detailed understanding of how the posture is controlled, developing of a new COP-based measure to capture both magnitude and direction within a single variable is required.

Aoki et al. (2014) used COP data to evaluate characteristic postural sway patterns based on recently adopted segment time series analysis employing maximum entropy method (Sawada et al., 1997). Identification of characteristic patterns was used to investigate postural instability in patients with unilateral vestibular dysfunction. Aoki et al. suggested that by applying this method to the COP data, the characteristic pattern which indicated an increased reflexive COP fluctuation indicating increased instability could be obtained.

Deschamps et al. (2014) investigated the impact of cognitive decline on postural control strategies between older adults with mild cognitive impairments and those with mild-to-moderate Alzheimer disease. Investigation was based on the COP measures including a relatively recent measure, average absolute maximal velocity (AAMV) which was described by Delignieres et al. (2011). In their study, Deschamps et al. demonstrated that the velocity based COP measures could be successfully employed to reveal the effect of cognitive impairments on postural control, confirming the effectiveness of AAMV measure in the assessment of postural balance. Based on the results of this work, it was argued that velocity-based COP measurements could be a key in the identification of new markers of early cognitive dysfunction, and particularly in the screening of individuals with increased risk of falling.

Another study was conducted by Ganesan et al. (2014) who evaluated the effect of lateral and medial wedges on postural sway in standing. By calculating a number of commonly used COP parameters such as mean and mean RMS distances, displacement range, mean velocity, they investigated how changes in the angular position of the ankle joints induced by standing on lateral and medial wedges affected the postural control. Results show that the use of either lateral or medial wedges might enhance postural control in standing.

2.3.1.1 Conclusion

In this section, several papers on the assessment of postural steadiness based on the COP data were reviewed. Traditionally, the COP data is provided by force platform devices which have several limitations such as high cost, and specific installation requirements. These limitations make the use of force platforms restricted to specialised biomechanics

laboratories where routine examination of the clinical and subclinical populations are not easily possible. In contrast to the conventional force platform, the DTS technology provides a portable, cost-efficient, and easy to use solution for producing COP data. Chapter 4 will present preliminary results for the suitability of DTS technology in the assessment of balance.

2.3.2 Kinematics of arm movement during reach in stroke survivors

One of the main challenges in the process of rehabilitation after stroke is restoration of arm motor functions. Impairments in arm function have been shown to severely limit level of autonomy in this population (Nakayama et al., 1994). Adequate and relevant assessment of motor dysfunction of the impaired upper limb is necessary to provide evidence for the severity of upper limb dysfunction and effectiveness of rehabilitation interventions employed (Cirstea & Levin, 2007). Several studies have used reaching task for this purpose.

The Reaching Task (reaching to a target while sitting) has been used to address a fundamental ability of the central nervous system in integrating multiple degrees of freedom (e.g. joints, body segments) during a movement (Cirstea & Levin, 2000). Such ability allows a person to perform a task in an infinite number of different ways. For example, contribution of different joints of the arm and/or trunk in bringing food to the mouth can be adapted based on the type of the food, or when the elbow joint contribution to the task is limited after being placed in a cast due to an injury. Successful reaching to objects is essential for independence during activities of daily living.

In healthy individuals, arm and trunk movements are so coordinated that during reaching to a target placed within 90% of the arm length, trunk does not contribute to the arm movement (Mark et al., 1997). Contribution of the trunk to arm movements starts beyond the critical boundary

(defined based on 90% one's arm length) of reach, where movement of the trunk starts before or simultaneously with the hand movement, and finishes after the hand stops to move (Rossi et al., 2002). Such pattern of coordination between the arm and trunk is disrupted after stroke leading to trunk recruitment in executing reaching to a target placed within the arm reach (critical boundary). Muscle weakness, spasticity, and abnormalities in the regulation of spinal reflexes are amongst suggested mechanisms which may contribute to the impaired control of movement after stroke. Specifically, it has been shown that the critical boundary of reach diminishes after stroke and trunk contributes significantly more to the arm movements during reaching to targets placed within the boundary (Levin et al., 2002). Contribution of trunk to reaching has been shown to be correlated to the level of motor impairments (i.e. stroke severity). Moreover, it has been suggested that there may exist a clinical threshold at which trunk contribution to the reaching alters as a result of changes in the impairment severity or in response to rehabilitation (Cirstea & Levin, 2000). Therefore, assessment of reaching tasks in stroke survivors and more specifically determination of trunk contribution to the reaching task might have a prognostic value in the rehabilitation of stroke survivors.

This section reviews some recent papers showing the use and effectiveness of tests based on reaching tasks in the assessment of motor deficits after stroke. The review reflects on the work conducted in Chapter 5 in which a Distributive Tactile Sensing Method was developed for discriminating between different levels of trunk bending in reaching task.

By investigating the relation between arm and trunk kinematics, Levin et al. (2002) examined control mechanisms governing compensatory strategies used by stroke survivors in executing reaching task. They recruited groups of healthy and hemiparetic individuals following stroke to evaluate the timing and pattern of recruitment of the hand and trunk during natural reaching movements to targets placed within and beyond the reach of the arm. By analysing kinematic data recorded with a motion

capture system, Levin et al. demonstrated that the critical boundary of reach was reduced after stroke. This was supported by the findings which indicated that the trunk a) was recruited for reaches to targets placed within the arm's length, b) contributed to arm displacement throughout the reach, and c) the amount of trunk displacement was inversely correlated with the amount of arm extension (i.e. increases in arm extension were associated with decreases in trunk recruitment). Results of this study showed that reaching task can successfully be used to investigate and determine motor deficits associated with reduced arm extension after stroke. Levin et al. suggested that even though some aspects of motor planning in hemiparetic individuals may be relatively unaffected by stroke, the reaching performance could still remain impaired.

Reaching task test was used by Cirstea and Levin (2000) to investigate the correlation between the damaged nervous system and the level of functional impairment of the affected upper limb after stroke. In a cross-sectional study, kinematic data recorded with 3D motion capture was obtained from groups of hemiparetic individuals following stroke and healthy controls. Arm and trunk movements during reaching task were described in terms of joint's trajectory, velocity, accuracy and interjoint correlation. Cirstea and Levin used this information to characterise motor deficits gained after stroke and analysed the relationship between arm and trunk movements in performing reaching task. Some important distinctions characterising the movement in subjects with moderate to severe stroke were reported. One of these was the non-typical use of the trunk in reaching a target placed well within the range of the arm's reach by stroke participants. In this study it was shown that the use of the trunk represents a compensatory strategy, and the trunk movement was significantly correlated with the clinically measured level of motor impairment. In addition, findings suggested that the use of compensatory

trunk strategy was significantly correlated with the deficit in motor function and degree of spasticity in moderate and severe stroke subjects.

Chen et al. (2013) proposed a self-efficacy measure that could measure effective reaching task and discriminate between more and less functionally able arms. Prior to this work, other self-efficacy measures based on reaching tasks had also been used such as the *confidence in arm and hand movement scale* (James et al., 2009), and single item measures related to confidence for accurate and rapid movement (Stewart, 2010). The self-efficacy measure described by Chen et al. represents the ratio of the confidently reachable targets (defined as *confidently reachable* by the participant's own judgement) to the total number of targets presented to the participants at different distances. By testing groups of healthy and hemiparetic individuals, a reaching self-efficacy score was obtained and used to compare differences in functional performance between individuals. Chen et al. reported significantly higher reaching self-efficacy score of the dominant arm compared with the non-dominant arm in the control group, and significantly lower self-efficacy of the paretic arm compared with the non-paretic in the stroke group. Due to its relatively high resolution, it was suggested that this reaching task self-efficacy measure can be applied to evaluate people who are just beginning to recover their reaching functions.

Reaching task was also used by Merdler et al. (2013) to describe temporal and spatial characteristics of 3D reaching movements using arm-plane variables obtained with 3D motion capture. In this work a new parameter representing a dynamic plane in which the reaching arm operates was introduced. This arm-plane parameter was formed by the proximal and distal arm segments where plane direction with respect to target space was formed by the direction vectors of the arm segments. Arm-plane based characteristics that accounts for the co-variation between

movements of the whole arm were used to identify their relationship with upper limb motor impairments in people with stroke. This new approach for representing the motion of the arm in reaching task was shown to be related to the severity of upper limb impairments. In this work Merdler et al. demonstrated that arm-plane motion analysis provides relatively new information about motor compensations involving the co-variation of shoulder and elbow movements. The validity of the technique was confirmed by the excessive trunk motion in stroke individuals compared with healthy controls. A main advantage of this reaching task assessment technique is that it provides a way of characterising 3D compensatory movements of the whole arm compared to individual joint planar kinematics. This type of characterisation was performed by obtaining and evaluating individual arm-plane-based measures such as the arm-plane angle, velocity and phase velocity, and arm-plane temporal angle.

In a cross-sectional study, Kordelaar et al. (2012) used reaching task to investigate pathological limb synergies between shoulder, elbow and trunk movements during a functional upper limb movement of people with stroke. By applying principal component analysis (PCA) to recorded 3D kinematic data, Kordelaar et al. identified components representing linear relations between the degrees of freedom of the upper limb (shoulder and elbow) and trunk across participants with stroke and healthy participants. Eighty five per-cent of variability in the trunk and arm joints during reaching task in participants with stroke could be explained by four of these PCA components. The four components corresponded to abnormal synergies such as shoulder abduction combined with elbow flexion, lateral trunk rotation and upward shoulder rotation, forward and axial trunk rotation and elbow flexion, and external shoulder rotation and excessive use of forearm pronation. This work demonstrated the usefulness of PCA in the identification of clinically meaningful interactions between compensatory trunk movements and the

presence of pathological synergies in the elbow and shoulder and trunk during reaching task in stroke survivors. The outcome of this study suggested that insight obtained via PCA into the mutual relationships between motor impairments and motor compensation during reaching task may help to investigate the learning of skill recovery in the first months after stroke.

2.3.2.1 Conclusion

In this section several papers on the assessment of upper-limb motor impairments based on functional examination of reaching tasks were reviewed. Generally, it has been shown that trunk contributes excessively to reaching in stroke survivors and abnormal synergies between upper limb degrees of freedom and trunk exists. Therefore, examination of trunk contribution to reaching forms an important component of the clinical assessment of stroke survivors. Traditionally, this type of examination requires analysis of kinematic data provided by motion capture systems which have some significant limitations which restrict their applicability in clinical settings. Some of these limitations are the high cost, requirement of trained specialist to accomplish post-processing of the collected data, and requirements for specific installation and calibration. In contrast to the gold standard motion capture systems, the mechanically simple DTS approach provides a solution of discriminating and quantifying trunk movements which can be associated with levels of upper-limb motor impairments for people with stroke hemiparesis. In Chapter 5, development of the DTS technology for discriminating different levels of trunk movement during reaching tasks is presented. Further in Chapter 6, the application will be evaluated in identifying the level of motor impairment in a group of stroke survivors.

2.4 Numerical methods for the analysis of elastic plates

In previous work the Distributive Tactile Sensing method has been applied to identifying properties of static and dynamic objects. In this work the applicability of the DTS method was extended to identifying real force parameters typically obtained with commercialised force plate devices. To theoretically verify this concept, a methodology that is able to estimate the locus of centre of pressure was developed based on FEM and FDM numerical mathematical models developed and discussed in Chapter 3. To justify the selection of FEM and FDM methods, this section briefly reviews on traditional numerical methods as theories describing elastic plates. Investigation has been subject to static loading only. Structural dynamics has not been considered as this analysis is mainly intended for determining the effect of plate vibrations (Szilard, 2004) which have not been of interest in this work. Due to the inherent mathematical difficulties in solving analytical elastic plate approaches (i.e. Ritz, Galerkin, Vlasov, Navier, Levy) and their practical limitations, numerical methods have been engaged to obtain approximate solutions to the governing differential equations of elastic plates. The review of this section has been conducted mainly through one of the classic books in the analysis of elastic plates, "Theories and Applications of Plate Analysis", Rudolph Szilard. The book addresses a large spectrum of plate problems and their analytical, numerical, computer-aided and engineering solution techniques.

Among the numerical techniques presently available in wide range of applications, the finite difference method (FDM) is one of the well-proven in the theory of plate analysis and it is probably the most transparent and general approach suited for solutions of various plate problems(Dolicanin et al., 2010; Kameswara Rao, 2011). The FDM applies two-dimensional discretization of plate continuum where the governing plate equation (Navier, 1823) is represented algebraically by corresponding finite

difference quotients at each mesh point. The FDM method allows for considerable improvement in accuracy by approximating the governing equation at several mesh points, known as multilocal methods. The FDM method is known for its implementation simplicity and can easily be solved by upscale calculator or computer algorithm for the solution of a set of algebraic equations that is readily available. Despite the advantages over other numerical techniques, the implementation of the FDM for the analysis of large plate structures, and structures with irregular geometry, loads and boundary conditions can be complex.

The versatile finite element method (FEM) is currently the most widely used numerical technique for the solution of structural-mechanics problems (Qatu, Asadi, & Wang, 2012; Thai & Kim, 2015). The FEM applies a physical discretization which means that the modelled continuum is replaced by discrete elements (finite elements) connected together to form a two or three dimensional structure. There are three major categories of the FEM approach, which have been developed for the analysis of various plate problems. These are FEM based on displacement, mixed or hybrid FEM, and equilibrium-based FEM, from which the one based on displacement is the most natural and most common in engineering.

In FEM, the plate continuum is represented by a number of finite elements connected only at a limited number of node points. The method assumes that if the load deformation characteristics of all elements can be defined individually, then by assembling the elements the load deflection behaviour of the plate can be approximated.

The FEM method is well suited for implementation by computer programs and a big number of software packages are commercially available (ANSYS, ADINA, NASTRAN, MARC). Alongside this advantage, the FEM model enables for fast and easy representation of structures with various geometries.

Another powerful numerical method for the analysis of plate and shell structures is the Gridwork (Framework) method (Hrennikoff, 1941) which is the forerunner of the more recent FEM. A gridwork is a two-dimensional plane consisting of intersecting jointed beams. The Gridwork method works as it replaces the continuum of the plate by an equivalent gridwork of beams defined by one of the following three procedures: deriving the equivalence of strain energies between the plate and the gridwork; deriving equivalence between the stress conditions between the original continuum and its substitute system; employing a limit approach of the corresponding finite difference equation of a substitute system.
Due to the similarities and relation between the gridwork and FEM methods, this modelling technique can be considered as a special case of the FEM. Although the FEM model has been exclusively dominant in the last decades, the gridwork method offers distinct advantages over the FEM, from which one of the most significant is that plate models can be solved relatively easy by using standard computer programs.

First introduced in 1968 by Cheung (1968), the Finite Strip Method (FSM) has been extensively used in the development of static solutions to thin plate problems (Ho & Tham, 1992). The FSM represents a semi-analytical and semi-numerical process that offers substantial computational advantages for specific class of plate problems by significantly reducing the number of equations to be solved. One such problem is a rectangular plate in which two opposite ends in one direction are assumed to be simply supported while the other two edges can have wide range of boundary conditions. The FSM method subdivide the plate into a small number of strips which represent two-dimensional finite elements having polynomial functions in one direction and a continuously differentiable smooth series in the other. After its first introduction in the late 1960s, the FSM has been improved to cover bigger range of boundary conditions other than simple supports in the longitudinal directions. In comparison to

the FEM where each nodal point has at least three degrees of freedom, the FSM replaces numerous elements by a single strip with just two degrees of freedom at the nodal lines. Consequently, the number of unknown displacements is drastically reduced. The approach is known for its considerable economy, which is expressed in simplified data manipulation in generating the assembled stiffness matrix of the structure as well as bandwidth reduction.

Another alternative to the FDM and FEM methods is the Boundary Element Method (BEM) which applies discretization only at the boundary of the plate continuum (Luo et al., 1998). The BEM method is divided in two modifications, direct method which defines the plate model in terms of variables describing physical meanings (displacement of boundary nodes), and indirect which uses variables whose physical meanings are not always clearly defined. Therefore, the direct BEM is more transparent and is generally preferred by engineers. The BEM method is based on Galerkin's variation approach which is applied to transform the governing plate equation into a set of integral equations on the plate boundary. In contrast to the above described mathematical modelling methods, the BEM method is relatively new approach which is currently under development. Due to its incompleteness in terms of development, as well as complex computer implementation, the method has not yet been acknowledged as a general purpose method.

2.4.1 Conclusion

This section briefly reviewed some of the currently more common numerical approaches for the analysis of elastic plates. For the analysis of elastic plates in this work, finite element and finite difference methods were chosen as these are systematic and straight forward in terms of

implementation, and provide principal understanding of the modelled plates with satisfactory level of accuracy. In particular, the finite element method was chosen as in the early stages of the project such model provided quick and easy implementation using ANSYS software package. The model was used in the identification of constructive parameters of DTS devices, demonstrated in Chapter 3. Later a finite difference model of elastic plate was solved mathematically and implemented in MATLAB. This has provided comprehensive understanding the functionality of modelled structures, and flexibility in conducting big amount of simulations. The model is used in the development and verification of application for determining the locus of centre of pressure described in Chapter 4. Additionally, the FDM model provides possibility for integrating additional components to the modelled plate to investigate responses of elastic plates subject to dynamic loadings. This will be shown in Chapter 5.

2.5 Neural Networks for applications of human movement

Recognition, classification and prediction are major decision making tasks of human activity. These occur when an object needs to be assigned into a predefined group based on a number of observed attributes related to that object. Many problems in science and medicine can be treated as discrimination, classification or prediction problems. Examples of applications include medical diagnosis, image and biochemical analysis, drug development, clinical forecasts, etc. (Amato et al., 2013; Zhang, 2000).In many of these applications, neural networks have outperformed traditional computational approaches, with their compelling adaptive capabilities in learning and adapting to changing environments (Schumann, Gupta, & Liu, 2010).

Pattern recognition and classification are one of the most active research and application areas of artificial neural networks. The modern era of neural networks has begun in the late 1980s by the introduction of the back propagation training method (Rumelhart and McClelland, 1986). Since then, the use of artificial neural networks in clinical applications has become widely investigated and it has been shown that neural networks provide a promising alternative to various conventional classification methods. This has been manifested by an increasing number of publications in medical journals in the last decades (Lisboa & Taktak, 2006).

In previous work on the Distributive Tactile Sensing, successful deployment of neural networks for pattern recognition has been demonstrated in clinical, sports and industrial applications (Tam et al., 2010; Elliot, 2007; Tongpadungrod, 2002; Stone et al., 1998). This section reviews few recent research papers, showing examples of artificial neural networks successfully used in the determination of important clinical and biomechanics information via pattern recognition and prediction applications relevant to the prime application of this thesis described in Chapters 5 and 6.

Using neural networks, recently Mane et al. (2015) presented a new technique for classifying low level hand movement based on single channel EMG data. Four healthy participants took part in this study, in which EMG onsets were acquired from the *Flexor Digitorum Superficialis* muscle for three different hand movements: closing palm, opening palm and wrist extension. Prior feature extraction, discrete wavelet transformation was used to condition the EMG signal, transforming it into multi resolution subset of coefficients using forth order signal decomposition. Pattern features were developed based on number of 2-dimensional local maxima points extracted from 5 seconds data recordings, and using 200 data sets for individual hand movements.

Classification was accomplished using Matlab's Neural Network Toolbox, implementing a network based on three-layer feed forward architecture with 10 hidden neurons and sigmoid activation function. Results of this study indicated 100% accuracy in detecting the palm opening movement in all subject, and 90% accuracy in palm closing and wrist extension movements.

According Mane et al., single channel EMG analysis can be more efficient approach over multi-channel due to its simplicity and computational cost. The work demonstrated that neural networks can be used to successfully discriminate between patterns of simple hand movements captured using EMG data from only one channel. Due to the simplicity of the approach applied by Mane et al., as well as the relatively high classification accuracy obtained, it was suggested that the use of wavelet analysis in combination with neural networks can be used in reducing the overall cost of a system, and in obtaining time-frequency domain information suitable for EMG feature extraction.

Joo et al. (2014) used artificial neural networks to predict gait speed in people using plantar pressure data acquired with insole plantar pressure measuring device (Novel Pedar-x system). Twenty healthy participants (10 males and 10 females) of age 24.5 ± 2.3 years took participation in this study. Joo et al developed two prediction models based on three-layer feed-forward neural networks with sigmoid transfer function to predict gait speed in stance and swing walking phases. Using an intuitive variable selection method (Zhang, 2011), numbers of 15 and 17 sensing values were used to determine the speed in the stance and swing phases, respectively. The sensors chosen for the stance phase were distributed mainly on the toes and heel, and the ones for the swing were distributed more widely over the centre of the foot sole. Gait experiment was conducted with three different speeds, slow/normal/fast, validated with data recorded with 3D motion capture system (Vicon 460, Oxford, UK).

The actual measurements and predicted values of gait speed were compared, resulting in correlation coefficients of 0.96 for normal walking, 0.98 for slow walking and 0.95 for fast walking. The work of Joo et al. implies that neural network based models such as the one of their work have the potential to be used in real clinical applications in understanding the progress and cause of diseases such as Parkinson, strike and diabetes.

In another recent study, Kaczmarczyk et al. (2009) used artificial neural networks to classify gait in people with stroke. In this application the performance of neural networks was compared with another two methods for classifying gait, cluster analysis and discriminant function analysis (McLachlan, 1992). Seventy-four hemiplegic patients, from whom 55 were diagnosed with ischemic and 20 with hemorrhagic stroke, participated in the study. Three different gait patterns were defined based on the type of foot position on the ground at first contact, accordingly forefoot, flatfoot and heel. Gait analysis was accomplished based on 3D motion data, acquired using Ariel Performance Analysis System (California, USA), subject to 18 markers placed at specific points according to a standard protocol for full body motion analysis. Kaczmarczyk et al. classified gait based on qualitative (cluster analysis) and quantitative (discriminant analysis and artificial neural networks) criteria, using the position of foot during first contact with ground and min/max angle values as a function of time for the knee and hip joints, respectively. Results in this study indicated classification accuracies of 85% obtained based on the cluster analysis, 50% for the discriminant function analysis and success of 100% for the neural network classification. Kaczmarczyk et al. suggested that appropriate applicability of artificial neural networks may allow for more effective treatment with appropriately targeted intervention. The work demonstrates that artificial neural networks can be superior to other methods (qualitative variable analysis and analysis of min/max joint angles) in classifying gait patterns of post-stroke patients, confirming

neural networks are suitable data processing and analysis tools that can be used in gait research.

Artificial neural networks have been used in predicting lower body joint loads and forces (Favre et al., 2012; Liu et al., 2009). Oh et al. (2013) used neural networks to predict ground reaction forces and their moments during gait based on kinematic data obtained in double support walking phase. The input variables were selected to have both dependency and independency, and were limited to the trajectory, velocity and acceleration data recorded from 48 healthy volunteers using 3D motion capture (Vicon, Oxford, UK). To verify the prediction results, normal gait experiments were carried out on three force plates (AMTI, MA, USA). A three-layer feed-forward neural network (one hidden layer) utilised a back-propagation training algorithm and sigmoid neurons on the hidden layer was used. Oh et al. reported correlation coefficients of 0.9 and 0.89 (averaged for the x, y and z components of the ground reaction forces and moments) between the predicted and actual ground reaction forces and moments, respectively. These results proved the possibility of obtaining ground reaction forces and moments using neural networks in contrast to the conventional inverse dynamics methods. Despite the relatively low level of accuracy, the work of Oh et al. demonstrated that neural networks provide a solution for avoiding some of the major limitations of the conventional force plates in regards to spatial constraints, usability and high cost.

Another example of neural networks used to predict contact forces is given by Ardestani et al. (2014). In their work, artificial neural networks were successfully applied to predict the medial condyle contact force at medial knee joints corresponding to two different gait modifications, medial trust and trunk sway. Using data in the form of ground reaction forces, motion trajectories of gait and EMG onsets, three multilayer neural

networks with different architectures were trained based on data of pre-rehabilitation gait patterns. The networks were recruited to predict the medial knee contact force associated with rehabilitation patterns, and were implemented in Matlab. The first neural network consisted of four layers (2 hidden layers) and 10 numbers of inputs (trajectories of 7 independent motion markers and the three components of the ground reaction force vector), and was trained based on pre-rehabilitation gait patterns for a single subject. This network was tested to predict the medial knee contact force of the same subject. The second neural network was with five-layer architecture (3 hidden layers) and 12 numbers of inputs (the three components of the ground reaction force vector and reading from 9 EMGs), trained and tested based on pre-rehabilitation gait patterns of four subjects. The third network consisting of five layers and 17 inputs (trajectories of 7 independent motion markers, 9 EMGs and the three components of the ground reaction force vector) was tested in predicting the knee contact forces for a subject who was not included in the network training. According to the results which were validated with in vivo measurements for medial trust and trunk sway, the three neural networks predicted satisfactory level of accuracy indicated in averaged cross correlation coefficient between predicted and measured knee contact forces of 0.95. The work of Ardestani et al. shows a good example of neural networks used in predicting medial knee contact forces based on mixture of data in the form of ground reaction forces, marker trajectories and EMG onsets. The work provides a solution to the conventional methods such as the mathematical inverse dynamics for a faster and easier way of obtaining knee contact forces.

2.5.1 Conclusion

This section reviewed several recent papers of artificial neural networks demonstrating how neural networks can be employed in clinical applications providing solutions of quick and simplified examination outcome. Although neural networks have some limitations and are currently in evolutionary development, in the recent years they have shown a big promise for the future in the development of automated clinical applications for evaluation of results, making diagnosis and solving other complex tasks. One such application is demonstrated in this thesis in which neural networks are employed to identify the level of upper limb motor impairment of people with post stroke. This is shown in Chapters 5 and 6.

Chapter 3

Mathematical Modelling

3.1 Introduction

Fundamentally the development of DTS experimental devices requires identification of constructive parameters for the application as meaningful outputs and influences affecting performance. The use of mathematical modelling in this project aimed to assess and identify appropriate constructive parameters of the DTS devices, as well as to obtain a comprehensive understanding of the behaviour of elastic plates subject to various static and dynamic loading. To achieve these aims two mathematical models of elastic plates based on finite element and finite difference methods (FEM and FDM) were developed. First, a geometrical FEM model was developed and implemented with the commercially available modelling software ANSYS Workbench. Then a plate model based on the finite difference method was explained by mathematical terms and implemented in Matlab.

The chapter describes the implementation and verification of four node quadrilateral flat plate that incorporates membrane and bending components of displacement. The finite elements and finite differences of the considered flat plate are obtained by superposing plate bending and membrane components. Plates of this type possess six degrees of freedom (DOF), three displacement (w_x, w_y, w_z), and three in-plane rotation DOFs (u_x, u_y, u_z).

Due to its simple implementation and manipulation flexibility, the versatile FEM model based on displacement was used to identify acceptable design parameters affecting the performance of DTS devices. The work conducted investigates different distributive plate thicknesses and compound materials, but it is focused on comparing the performance of distributive surfaces subject to different types of plate supports. Figure 3.1 illustrates a performance tree showing the salient design parameters of DTS devices (Section 3.5).

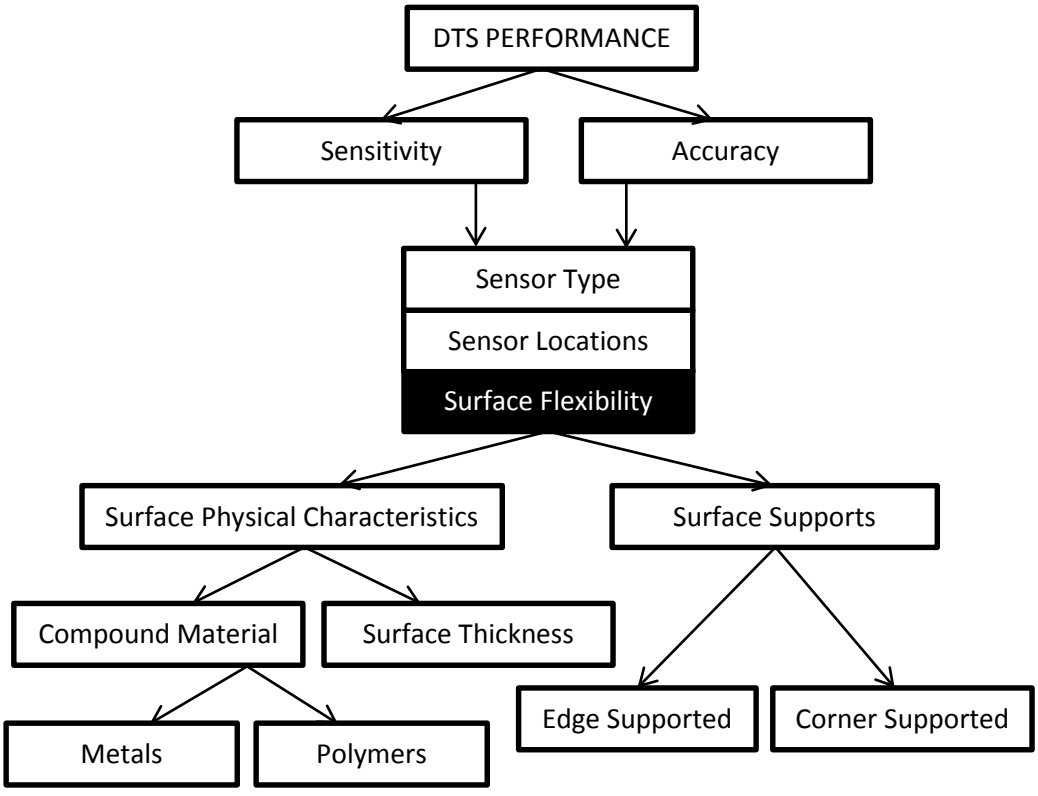

Figure 3.1 – DTS performance tree illustrating the fundamental design parameters affecting the sensitivity and accuracy of DTS devices.

The developed geometrical FEM model was verified by comparing simulated surface deflections with that of a real distributive surface. Derived surface deflections were then used to test the accuracy of the

distributive surface in position detection of static point loads. The investigation resulted in deriving average percentage errors of 0.6% and 3.6% for corner and edge supported boundary conditions respectively.

The work conducted over the FEM plate model showed that the overall sensitivity of the distributive surfaces can be controlled by using plates with different thicknesses and material elasticity. It was found that corner supported boundary conditions can provide optimised sensitivity and accuracy over the edge supported boundary conditions.

Further a mathematical model of the distributive surface was developed based on the FDM method and implemented in Matlab. In contrast to the FEM, which applies physical discretization, the FDM is based on mathematical discretization of the plate continuum. The mathematical realization of a FDM plate model and its Matlab implementation provided the opportunity to simulate the performance of complete DTS systems by combining it with other modelled structures as force inputs. The FDM was chosen as it is more transparent to the user and provides simpler mathematical implementation which leads to better understanding of modelled structures and their behaviour. This makes the finite difference method more suitable to manipulation and integrating additional components to it. Figure 3.2 illustrates a diagram of the FDM model, showing the applicability of the model in this thesis.

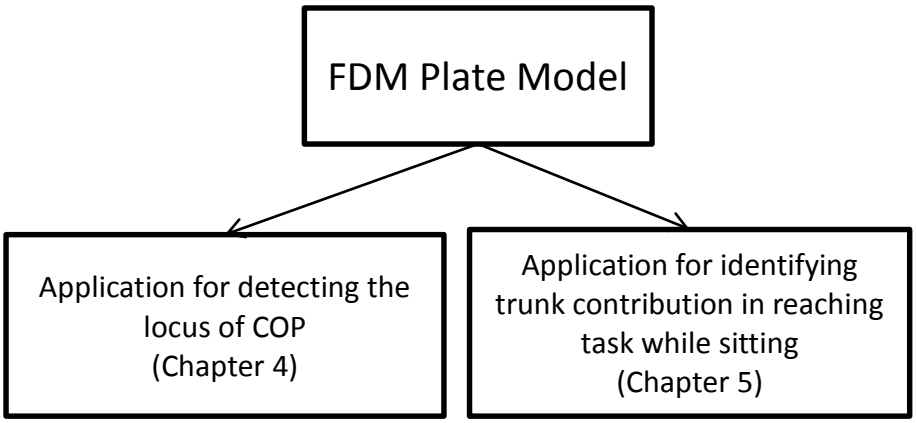

Figure 3.2 – Application diagram of the FDM plate model.

Both FEM and FDM models were developed with mesh sizes of 40 x 40 elements in both x and y directions based on a procedure for calculating more accurate values of the mesh-point deflections by using Richardson's extrapolating formula. Verification of the models was accomplished by comparing surface displacement with that of a real distributive surface.

The modelling work presented in this chapter provided explicit analysis over the FEM and FDM models of elastic plates. The development of FDM model with a convergence error of 0.33% has led to realistic performance of the modelled plate. Both FEM and FDM plate models have verified through agreement with measurements of deflection on the real surface.
In Chapter 4 the FEM and FDM plate models were used to develop and simulate an application for detecting the locus of centre of pressure. The application was used to compare the DTS technology with that of a commercialised force platform in detecting and tracking centre of pressure.
In Chapter 5 the model was extended to incorporate a biomechanical module as a dynamic force input to simulate a complete DTS system in performing reaching task. The model was simulated in a quasi-static mode in order to generate data needed to train neural networks applied to discriminate different levels of trunk contribution in performing reaching task.

3.2 Geometrical model of elastic plate by Finite Element Method (FEM)

In Finite Element Method, the accuracy of modelled structures is determined by the size of finite elements (the mesh density of discretised structure). According to finite element theory, the models with fine mesh (small element size) yield to highly accurate results but it may take longer in terms of convergence and computing time. On the other side, models with coarse mesh (large element size) may lead to less accurate results in return

to saving time and computing resources. In addition, very fine meshes are not generally desirable as they significantly increase the complexity of the models. Coarse meshes with large element sizes are used in simplified models for providing a quick and rough estimation of designs. The purpose of this modelling work was to develop elastic plate models with medium size meshes allowing fast convergence time and relatively high displacement accuracy.

The geometrical FEM model was developed with *1600* mesh elements (*n=40* elements for both *x* and *y* directions). This number was obtained based on recommended by Szilard procedure for defining the number of the mesh elements. The procedure is based on calculating more accurate values for the mesh-point deflections by Richardson's extrapolating formula (Szilard, 2004b; Szilard, 2004d):

$$w_i^{(3)} = w_i^{(2)} + \frac{w_i^{(2)} - w_i^{(1)}}{2^{\mu} - 1} \tag{3.12}$$

where μ represents the error order of the biharmonic operator, which depends on the convergence characteristics of the numerical method applied ($\mu = 2$ for Finite Element and Finite Difference Method).

Figure 3.3 represents a percentage error graph calculated for *n=4÷80*. Number of *40* mesh elements along x and y directions (*error ≈ -0.95%)* was chosen as a higher number of mesh elements didn't lead to considerably smaller error but significantly slower mesh convergence.

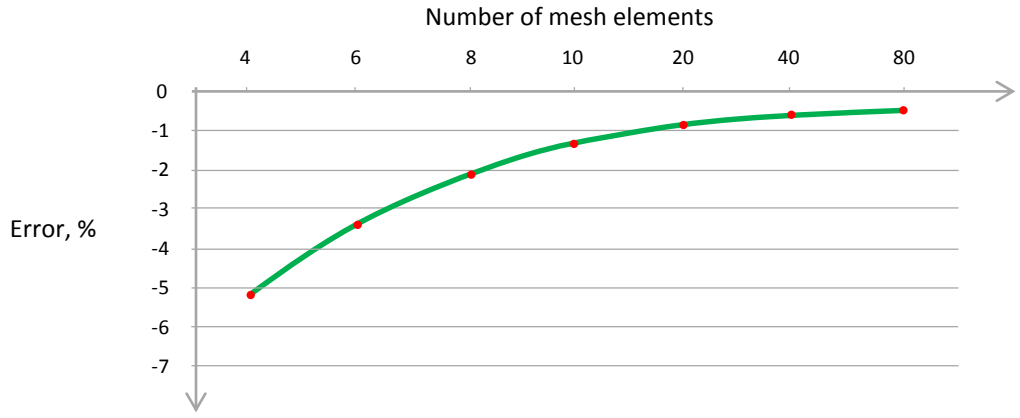

Figure 3.3 – Plot of percentage error calculated for FEM meshes consisting of different number of elements, from 4 to 80 elements in each x and y directions.

3.3 Static model of elastic plate by Finite Difference Method (FDM)

This section describes the mathematical implementation of an elastic plate model by finite difference method. The developed FDM plate mathematical model is based on solutions described by Szilard (2004c) and Kameswara Rao (2011). It has been developed with corner and edge supported boundary conditions subject to uniformly distributed and concentrated transverse loadings and implemented in Matlab.

Mathematical implementation of the finite difference plate model is based on discretization of the plate continuum, in a 2-dimensional mesh. In the finite difference method, corresponding finite difference quotients at each mesh point are represented by the partial derivatives in the governing plate equation. Therefore the differential equation governing displacement $w(x,y)$ is transformed into algebraic equations at each mesh point *'i'* yielding the displacement w_i.

The governing differential equation of elastic plate is defined by Navier in 1823 (Szilard, 2004a) as:

$$\frac{\partial^4 w}{\partial x^4} + \frac{2\partial^4 w}{\partial x^2 \partial y^2} + \frac{\partial^4 w}{\partial y^4} = \frac{p_{zT}(x,y)}{D} \tag{3.1}$$

where x and y are the Cartesian plate coordinates; w is the plate deflection; p_{zT} is the total applied force; D is the plate flexural rigidity. The flexural rigidity D is given by:

$$D = \frac{Eh^3}{12(1-v)} \tag{3.2}$$

where E is the Young's modulus of elasticity; h is the plate thickness; v is Poisson ration.

To obtain finite difference expressions for the derivatives, the function *f(x)* is approximated in a given interval by an interpolating polynomial. A better polynomial approximation at so-called pivotal point *'m'* (describing the mesh elements) yields better finite difference expressions and therefore improved accuracy. The accuracy of the plate model is based on fourth order derivative and is described with the relation between the pivotal point *'m'* and its equally placed points illustrated in Figure 3.4 for the one dimensional case.

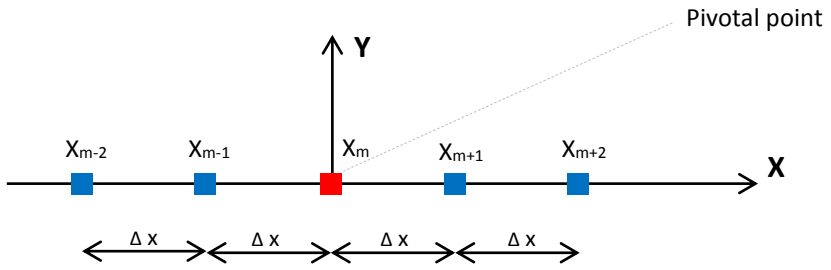

Figure 3.4 – One-dimensional graphical representation of finite differences.

The first, second, third and fourth derivatives of the original function *y=f(x)* considered in the one-dimensional case are defined as follows:

Ist derivative

$$\left(\frac{dy}{dx}\right)_m \approx \left(\frac{\Delta y}{\Delta x}\right)_m = [\phi'(x)]_m = \frac{1}{2(\Delta x)}(y_{m+1} - y_{m-1}) \tag{3.3}$$

IInd derivative

$$\left(\frac{d^2y}{dx^2}\right)_m = \left[\frac{d}{dx}\left(\frac{dy}{dx}\right)\right]_m \approx \left(\frac{\Delta^2 y}{\Delta x^2}\right)_m = \phi''^{(x)m} = \frac{1}{(\Delta x)^2}(y_{m+1} - 2y_m + y_{m-1}) \tag{3.4}$$

IIIrd derivative

$$\left(\frac{d^3y}{dx^3}\right)_m \approx \left[\frac{\Delta}{2(\Delta x)}\left(\frac{\Delta^2 y}{\Delta x^2}\right)\right]_m = \frac{1}{2(\Delta x)^3}(\Delta^2 y_{m+1} - \Delta^2 y_{m-1}) =$$

$$= \frac{1}{2(\Delta x)^3}(y_{m+2} - 2y_{m+1} + 2y_{m-1} - y_{m-2}) \tag{3.5}$$

IVth derivative

$$\left(\frac{d^4y}{dx^4}\right)_m \approx \left(\frac{\Delta^4 y}{\Delta x^4}\right)_m = \left[\frac{\Delta}{\Delta x}\left(\frac{\Delta^3 y}{\Delta x^3}\right)\right]_m = \frac{1}{(\Delta x)^4}\left(\Delta^3 y_{m+\frac{1}{2}} - \Delta^3 y_{m-\frac{1}{2}}\right) =$$

$$= \frac{1}{(\Delta x)^4}(y_{m+2} - 4y_{m+1} + 6y_m - 4y_{m-1} + y_{m-2}) \tag{3.6}$$

The derived expressions can also be obtained by the use of a table of central differences with discrete points located symmetrically with respect to the pivotal point *'m'*, Table 3.1.

x	y	Δy	$\Delta^2 y$	$\Delta^3 y$	$\Delta^4 y$
x_{m-2}	y_{m-2}				
		$\Delta y_{m-(3/2)}$			
x_{m-1}	y_{m-1}		$\Delta^2 y_{m-1}$		
		$\Delta y_{m-(1/2)}$		$\Delta^3 y_{m-(1/2)}$	
x_m	y_m		$\Delta^2 y_m$		$\Delta^4 y_m$
		$\Delta y_{m+(1/2)}$		$\Delta^3 y_{m+(1/2)}$	
x_{m+1}	y_{m+1}		$\Delta^2 y_{m+1}$		
		$\Delta y_{m+(3/2)}$			
x_{m+2}	y_{m+2}				

Table 3.1 – Derivation of central differences

The finite difference representation of a 2-dimensional plate mesh and its pivotal point *'m,n'* is illustrated in Figure 3.5.

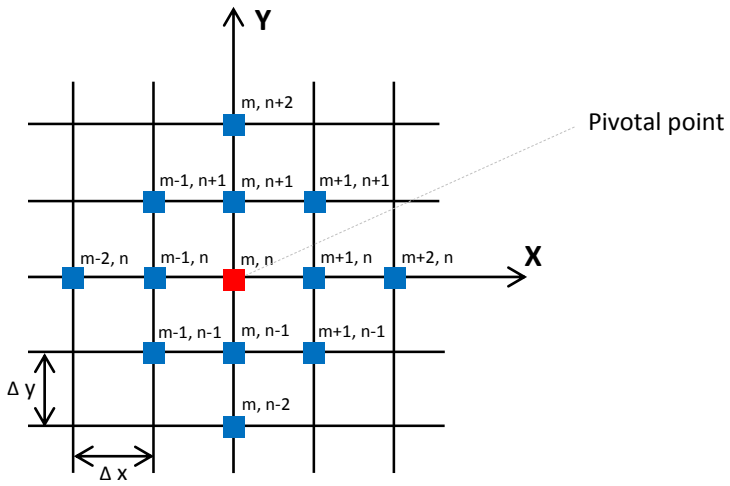

Figure 3.5 – Two-dimensional finite difference representation of a plate mesh.

Having obtained the fourth derivative of the original function, the separate parts of the governing plate equation can be expressed as:

$$\left(\frac{\partial^4 w}{\partial x^4}\right)_{m,n} \approx \frac{1}{\lambda^4}\left(w_{m+2,n} - 4w_{m+1,n} + 6w_{m,n} - 4w_{m-1,n} + w_{m-2,n}\right) \quad (3.7)$$

$$\left(\frac{\partial^4 w}{\partial y^4}\right)_{m,n} \approx \frac{1}{\lambda^4}\left(w_{m,n+2} - 4w_{m,n+1} + 6w_{m,n} - 4w_{m,n-1} + w_{m,n-2}\right) \quad (3.8)$$

$$\left(\frac{\partial^4 w}{\partial x^2 \partial y^2}\right)_{m,n} \approx \frac{1}{\lambda^4}[4w_{m,n} - 2\left(w_{m+1,n} + w_{m-1,n} + w_{m,n+1} + w_{m,n-1}\right) +$$
$$+ w_{m+1,n+1} + w_{m+1,n-1} + w_{m-1,n+1} + w_{m-1,n-1}], \quad (3.9)$$

where $\Delta x = \Delta y = \lambda$.

Therefore the finite difference representation of the plate governing equation becomes:

$$(D\nabla^2\nabla^2 w)_{m,n} \approx \left[20w_{m,n} - 8\left(w_{m+1,n} + w_{m-1,n} + w_{m,n+1} + w_{m,n-1}\right) + \right.$$
$$+2\left(w_{m+1,n+1} + w_{m-1,n+1} + w_{m+1,n-1} + w_{m-1,n-1}\right) +$$
$$\left. + w_{m+2,n} + w_{m-2,n} + w_{m,n+2} + w_{m,n-2}\right] + \varepsilon(\lambda^2) = \frac{\lambda^4 (p_z)_{m,n}}{D} + \frac{\lambda^2 (P_z)_{m,n}}{D} \quad (3.10)$$

where p_z and P_z *are* the distributed and concentrated load components of pivotal point '*m,n*' (Kameswara Rao, 2011); ε is the error term describing the discrepancy between the exact expression of a biharmonic operator (∇^2) and its finite difference representation. The error term is obtained from the expression:

$$\varepsilon^{(1)}{}_{m,n} \approx \frac{w^{(0)}{}_{m,n} - w^{(1)}{}_{m,n}}{2^{\mu} - 1} = \frac{w^{(0)}{}_{m,n} - w^{(1)}{}_{m,n}}{3} \quad (3.11)$$

($\mu = 2$ for Finite Element and Finite Difference Method).

Following the procedure for defining the number of mesh elements (Richardson's extrapolating formula – Section 3.2), the FDM plate model was also developed with *1600* mesh elements (*n=40* elements for both *x* and *y* directions). Figure 3.6 represents a percentage error graph calculated for *n=4÷80*. Number of *40* mesh elements along x and y directions (*error ≈ -0.33%)* was chosen as a higher number of mesh elements did not lead to considerably smaller error but significantly slower mesh convergence. According Szilard (Szilard, 2004b), discretisation with very fine meshes may create round-off errors affecting the accuracy of the model.

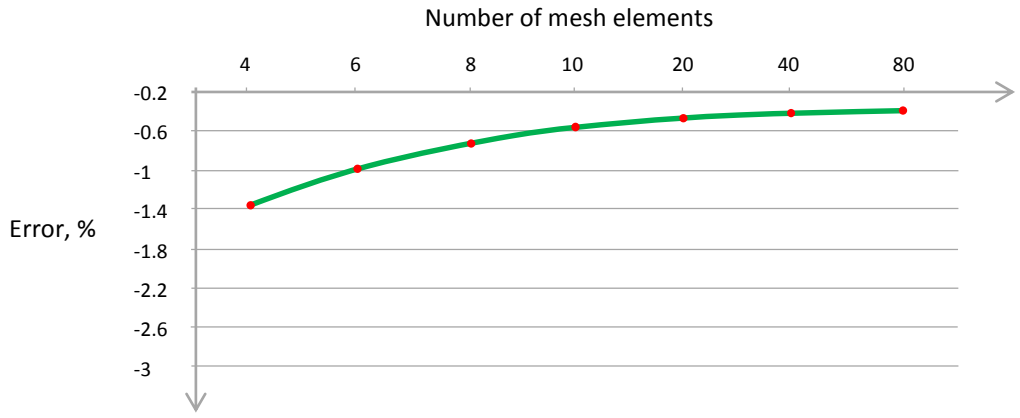

Figure 3.6 – Plot of percentage error calculated for FDM meshes consisting of different number of elements, from 4 to 80 elements in each x and y directions.

For the purposes of this project, the developed plate model was defined with edge and corner supported boundary conditions defined as follows:

$m_{x(m,n)} = 0;$ $\qquad$ $m_{y(m,n)} = 0;$

$$w_{m,n} = 0 \qquad and \qquad \left(\frac{\partial w}{\partial x}\right)_{m,n} \approx \frac{1}{2\lambda}\left(w_{m+1,n} + w_{m-1,n}\right) = 0, \qquad (3.12)$$

where m_x and m_y are the 2-dimensional components of the force moments.

The 2-dimensional finite difference representation of a concentrated load at pivotal point *'m,n'* is derived based on Simpson's one-third rule of double numerical integration for four squares (Soare, 1967; Szilard, 2004b).
The obtained finite difference representation of a concentrated load applied at pivotal point '*m,n'* is:

$$(P_z)_{m,n} = \frac{1}{36}\{p_{m-1,n-1} + 4p_{m,n-1} + p_{m+1,n-1} + 4p_{m-1,n} + 16p_{m,n} + \\ +4p_{m+1,n} + p_{m-1,n+1} + 4p_{m,n+1} + p_{m+1,n+1}\} \tag{3.13}$$

Having derived the finite difference representation of the elastic plate governing equation and the concentrated point load, a Matlab code was written to implement the above stated calculations defining the complete plate model. In the next section the FDM model is verified alongside the geometrical FEM plate model developed with ANSYS Workbench.

3.4 Verification of the FEM and FDM plate models

The two mathematical models of elastic plate based on finite element and finite difference methods were verified by comparing the simulated plate deflections with that of real distributive surfaces. The models were defined as square shaped plates of dimensions 430 x 430mm, matching the size requirement of the further developed experimental setup of a DTS floor platform described in Chapter 4. The models were tested under corner supported boundary conditions as these provide minimal surface support and hence more natural deformations of the modelled surfaces. The verification was based on two types of surfaces, an acrylic surface of thickness 4mm and a steel surface of thickness 3mm. To define the material characteristics of the simulated surfaces, Young's modulus and Poison ratio were selected from the relevant standard ranges of acrylic and steel

materials to match the performance of the real physical surfaces (Acrylic surface: *Young's modulus 3.5GPa, Poison ration 0.31;* Steel surface: *Young's modulus 198.7GPa, Poison ratio 0.27* ("Materials Data Book," 2003; "The Engineering Toolbox," 2015). Due to the symmetrical shape of the surfaces, deflections were measured at three points across the surface corresponding to the three most common sensor positions investigated in this work (Figure 3.7). Simulated surface deformations were provoked by a single transverse force (F_z) applied in the middle of the surface.

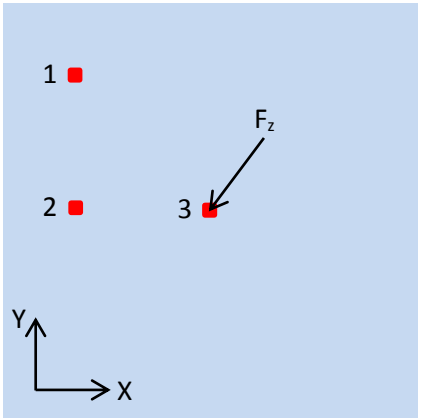

Figure 3.7 – Illustration of the modelled distributive surface with the locations of three points in which deflection was measured (1, 2 and 3).

In this study, deflection point 1 was considered as a major sensing position. Therefore, this point was chosen to reference the deflections of the simulated surfaces with the real ones. Surface responses were tested with four different simulation loads (for the acrylic surface – *0.25, 0.5, 0.75, 1kgf*; for the steel surface – *5, 10, 15, 20kgf*) as the biggest load was selected to cause maximum surface deflection not exceeding the thickness of the surface.

3.4.1 Surface deflection measurements

The deflections of the real physical surfaces were measured by the use of IR displacement sensor, used in the design of the first for this project experimental setup (Chapter 4). Micromanipulator "Eppendorf - TransferMan NK2" (Figure 3.8A) was used to correlate the non-linear voltage measurements of the IR sensor in respect of distance. The measurements were derived by using a metal bar attached to the micromanipulator as shown in Figures 3.8B.

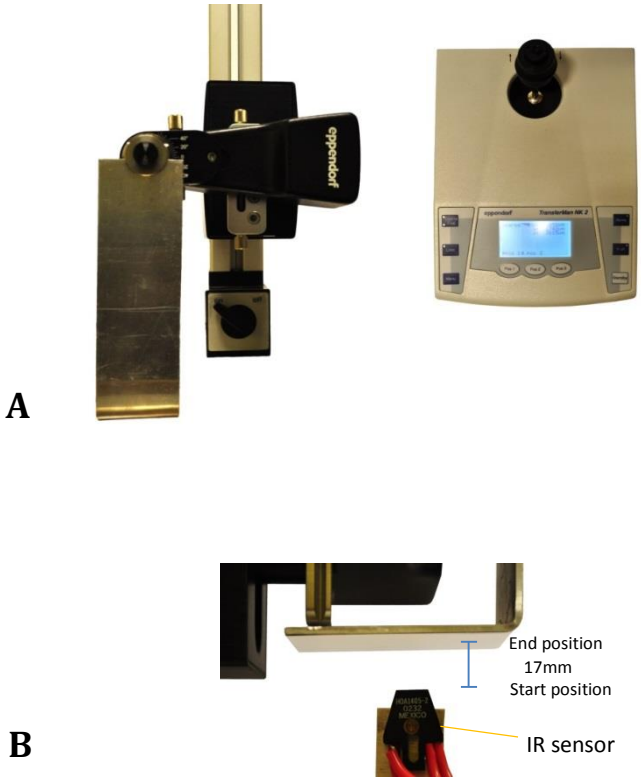

Figure 3.8 – Micromanipulator "Eppendorf - TransferMan NK2" (A) used to Measure the range of operation (established within distance of 17mm) of IR displacement sensor "HOA 1405-2" (B).

A piece of white reflective photo paper was attached to the underside of the metal bar to provide normal reflection of the emitted from the sensor IR light, ensuring normal sensor reading. The micromanipulator was set to move the bar vertically from the start position, in which the bar touches the sensor, up to the end position within a distance of *17mm*. The speed of the bar was set to *100µm/s* and sensor readings were recorded with sampling rate of *20Hz* ensuring the acquisition resolution is higher than the one of the sensor (sensor wavelength – *8.9µm*). The sampling rate was calculated by the formula:

Sampling rate > actuator speed / sensor wavelength (3.14)

Sampling rate > 100µm / 8,9µm ***Sampling rate > 11Hz***

Figure 3.9 shows obtained Voltage – Distance characteristics of a sensor "HOA 1405-2". As illustrated in the graph, the operational range of the sensor "HOA 1405-2" has a non-linear voltage-distance characteristic. In this work, the relatively straight part of the characteristic from *7* to *12mm* was used as an operational range of this sensor. The range corresponding to distance of approximately 5mm was sufficient for the applications considered in this project.

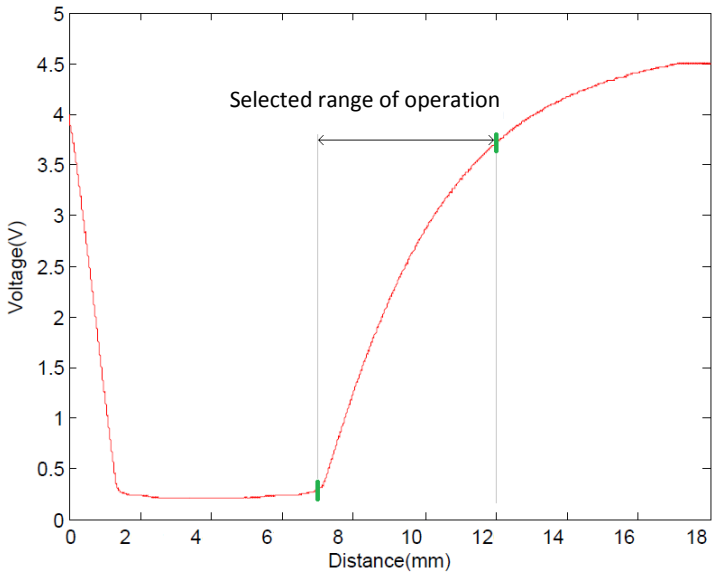

Figure 3.9 – Voltage - Distance characteristics of IR sensor "HOA 1405-2".

3.4.2 Verification results

Figure 3.10 shows the developed in ANSYS Workbench FEM plate mesh of tetragonal type. The mesh is discretised by 40 divisions in x and y directions resulting in element size of 10.75mm (430mm / 40divisions).

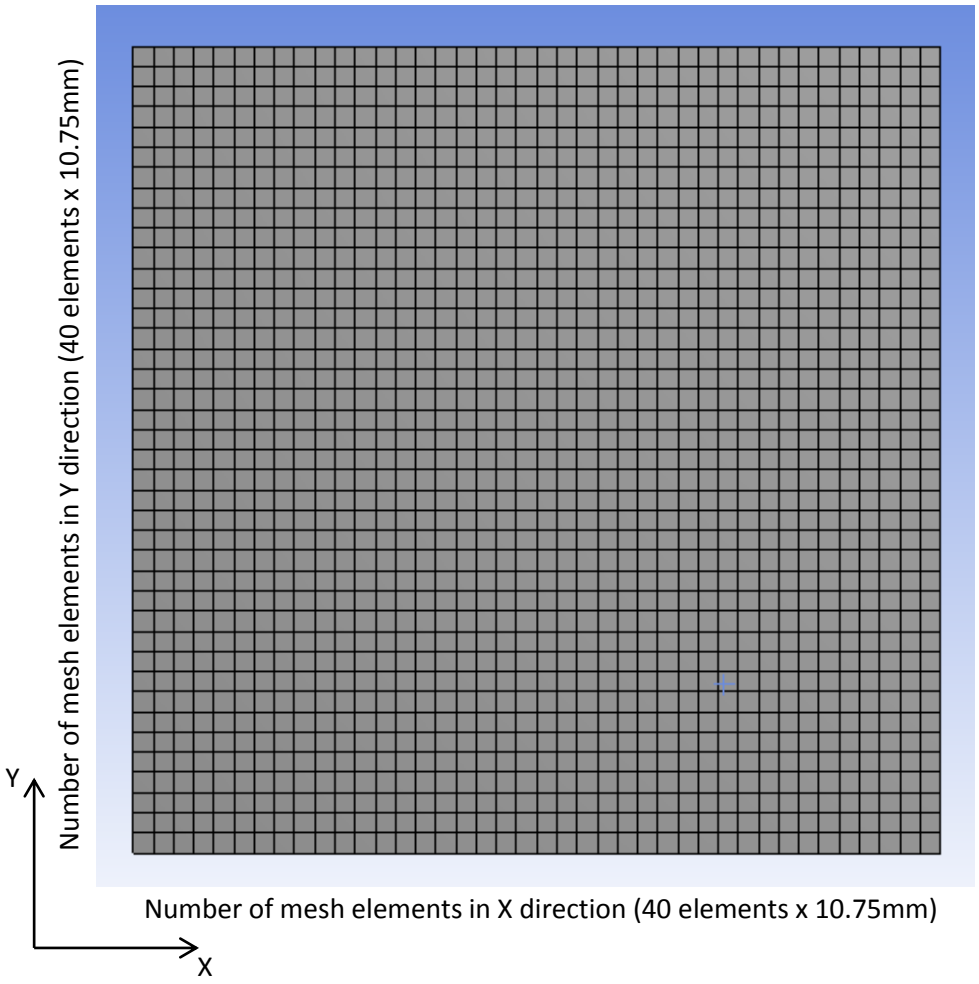

Figure 3.10 – Mesh of FEM plate model with 40 elements on both x and y coordinates.

Figure 3.11 shows illustrations of the developed and implemented in Matlab FDM elastic plate models based on corner and edge supported boundary conditions.

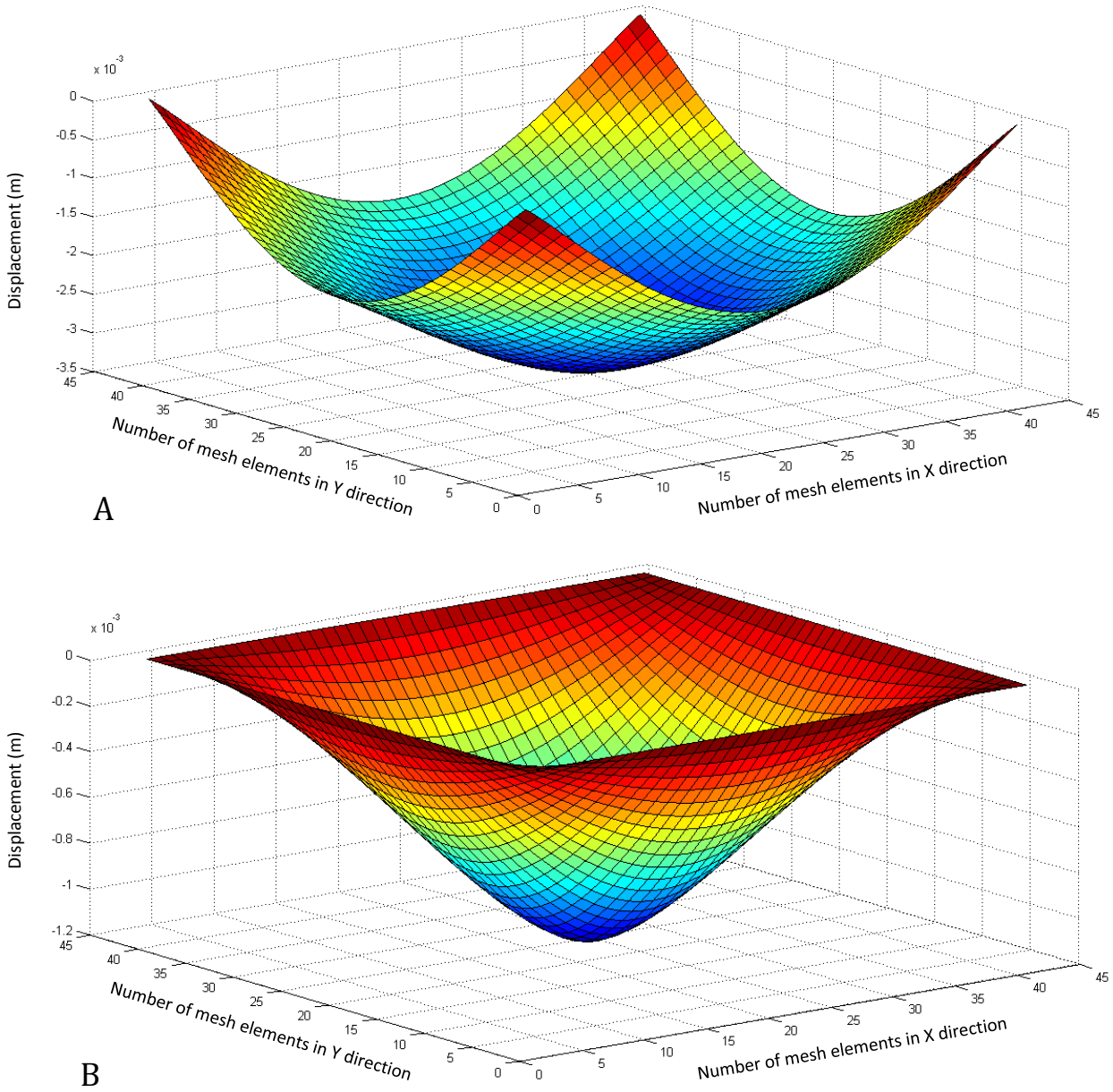

Figure 3.11 – FDM elastic plate models based on corner (A) and edge (B) supported boundary conditions.

Results of the verification test are presented in Tables 3.2 and 3.3 in the form of displacement, which was obtained from the considered in the real and simulated surfaces three deflection points (According Figure 3.7 sensing positions 1, 2 and 3). In order to show the deformation differences between the surfaces, deviation from the real surface deflections were calculated and included in the results. In addition, Figures 3.12 and 3.13 compare plots representing the deformation behaviour of the acrylic and steel surfaces, respectively. The plots are derived based on the results presented in Tables 3.2 and 3.3.

Acrylic (Young's M -3.5GPa, Poison ratio - 0.31, thickness - 4mm)								
Load (kgf)	0.25		0.5		0.75		1	
	Deflection(mm) - real DTS surface							
Sens. position 1	0.5		1		1.446		1.93	
Sens. position 2	0.79		1.53		2.23		2.98	
Sens. position 3	1.03		2.1		3		3.97	
	Deflection(mm)FEM							
		Deviation (mm)		Deviation (mm)		Deviation (mm)		Deviation (mm)
Sens. position 1	0.508	0.008	1.015	0.015	1.523	0.077	2.03	0.1
Sens. position 2	0.677	-0.113	1.354	-0.176	2.032	-0.198	2.709	-0.271
Sens. position 3	0.857	-0.173	1.715	-0.385	2.572	-0.428	3.43	-0.54
	Deflection(mm)FDM							
		Deviation (mm)		Deviation (mm)		Deviation (mm)		Deviation (mm)
Sens. position 1	0.5	0	1	0	1.501	0.055	2.002	0.072
Sens. position 2	0.705	-0.085	1.41	-0.12	2.116	-0.114	2.821	-0.159
Sens. position 3	0.912	-0.118	1.825	-0.275	2.737	-0.263	3.649	-0.321

Table 3.2 – Surface deflections of the real, FDM and FEM acrylic surfaces subject to transverse single loads of 0.25, 0.5, 0.75 and 1kgf.

Steel (Young's M -198.7GPa, Poison ratio - 0.27, thickness - 3mm)								
Load (kgf)	5		10		15		20	
	DTS surface							
Sens. position 1	0.34		0.64		0.91		1.19	
Sens. position 2	0.52		1		1.4		1.78	
Sens. position 3	0.72		1.36		2.01		2.61	
	Deflection(mm) FEM							
		Deviation (mm)		Deviation (mm)		Deviation (mm)		Deviation (mm)
Sens. position 1	0.342	0.002	0.684	0.044	1.026	0.116	1.3675	0.1775
Sens. position 2	0.472	-0.048	0.943	-0.057	1.415	0.015	1.886	0.106
Sens. position 3	0.617	-0.103	1.233	-0.127	1.849	-0.161	2.466	-0.144
	Deflection(mm) FDM							
		Deviation (mm)		Deviation (mm)		Deviation (mm)		Deviation (mm)
Sens. position 1	0.34	0	0.68	0.04	1.02	0.11	1.36	0.17
Sens. position 2	0.496	-0.024	0.991	-0.009	1.487	0.087	1.983	0.203
Sens. position 3	0.663	-0.057	1.325	-0.035	1.988	-0.022	2.65	0.04

Table 3.3 – Surface deflections of the real, FDM and FEM steel surfaces subject to transverse single loads of 5, 10, 15, 20kgf.

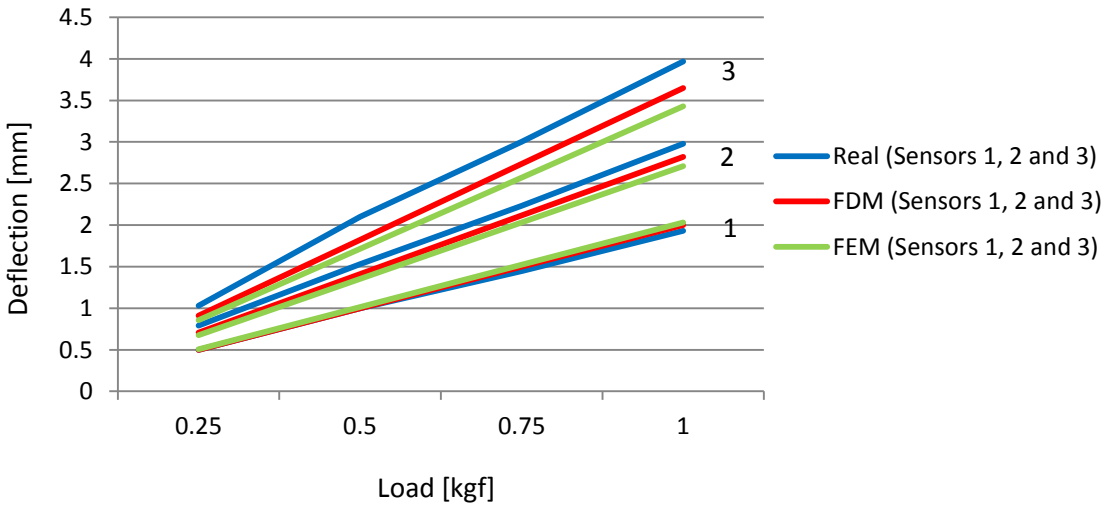

Figure 3.12 – Plots representing the deformation behaviour of the real, FEM and FDM acrylic surfaces in the three sensor locations subject to 0.25, 0.5, 0.75 and 1kgf transverse loads.

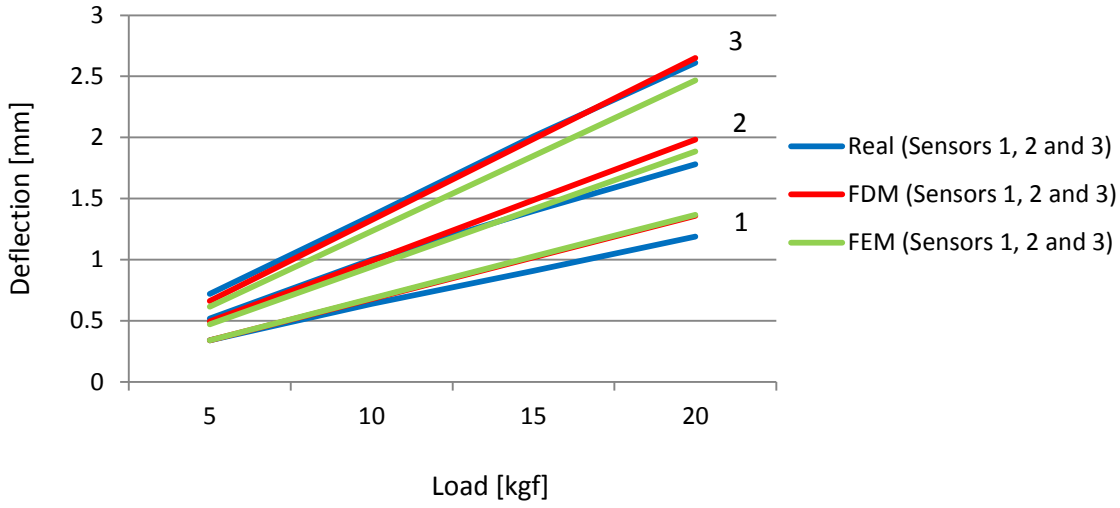

Figure 3.13 – Plots representing the deformation behaviour of the real, FEM and FDM steel surfaces in the three sensor locations subject to 5, 10, 15 and 20kgf transverse loads.

3.4.3 Verification of Theoretical Models

The results verify that both FEM and FDM plate models respond in a very similar manner to the real physical surface. The simulated plate models have been investigated with loads causing deflections higher than one tenth of the plate thickness. According Szilard (2004b), this leads to increased discrepancy of the deflections between the real and simulated surfaces and hence increased deviations from deformations of real surfaces. Considering this limitation, the obtained deflections of the real and simulated surfaces have demonstrated acceptable and satisfactory performance of the surfaces. The similar deformation behaviour of the surfaces shown in the graphs of Figures 3.12 and 3.13 has a significant importance to the use and applicability of the simulated plate models in this thesis. This is due to the fact that in many applications of the DTS method it is important to know how the distributive surface deforms, rather than the exact displacement of surface deformations.

In the Distributive Tactile Sensing approach, interpreting sensing data in the form of proportions between deflections at specific sensing locations can be advantageous when external conditions such as temperature and moisture have an effect of the surface flexibility, or the effect of increasing or decreasing load magnitudes has to be minimized. This is possible as in certain cases proportion measurements tend to maintain relatively constant values subject to increasing or decreasing surface deflections. For example, a fluctuating point load applied at particular position over a flexible surface would cause fluctuating surface deformations resulting in relatively constant proportion values between certain deflection points. In this project, such interpretation methods were used to investigate the accuracy of distributive surfaces, as well as to detect the locus of centre of pressure. In support of the above stated assumptions, Tables 3.4 and 3.5 represent some additional verification results of comparing two groups of proportions between displacements obtained from the following sensing positions: group 1 - sensing positions 1 and 2; group 2 - sensing positions 1 and 3, according Figure 3.7. Proportions were calculated based on the surface deflections presented in Tables 3.2 and 3.3. The results obtained confirm the above stated assumption indicating that the increasing effect of an applied single load does not considerably affect the values of relevant to each group proportions.

Acrylic			Loading (kgf)			
			0.25	0.5	0.75	1
Group 1	S1/S2	real	0.632911	0.653595	0.64843	0.647651
Group 1	S1/S2	FDM	0.70922	0.70922	0.709357	0.709677
Group 1	S1/S2	FEM	0.750369	0.749631	0.749508	0.749354
Group 2	S1/S3	real	0.485437	0.47619	0.482	0.486146
Group 2	S1/S3	FDM	0.548246	0.547945	0.548411	0.548643
Group 2	S1/S3	FEM	0.592765	0.591837	0.592146	0.591837

Table 3.4 – Proportions of deflection points S1-S2 (Group 1), and S1-S3 (Group 2) for surface of acrylic material, subject to transverse loadings applied in the middle of the surface (0.25, 0.5, 0.75, 1kgf).

Steel			Loading (kgf)			
			5	10	15	20
Group 1	S1/S2	real	0.653846	0.64	0.65	0.668539
Group 1	S1/S2	FDM	0.685484	0.686176	0.685945	0.68583
Group 1	S1/S2	FEM	0.724576	0.725345	0.725088	0.72508
Group 2	S1/S3	real	0.472222	0.470588	0.452736	0.455939
Group 2	S1/S3	FDM	0.512821	0.513208	0.513078	0.513208
Group 2	S1/S3	FEM	0.554295	0.554745	0.554895	0.554542

Table 3.5 – Proportions of deflection points S1-S2 (Group 1), and S1-S3 (Group 2) for surface of steel material, subject to transverse loadings applied in the middle of the surface (5, 10, 15, 20kgf).

Following verification, the FEM and FDM plate models were ready for the intended purposes of this project. The remaining text in this chapter will demonstrate how the versatile FEM model was used to investigate design parameters affecting the performance of DTS devices.

3.5 Salient design parameters of DTS devices by FEM

Similar to other sensing systems the performance of DTS devices can be assessed, optimised and controlled by measuring the two main parameters relevant to the nature of DTS technology, sensitivity and accuracy. For a given application, the sensitivity and accuracy of DTS devices depend on the deformation characteristics of deforming surfaces used, as well as the performance and characteristics of the deployed sensing elements and their locations (DTS performance tree – Figure 3.1). The investigation undertaken in this section is focused on the deformation characteristics of the distributive surface, not the types of sensing elements used and their specifications.

The sensitivity of the distributive surface can be defined as the ability of the surface to respond to force stimuli with small magnitudes and/or small changes in force stimuli with various magnitudes. For example, particularly high sensitivities can be achieved by using surfaces with high flexibility which deform in response to small contact forces. The accuracy of the distributive surface can be defined as its ability to respond differently to small contact changes, corresponding to the magnitude or the position of the applied force. Due to the deformation nature of elastic surfaces, it is always the case that the sensitivity and accuracy of the distributive surface varies in different areas over the surface. In order to optimise the performance of DTS devices, the deformation characteristics of distributive surfaces can be controlled by appropriate selection of surface materials, thicknesses and supports. It has to be noted that in certain cases, for example when the distributive surface responds to contact forces of large magnitude, high sensitivities might not be sought after as this would bring undesired additional surface deformations. Hence the selection of specific DTS characteristics might be suitable for certain applications but not for others.

As the DTS technology provides the possibility of using surfaces of different compound materials and thickness, its applicability covers a wide range of contact loading. By using distributive surfaces of the acrylic and structural steel materials and thicknesses in the range of *2* to *6mm,* the DTS devices could be adjusted for applications subject to contact loading in the range of *1N to 1000N*.

Boundary conditions are the other significant factor affecting the performance of DTS device. In previous projects of the DTS technology, the majority of developed applications were based on edge supported distributive surfaces. In this work corner and edge supported boundary conditions were investigated and used. As would be expected, it was found that corner supported surfaces provide higher flexibility and in certain cases higher accuracy in comparison with edge supported surfaces. The DTS

approach allows implementation of various types of surface support which can be effective in optimising the performance of DTS devices. This was demonstrated in this section by investigating the performance of elastic surfaces using the FEM plate model.

3.5.1 Investigating DTS accuracy in position detection to identify appropriate surface supports

In this section the developed FEM plate model was investigated through conducting number of simulations via ANSYS Workbench commercially available software. The purpose of this modelling work was to compare the performance of distributive surfaces under edge and corner supported boundary conditions. This was accomplished by introducing a technique for testing accuracy of the distributive surface for detecting the position of static transverse point loads. The technique for evaluating accuracy of the distributive surface is described by the use of the illustration shown in Figure 3.14.

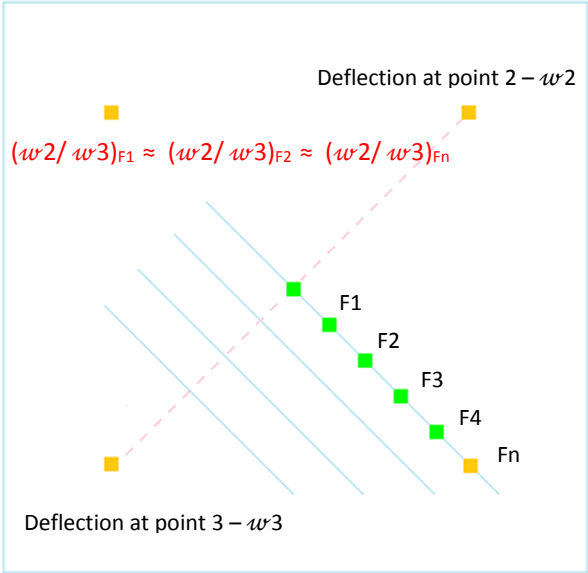

Figure 3.14 – Technique for evaluating the accuracy of DTS surface in position detection described by diagonal nodal positioning of point loads F1-Fn (subject to deflection proportions of two opposite corner points).

The proposed technique applies to distributive surfaces of a square shape. It compares the deflection proportions of two corner points of the surface which are opposite each other (e.g. point 2 and point 3 in Figure 3.14). The proportions of interest are subject to static point loads applied along any line perpendicular to the line connecting the two corresponding corner points. It is important for the technique that the selected corner points are symmetrical to each other along the diagonal lines of the surface. The proposed technique is based on the assumption that for all static loads (F1 to Fn), the corresponding proportions ($w2/w3$) have approximately the same values. Thus any point load across the distributive surface has two particular deflection proportions which can be associated with the x and y coordinates of the surface. Complete realisation of such a position detection technique will be presented in Chapter 4 to determine the locus of centre of pressure.

The above described principle for identifying the position of a load applied to the distributive surface is also applicable to proportions calculated between two neighbour deflection points (point1 and point3) as shown in Figure 3.15.

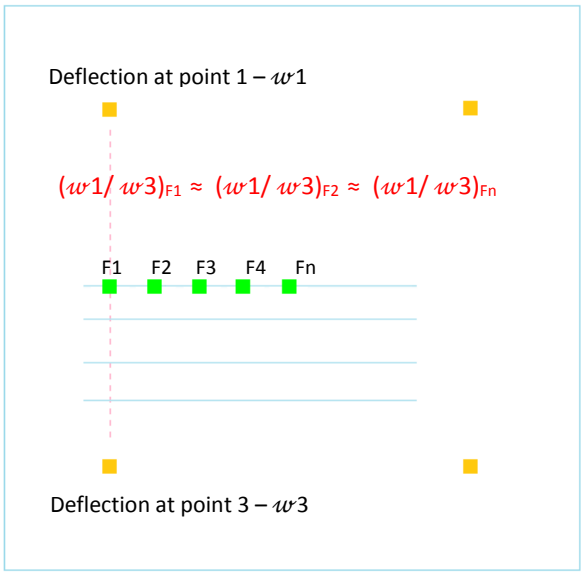

Figure 3.15 – Technique for evaluating the accuracy of DTS surface in position detection described by horizontal nodal positioning of point loads F1-Fn (subject to deflection proportions of two neighbour corner points).

In this case the two neighbour corner points are symmetrical to each other along the middle horizontal or perpendicular lines of the surface. Therefore the proportions between deflections $w1$ and $w3$ for the corresponding point loads (F_1 to F_n) have approximately the same values.

In this work the accuracy of the distributive surface is investigated based on the above described two types of proportions, corresponding to the neighbouring (Figure 3.14) or opposite (Figure 3.15) corner points. The accuracy of the distributive surface was tested by measuring the variation in deflection proportions between two corner points (points 2 and 3, and 1 and 3 for the two cases respectively), subject to the corresponding for each proportion point loads. The investigation of identifying the accuracy of the distributive surface was conducted based on edge and corner supported boundary conditions illustrated in Figure 3.16.

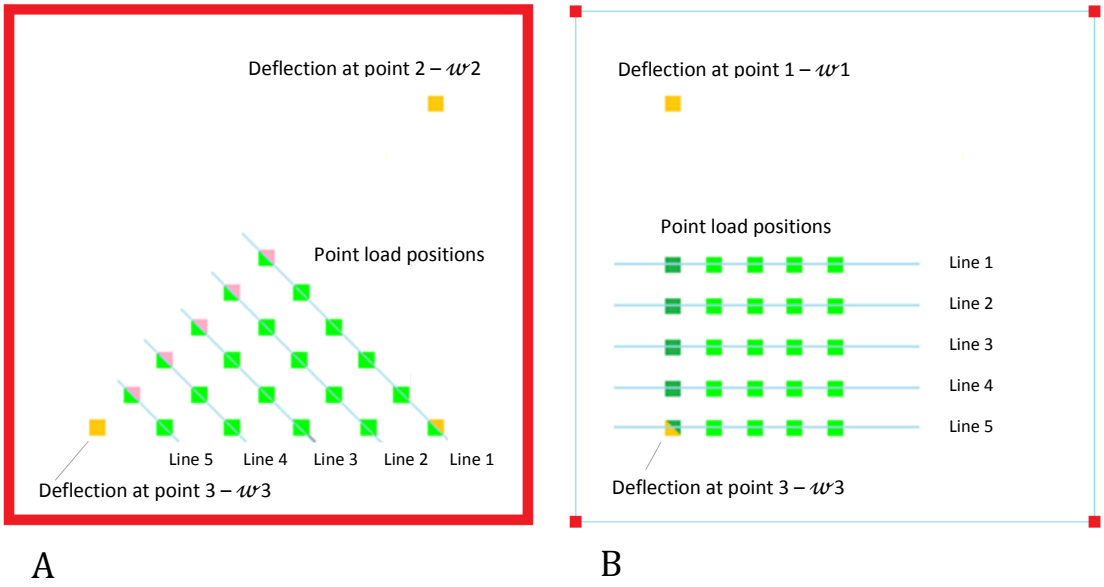

Figure 3.16 – Edge supported (A) and Corner supported (B) boundary conditions of the distributive surface.

The simulated results corresponded with an acrylic surface of thickness *4mm*. Loads with magnitudes of up to *10N* were simulated, causing

maximum deflection in the centre of the surface of *1.04* to *3.43mm* for edge and corner supported surfaces, respectively.

For the two examples of the technique for identifying the accuracy of distributive surfaces, subject to opposite and neighbour deflection points, the simulations were conducted with numbers of 20 and 25 point loads, respectively. The point loads were applied separately along five lines as shown in Figure 3.16. The symmetry enabled representative simulation modelling over a quarter of the surface. As the obtained simulation data was interpreted in the form of proportions, different thicknesses and compound materials of the surfaces, as well as magnitudes of the applied loads, had a negligible effect on the results. This is due to the fact that, as it was shown in Section 3.4.3, proportions between selected deflection points tent to have relatively constant values subject to specific position of an applied point load but different mechanical characteristics of distributive surfaces and magnitudes of the applied load. Respectively the use of proportion values is particularly useful in position detection applications.

3.5.2 Simulation results

Surface deflections from conducted simulations were used to test the accuracy of the distributive surface based on the above described technique for testing the accuracy of the distributive surface. Obtained proportion values were compared separately along each line where the simulation loads were applied. The load points adjacent to the line connecting the two corner points (for both accuracy methods) were used as referential. The results from this investigation were based on calculating the differences between the deflection proportions for each line and presenting them as a percentage error derived by the following formula:

(Measured value – Reference value) / Reference value * 100 = % Error (3.15)

Mean percentage errors were calculated for the two techniques for identifying the accuracy of distributive surfaces in corner and edge supported plate models. The errors were calculated separately and together for all lines along which the loads were applied. The results from the conducted simulations are summarized and presented in Table 3.6.

	Mean % Error in proportion value deviation for each line					
Opposite corner points	**Line 1**	**Line 2**	**Line 3**	**Line 4**	**Line 5**	**Mean % Error**
Edge Supported	0.023	3.258	5.144	5.285	4.078	3.558
Corner Supported	0.005	2.518	2.682	1.791	0.648	1.529
	Mean % Error in proportion value deviation for each line					
Neighbour corner points	**Line 1**	**Line 2**	**Line 3**	**Line 4**	**Line 5**	**Mean % Error**
Edge Supported	0.056	4.376	9.47	16.045	23.005	11.032
Corner Supported	0.009	0.332	0.63	0.827	1.005	0.56

Table 3.6 – Obtained accuracy of deviation in proportion values for the simulated surfaces presented in percentage errors for edge and corner supported boundary conditions, and opposite and neighbour corner points.

Figure 3.17 illustrates the obtained errors in proportion values deviation graphically for the two variations of the accuracy method in edge and corner supported surfaces. The plots represent the increasing and decreasing behaviour of the calculated errors at the five lines of each of the four simulation conditions. The four plots are described from top to bottom as follows:

1 - Edge supported boundary conditions – opposite corner points;
2 – Corner supported boundary conditions – opposite corner points;
3 – Edge supported boundary conditions –Neighbour corner points;
4 – Corner supported boundary conditions – Neighbour corner points.

The errors plots in proportion values deviation obtained for opposite and neighbour corner points under edge supported boundary conditions (Plots 2 and 1, respectively) shows considerably higher increases than the corresponding ones obtained for corner supported boundary conditions (Plots 4 and 3). The smallest mean error shown on Plot 4 was obtained based on neighbour corner points under corner supported boundary conditions.

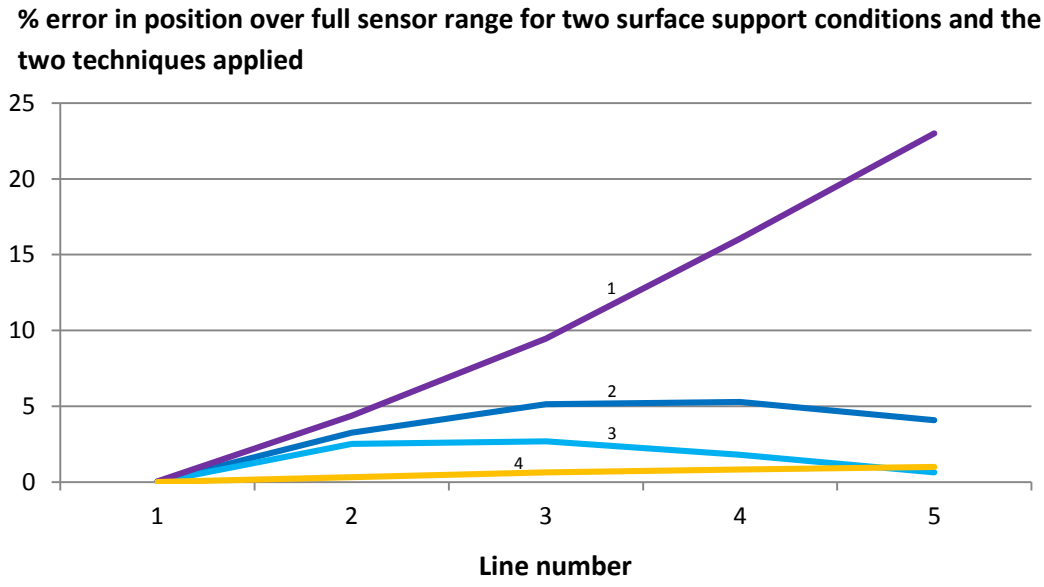

Figure 3.17 – Graphical illustration of the obtained mean percentage errors in proportion values deviation indicating the accuracy of the simulated surfaces according table 3.6.

3.5.3 Discussion

In this experiment the FEM plate model was used to test the accuracy of the distributive surface in detecting the position of static point loads. Testing the performance of the distributive surface under edge and corner supported boundary conditions caused different deformation responses of

surfaces. Hence different distributive surface accuracies were obtained for the two types of boundary conditions. Derived average errors in the range of 0.6% and 11% for corner and edge supported surfaces suggested that the type of surface supports has a significant effect on the overall performance of DTS devices. Results from this investigation implies that corner supported distributive surfaces can provided better accuracy in comparison with edge supported in detecting the positions of a single point loads. An explanation for this is that edge supported surfaces restrict the ability of the elastic surfaces to deform in the areas of support. This affects the uniform deformation behaviour of surfaces, which in the current application of position detection, leads to undesired increase of variation in measured proportion values.

3.6 Conclusion

In this chapter two mathematical models of elastic plates based on finite element and finite difference methods were developed and verified. It was demonstrated that mathematical models can be successfully used in investigating the design of DTS devices by providing important information relevant to the sensitivity and accuracy of the devices.

In the next chapter, the knowledge gained over the developed FEM plate model will be applied in designing the first for this project experimental setup as DTS floor platform.

The development of FDM plate model by mathematical terms and its software implementation in Matlab have provided advanced understanding the behaviour of elastic plates. In Chapters 4 and 5 the FDM plate model will be used to simulate the performance of complete DTS systems in applications for detecting the locus of centre of pressure and performing functional reaching task.

CHAPTER 4

DTS approach applied to detect the locus of centre of pressure

4.1 Introduction and aim

To date, the Distributive Tactile Sensing approach has been used for discriminating types or categories of human motion. However the DTS approach is also suitable for discriminating other types of information associated with estimation of motion related parameters. In this chapter the aim is to demonstrate the DTS approach in determining important parameters associated with force measurement used in the assessment of postural steadiness in biomechanics.

An experimental device in the form of a DTS floor platform was constructed. Using the principles of position detection described in Chapter 3, a linear approach was developed and applied to discriminate the character of the widely used biomechanics force parameter 'Centre of Pressure'. This enables contrast between the performance of the DTS system with that of a standard force platform (FP). Currently such force platforms are the gold standard in the clinical assessment of postural steadiness.

Force platforms are tactile sensors which measure force generated by a person who is in contact with the platform and present it in the form of a single resultant ground reaction force. They consist of a rigid rectangular

surface, usually of dimensions 400 x 600mm. The more recent force platforms can accurately determine the three-dimensional components of the applied force and its moments, as well as the force point of application known as centre of pressure (COP). As these devices provide very accurate measurements they have been used in clinical and biomechanical research during the years. Most modern force platforms can detect the COP locus with a maximal error of 2mm ("Kistler FP - Type 92600AA, product specification", 2015.). A major advantage of force platforms is that they are suited for identifying new postural disorders by analysing collected data post-examination. Alongside the positives, force platforms have some significant practical limitations. One of them is that force platforms require trained specialist to perform post-examination data processing which can be relatively time consuming and costly. Force platforms are considerably expensive which make their usage not feasible for many people who need examination. In the recent years, the disadvantages of such devices has drawn attention towards more practical and cost-efficient engineering solutions to the conventional force platforms.

In this chapter the DTS approach has been applied to a novel tactile sensing device which overcomes some of the complications with the traditional force platforms. The simplicity and implementation flexibility of the DTS approach has led to developing a cost-efficient portable device which can be applied readily in clinical and home environments. Through the process of discrimination the DTS approach has been applied to accurately estimate important force parameters, traditionally obtained with force platform devices. The chapter describes the development of application for detecting the locus of centre of pressure. Preliminary results are presented indicating suitability of the DTS technology in the assessment of postural steadiness.

4.2 Construction and operation of DTS devices

The fundamental mechanical construction of the DTS devices is illustrated in Figure 4.1. The DTS devices consist of a rigid base plate on which a flexible surface is simply supported. A small number of coupled sensing elements (typically 3 to 5) with outputs related to deflections are applied. These are coupled through the deflection of the surface in responses to applied loads. In this example proximity sensors are mounted underneath the surface in selected points in which deformations are typically more pronounced.

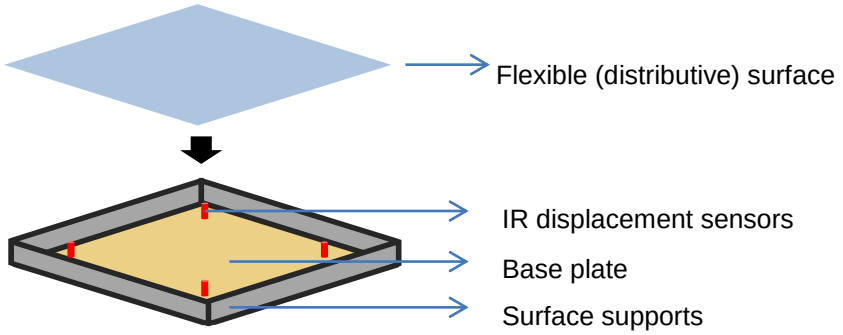

Figure 4.1 – Mechanical construction of DTS devices.

Figure 4.2 illustrates the configuration and software functions that are used to interpret the collected data and to output information directly in real-time. Therefore the operational principle of DTS devices consists of the following flow of processes:

- Interaction of the top distributive surface with contact forces generated by the moving human body.
- Surface deformation activates of all sensing elements.
- Time series sensing data is recorded in the form of transients.
- Raw sensing data is conditioned and analysed in real-time.

- Appropriate interpretation techniques are applied to the conditioned data, extracting specific sensing features.
- Surface contact information is derived associating the extracted features with different types of contact or specific parameters.
- A state of motion condition or a specific parameter (i.e. COP) is estimated based on the derived information.

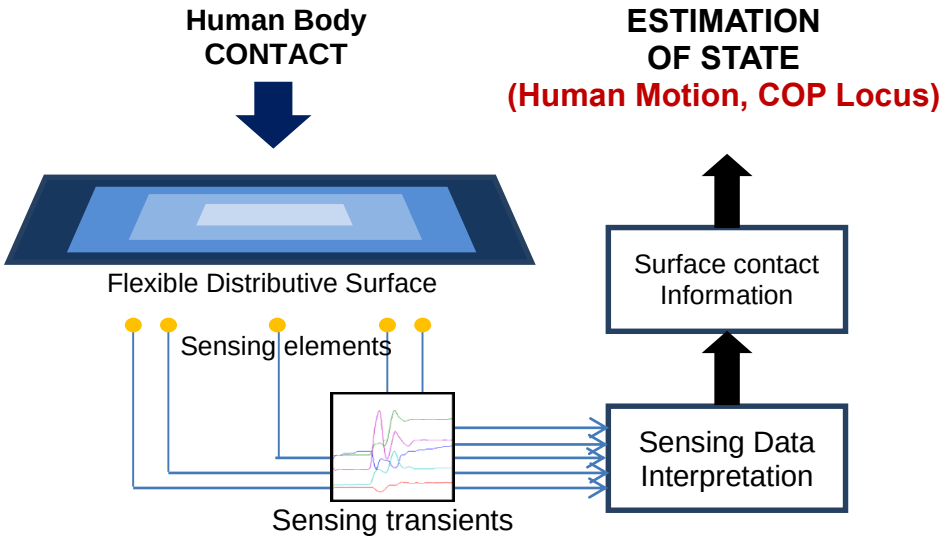

Figure 4.2 – General configuration and operational principle of DTS devices.

In this chapter the DTS approach was applied to an experimental device as a DTS floor platform for standing applications. The design of the device was defined based on the approach of Chapter 3, analysed as an FEM model of elastic plate. The same model was used to develop a methodology for estimating the locus of COP subject to a static point load applied vertically over a 2-dimensional surface of square geometry. The developed methodology was applied to the DTS floor platform. Accuracy of the developed application for detecting and tracking the COP locus was verified by comparing output generated from simulated and real systems of x and y COP coordinates with that of the actual COP point of application.

Then, a comparison between DTS floor platform and commercialised force platform (Kistler, USA) was accomplished by recording COP data simultaneously from both devices. For that purpose both systems were synchronised by placing the DTS device on top of the force platform. Data was recorded from a group of healthy volunteers standing on top of both devices with one or two feet representing a progressively more challenging situation for maintaining balance, respectively. The average deviation in the COP of 0.4mm between both devices showed the DTS approach can provide an alternative and accurate solution for determining the locus of COP to the conventional force platforms. This reinforces the possibility that the DTS approach can be used successfully to determine biomechanical parameters detectable from force measurement.

4.3 Design of DTS floor platform

The first experimental setup developed in this work as DTS floor platform is shown in Figure 4.3. The DTS floor platform consists of steel contacting surface of size 430 x 430mm and thickness of 3mm. The plate dimension and thickness are chosen to suit variable sizes of human feet and an average human weight of 70kgf (686N).

A B

Figure 4.3 – Distributive Tactile Sensing (DTS) Floor platform for standing applications: A – Complete device; B – Inside view of the device with electronics mounted on a wooden base.

The sensors, data acquisition hardware, sensors electronic board, and cabling were installed on a wooden base. Four steel bars (height – 40mm, width – 40mm) were attached to the wooden base around the periphery and provided a stable approximation towards a single support for the distributive surface. Four removable M6 female screws of height 4.8mm were provided in the corners on top of the steel bars to optionally switch between edge and corner supported distributive surfaces. Four wooden bars with round edges were attached to the sides of the device to maintain the top distributive surface fixed in place and prevent human body contact with sharp edges and corners. Corners protectors were used to prevent lifting up of the top surface when the device is in use. Connectivity of the DTS floor platform with a data processing and user interface system (laptop or PC) was accomplished by single USB connection. The connection provides power to the sensing elements.

4.3.1 Sensing system

The Distributive Tactile Sensing approach was implemented using IR displacement sensing elements as these provide stable voltage measurements with high analogue resolution, and have successfully been deployed in previous DTS projects. A small number of coupled sensing elements were positioned at strategic points to continually capture the coupled transient response of surface deformation. For the application described in this chapter, four sensing elements were placed at equivalent positions near the corners of the distributive surface (150mm diagonally from the corners).

The type of sensor selected for this project is based on IR displacement measurement as a proximity sensor. The working principle of this sensor is illustrated in Figure 4.4 and is described in the following steps:

1. IR light is generated and emitted from the sensors emitting diode.

2. The emitted light is reflected in an IR reflective surface and redirected back to the sensor.
3. The IR light is received back from the sensors IR phototransistor.

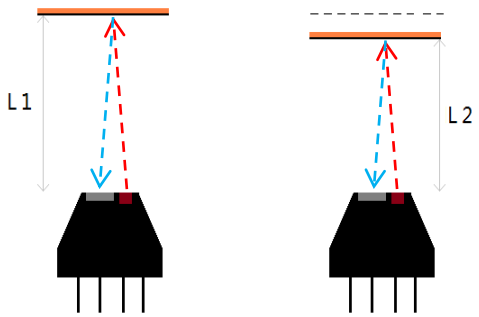

Figure 4.4 – Work principle of IR displacement sensor – "HOA 1405-2".

A reflection angle (defined by the emitted and reflected IR light beams), corresponding to the distance between the sensor and reflective surface, defines the intensity of IR light that reflected back from the sensor. This can be calibrated to measure distance. For the DTS floor platform, the sensing element used is "HOA 1405-2" (Honeywell, USA) proximity type. The sensor provides non-linear voltage measurement in a distance range of 10mm with an offset of 7mm, and utilises a wavelength of 8.9µm. An electronic board was implemented to connect all sensing elements with a data acquisition device, providing power for the elements and data transfer to a computer. Connection for each sensing element was accomplished via the electronic circuit of Figure 4.5. In the diagram, two resistors (R1 and R2) are used to provide normalised current to the sensor emitting diode (D) and phototransistor (Q), respectively.

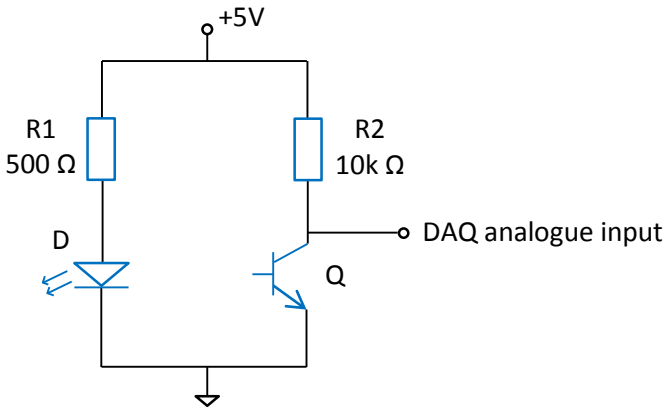

Figure 4.5 – Electronic diagram used to power supply and get readings from sensing elements via DAQ hardware.

4.3.2 Data Acquisition

Data acquisition (DAQ) hardware was used to convert the analogue voltage output of the sensing system into digital values utilised by data interpretation software on a computer. The DAQ hardware USB-6008 (National Instruments, USA) was integrated into the DTS sensing unit. The DAQ converted 11 bits in the range of ±5V with a sampling rate of 100Hz to 10kHz on 8 channels.

4.4 Methodology for detecting the locus of centre of pressure over 2-dimensional square surface

The methodology for detecting the locus of centre of pressure presented in this section was developed based on the technique for evaluating the accuracy of the distributive surface described in Chapter 3. In Section 3.4.1, it was demonstrated that an applied point load over a 2-dimensional elastic plate corresponds to a particular value, calculated as a proportion between surface deflections at two corner points. This concept has been

illustrated in Figure 4.6A where a point load F1 has been associated with a proportional value between deflection at points $w1$ and $w3$.

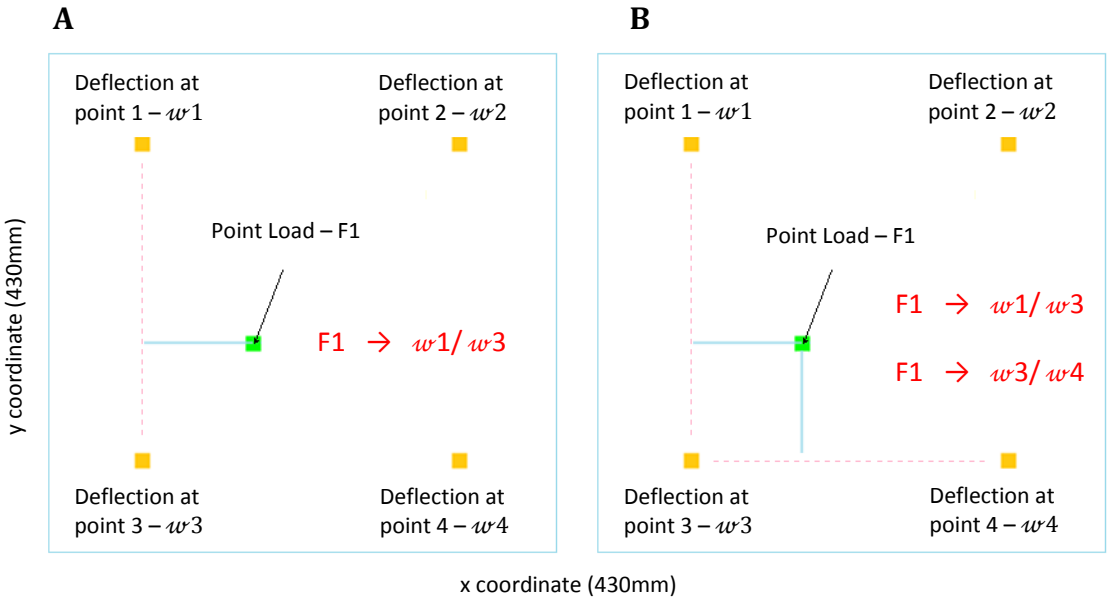

Figure 4.6 – Illustrations demonstrating the principle of detecting the locus of COP over two dimensional square surface: A – detecting one of the two coordinates of an applied point load by using proportion values $w1/w3$; B – detecting two of the COP locus coordinates by using proportion values $w1/w3$ and $w3/w4$.

The same principle can be applied to derive a second proportionality between deflection points $w3$ and $w4$ as shown in Figure 4.6B. Therefore each point load applied over the surface has two specific proportion values which can be associated with the 2-dimensional coordinates of the applied point load.

The methodology for detecting the locus of centre of pressure can be implemented using different combinations of deflection points. For example the x coordinate of the COP locus can be obtained by either w1/w2, or w3/w4 (w1/w3, or w2/w4 for the y coordinate) proportion values. This means that the COP locus can be obtained by using selection of

only three deflection points (i.e. w1, w3 and w4). Using only three deflection points for the considered sensor locations, however, would lead to achieving high accuracies only within half of the surface area (defined by the three deflection points). This is due to the increasing deviation between proportion values of receding COP locus.

In this thesis the locus of centre of pressure has been obtained by using four deflection points (w1, w2, w3 and w4 illustrated in Figure 4.6). The x and y coordinates of the COP locus, have been derived by averaging the following pairs of deflection points: w1-w3 and w2-w4 for the x coordinate, and w1-w2 and w3-w4 for the y coordinate. This has led to simplified and relatively generous interpretation of the COP methodology, aiming to unify the relations between proportion values of COP locus applied across the surface.

Due to non-linearity of elastic surface deformations, a linearization has been applied to correlate the considered in this application proportion values with the corresponding distances along x and y directions. The linearization was subject to five equally distributed points along the two coordinates. It was accomplished by a system of five fourth-order polynomial equations of type:

$$f(x_n) = a_0 + a_1x_n + a_2x_n^2 + a_3x_n^3 + a_4x_n^4 \quad (4.1)$$

where $f(x_n)$ is the real coordinate of the centre of pressure based on five equally distributed points n (n=1:5) across the x (or y) dimension of the surface; x_n is the obtained (based on measurements from the sensors) proportion value at point n.

This type of linearization provided the opportunity to calibrate the DTS system according to areas of the distributive surface where an optimal accuracy is desired. This was achieved by selecting the desired x and y axes across the surface, which were equally separated by five points where the linearization has been applied. In this work linearization was

accomplished according to the midline of the x and y axes, achieving optimal accuracy in the centre of the distributive surface.

The principle for detecting the locus of centre of pressure is based on the assumption that applying multiple loads over the distributive surface would cause deformation corresponding to a resultant over the surface COP locus. For example as shown in Figure 4.7, two (or more) equivalent point loads applied at opposite and equal from the middle of the distributive surface locations will cause surface deflection corresponding to proportions with very similar values as that of a single point load applied in the middle of the surface. Therefore the deformation of elastic plates corresponds to a resultant of multiple loads point of application relevant to the COP locus.

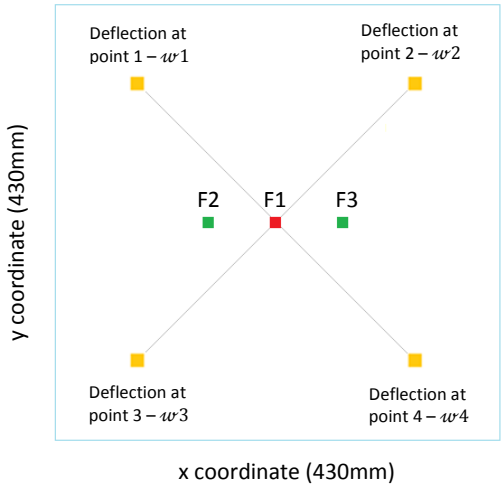

$$(w1/\ w3)_{F1} = (w1/\ w3)_{F2,F3}$$

$$(w3/\ w4)_{F1} = (w3/\ w4)_{F2,F3}$$

Figure 4.7 – Illustration comparing the relevant for the COP application proportion values subject to single point load (F1) applied at the middle of the distributive surface and multiple point loads (F2 and F3) with equivalent magnitudes applied at equal distances from the middle of the surface.

The above described methodology for detecting the locus of COP was applied to the FDM plate model described in Chapter 3 and the

experimental DTS floor platform developed in this chapter. Implementation of the application was accomplished by developing Matlab user interfaces for the simulated and real systems to detect the locus of centre of pressure automatically and in real time. The application was accomplished based on corner supported boundary conditions, as in Chapter 3 these were found to provide better accuracy for the relevant application in comparison with edge supported boundary conditions.

4.5 Verifying the methodology for detecting the locus of centre of pressure

The ability of the DTS floor platform to detect the locus of COP has been verified in an experiment where x and y COP coordinates data obtained from the simulated and physical systems were compared with that of the actual COP point of application. Comparison was accomplished based on calculating the deviation of COP locus in x and y directions.

In contrast to the simulated system where the deflection proportions were calculated based on the plate models surface displacement, in the real DTS floor platform the deflection proportions were subject to the voltage measurements provided by the sensing elements. Prior to applying the methodology for detecting the locus of COP, sensing data was filtered to eliminate small signal disturbances. A window filtration method which uses time history of the acquired data was applied. Selected method works by averaging a fixed number (referred as window size) of consequent samples, throughout the length of the time series. A shift value defines the shift of the window at each step of the filtration process. In this application filtration was implemented with window size of 3 and shift value of 1. In real time applications the presence of a time lag relevant to the window size (the larger the window size, the larger the time lag) was considered.

Due to the symmetrical shape of the distributive surface, verification of COP locus was accomplished at selected area as shown in Figure 4.8. The figure illustrates the 2-dimensional square distributive surface of the DTS floor platform, scaled in x and y directions according the positions of sensing elements. COP measurements were obtained at fifteen equally distributed positions (P_1 – P_{15}). As discussed in Section 3.4.3, the magnitude of the applied contact forces can be negligible in the case of this application. In this experiment a point load with magnitude of 50kgf (490N) was used. Estimated COP coordinates of the simulation and real systems were used to calculate corresponding deviations from the real COP point of application. The measurements from the physical distributive surface were repeated five times and the average COP locus for each point is presented in the results section.

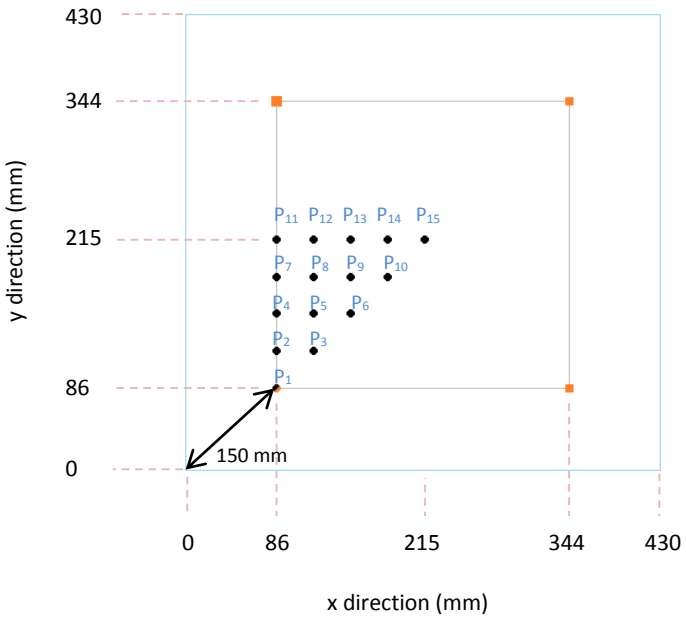

Figure 4.8 – Positions (P_1 – P_{15}) of the applied point loads used in the verification of the methodology for detecting the locus of centre of pressure.

4.5.1 Results

Results of the measured COP locations, subject to simulated and real DTS device, are presented in Table 4.1. The results are presented in the form of deviation of the derived COP locus from the actual point of application for each point load (P_1 – P_{15}). To contrast the overall accuracy between simulated and real DTS systems, the root mean square error (RMSE) calculated for the x and y coordinates is presented in the results.

	Transverse load application point over distributive surface (430x430mm) **- x, y coordinates**		COP locus - simulated system (**DEVIATION** from the real COP application point)			COP locus – real DTS device (**DEVIATION** from the real COP application point)		
	x (mm)	y (mm)	x (mm)	y (mm)	total (mm)	x (mm)	y (mm)	total (mm)
Point1	86	86	2.7	-1.53	3.15	2.03	1.78	2.7
Point2	86	118.25	0.03	2.37	2.37	0.25	-6.86	6.86
Point3	118.25	118.25	0.5	0.57	0.75	3.81	-3.81	5.39
Point4	86	150.5	0.75	2.56	2.66	-0.51	1.02	1.14
Point5	118.25	150.5	0.27	1.62	1.64	2.29	2.54	3.42
Point6	150.5	150.5	0.57	1.23	1.36	1.52	-1.52	2.16
Point7	86	182.75	2.14	0.06	2.15	2.54	2.54	3.6
Point8	118.25	182.75	0.61	0.03	0.61	1.27	3.05	3.3
Point9	150.5	182.75	0.71	-0.22	0.75	-0.51	0.25	0.57
Point10	182.75	182.75	0.76	-0.2	0.78	1.27	1.52	1.9
Point11	86	215	3.43	-2.79	4.42	1.27	-0.76	1.41
Point12	118.25	215	0.79	-1.83	2	0.51	1.02	1.14
Point13	150.5	215	0.81	-1.8	2	1.52	0.51	1.61
Point14	182.75	215	0.8	-1.8	2	0.76	0	0.76
Point15	215	215	0.88	-1.8	2	0.51	0.51	0.72
			RMSE			**RMSE**		
			1.39	**1.63**	**2.15**	**1.66**	**2.51**	**3**

Table 4.1 – Derived COP locus for the simulated and real DTS devices subject to application of point loads.

Figure 4.9 illustrates the derived locus of the COP in simulated and real DTS systems for a 2-dimensional distributive surface, alongside the real COP points of application. The illustration reflects the area of the distributive surface in which the measurements were taken. The figure is used to visually illustrate the obtained accuracy of the simulated and real DTS systems in detecting the COP locus. As it can be seen, the accuracy of the simulated and real systems has shown to be higher in the middle area of the surface compared with the side areas of the distributive surface. This confirms the accomplished linearization according to the middle x and y axes led to higher accuracy of the distributive surface in the middle of the surface in comparison with the further from the middle areas.

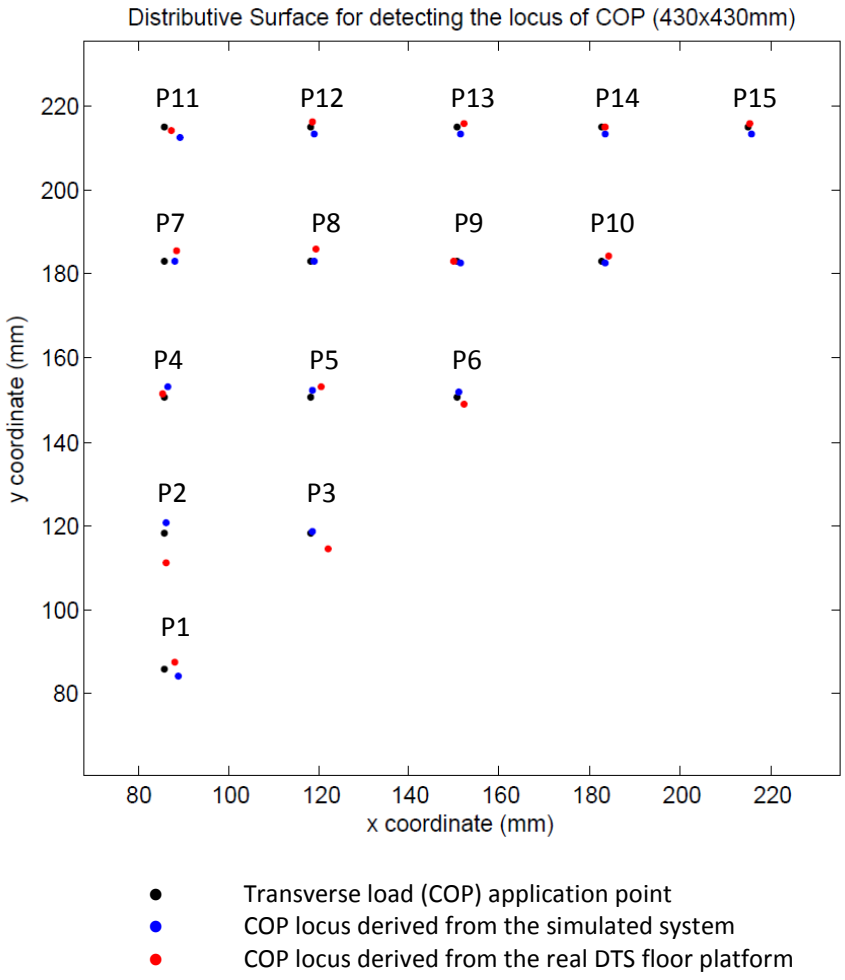

Figure 4.9 – Derived COP locus of simulated and physical DTS systems subject to applied over the surface single point load.

4.6 DTS floor platform vs. "Kistler" force platform in detecting and tracking the locus of centre of pressure

In this experiment the ability of the DTS floor platform to detect and track the COP locus subject to irregular forces exerted by the human body was compared with that of a "Kistler" force platform in a real-time application test. For that purpose, the DTS floor platform was installed on top of a floor mounted force platform, as shown in Figure 4.10. Due to the larger size of the DTS device in one of the dimensions, an adaptor plate was used to achieve compatibility for simultaneous data recording. The coordinate systems of both devices were aligned such that results are contrasted more readily.

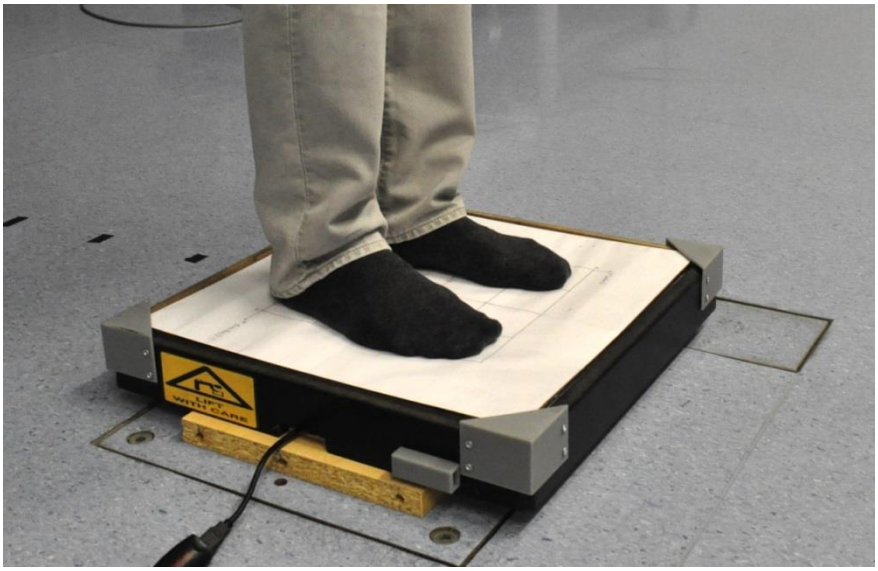

Figure 4.10 – DTS floor platform installed on top of a "Kistler" force platform.

To compare the outcome of both devices, COP data was recorded for a group of five healthy volunteers (V1 to V5) of various weights standing on top of the DTS and FP devices. Two 25 seconds trials were recorded for each volunteer while maintaining balance on one or two legs. The

volunteers were instructed to step in the middle area of the DTS floor platform so that measurements were obtained from the more accurate areas of the surface. The data recorded in the first 5 seconds was discarded to eliminate signal noises and fluctuations due to initial contact with the devices. Collecting data from both devices was synchronised using an analogue signal triggered from a laptop interfacing with the DTS floor platform. Data was recorded with a sampling rate of 100Hz. The performance of the DTS device was compared with that of the force platform by obtaining the average deviation of the COP locus between both systems.

4.6.1 Results

The average deviation of COP locus between DTS and FP systems was obtained by calculating the root mean square error (RMSE) for the recorded COP *x* and *y* coordinate time series. Table 4.2 presents the result of the calculated RMSE for the 5 volunteers tested while performing the balance test with one or two feet. Average from all trials RMSE of 1.05mm was obtained considering the data was recorded for a period of 20 seconds within relatively small area of the distributive surface (approximately 50mm^2). The majority of obtained RMSEs subject to performing balance equilibrium with two feet indicated smaller average deviation in comparison with that of performing balance equilibrium with one foot. An explanation for this is the fact that when a person maintains balance with one foot the locus of COP travels faster and within a larger area over the distributive surface in contrast with maintaining balance with two feet.

	RMSE (mm)									
	2 feet					**1 foot**				
Volunteer	V1	V2	V3	V4	V5	V1	V2	V3	V4	V5
COP-x	0.6	0.77	0.49	0.94	0.42	1.09	1.05	0.68	1	1.04
COP-y	0.48	0.61	0.4	0.95	0.74	1.6	2.8	1.66	1.14	2.5
	Average of all trials: $COP_{(x-y)}$ – 1.05									

Table 4.2 – Root Mean Square Error calculated for the five volunteers maintaining balance equilibrium with one and two feet.

In support of the results presented in Table 4.2, Figures 4.11 and 4.12 show plots of recorded COP x and y time series of selected trials subject to performing balance with one and two feet, respectively. The figures show the overlapping behaviour of x and y coordinates obtained with the DTS device compared with that of the FP system. Due to the different approaches applied by the DTS and force platform system to obtain COP data (based on flexible and rigid surfaces, respectively), some differences between the plotted time series of both systems can easily be noticed. For example in some trials like the one in Figure 4.11, the plots of the DTS time series showed an increased deviation from that of the force platform in the highest up and down peaks of the signals. An explanation for this is that when the COP locus changes its direction of travel reversibly and relatively quickly, the dynamic effect of DTS surfaces influences the obtained COP locus differently than the one of the rigid force platform.

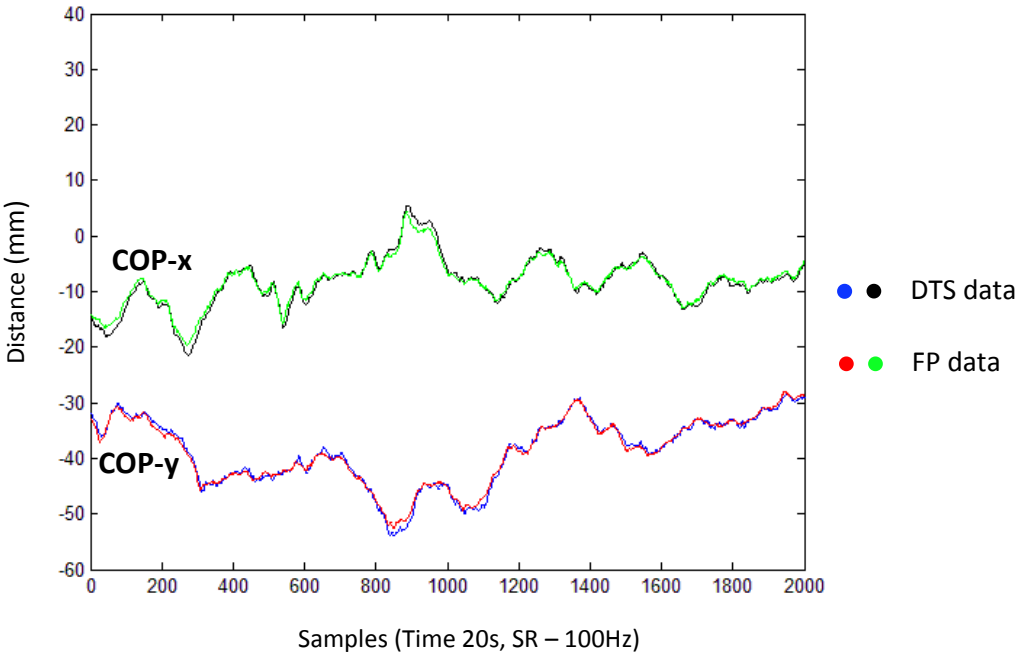

Figure 4.11 – Plot of COP x and y time series subject to maintaining balance with 2 feet (volunteer V3 according Table 4.2).

In contrast to Figure 4.11, Figure 4.12 shows COP time series obtained based on maintaining balance on one foot. In this example the behaviour of the x and y time series signals is relatively sharper due to the fact that when a person maintains balance with one foot, the body is more unstable. In order to keep the body's centres of mass and pressure within their limits, the body induces forces which are more variable compared with the case when the balance is maintained with two feet. This leads to increased COP velocities and areas of operation, which explains the different behaviour of the COP locus in the two balance conditions considered in this application. The above stated assumptions are also confirmed by obtained stabilograms (the 2-dimensional trajectory of COP locus over 2-dimensional surface) of COP locus shown in Figure 4.13.

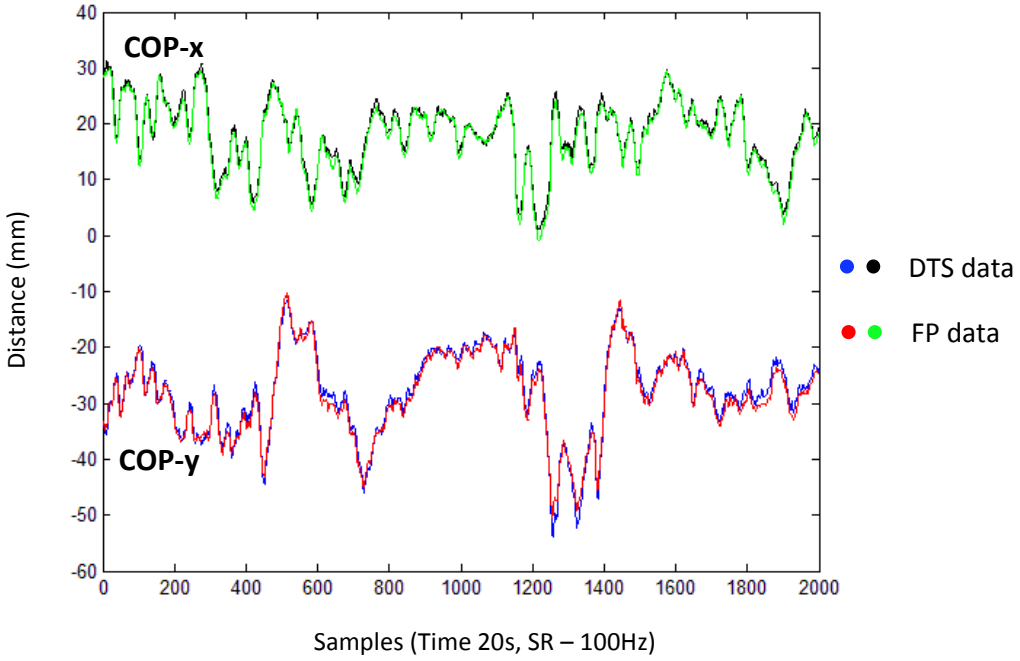

Figure 4.12 – Plot of COP x and y time series subject to maintaining balance equilibrium with 1 foot (volunteer V4 according Table 4.2).

The stabilograms of COP locus illustrated in Figure 4.13 are obtained from selected trials recorded in this experiment. The figure illustrates the detailed and matching shapes of COP locus obtained with DTS and FP systems, considering the stabilograms reflect a relatively small area of operation.

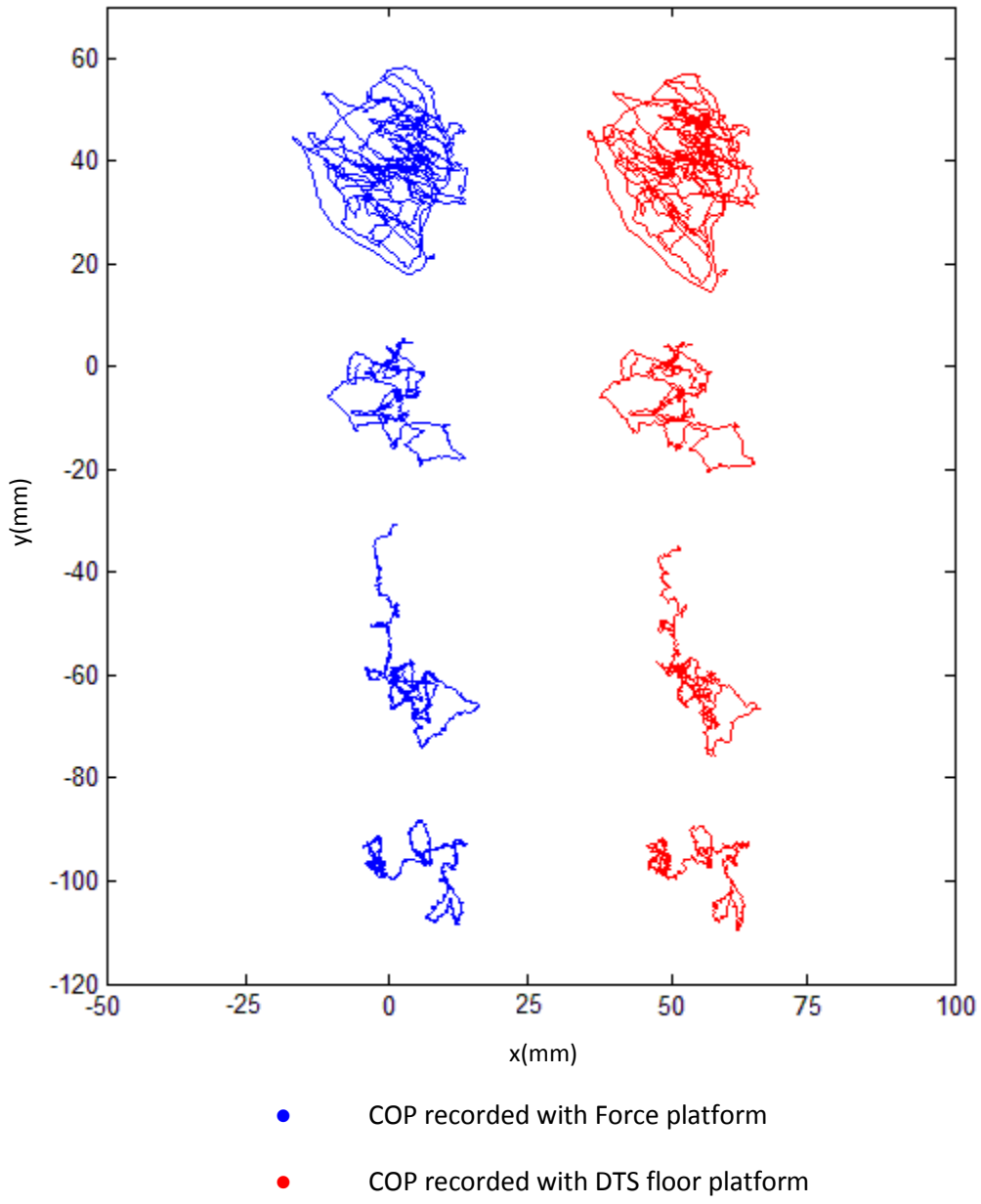

Figure 4.13 – Comparisons between COP stabilograms derived from DTS and FP devices for selected trials (from top to bottom: volunteer V4 (two feet); volunteer 3, 4 and 5 (one foot)).

4.7 Discussion

Results demonstrated that the COP locus can be derived with an average deviation of 2.15mm for the simulated and 3mm for the real DTS systems from the actual position of the applied COP locus. Simulation results have shown that the locus of COP can be derived more accurately in certain areas over the distributive surface compared with others due to the non-linear deformation characteristics of elastic plates. During simulation experiments, it was found that the middle horizontal and vertical cross-sectional lines over the 2 dimensional distributive surfaces are the most appropriate lines for calibrating the system along the x and y coordinates. An explanation for this is the fact that the behaviour of proportions of corner points based on loads applied at these two lines is less variable. Therefore in the central areas of the distributive surface associated with higher surface accuracy deviation of less than 1mm from the actual COP point of application was obtained, while in the less accurate areas around the edges of the surfaces deviation exceeded 4mm. These findings have been confirmed practically by testing with the DTS floor platform to detect and track the locus of COP in real time. In the conducted experiments with DTS and FP devices, the centre of pressure resulting from irregular and multiple loads (human feet) was derived with minor deviation from the one obtained with the force platform. Interestingly a study conducted by Dias et al. (Ache Dias et al., 2011) in evaluating a new stabilometric FP system implies that FP devices including commercial force platforms also tend to be more accurate in the middle areas of the FP surfaces in comparison with the edge areas.

Testing with the force platform which is a gold standard in the evaluation of postural steadiness was important in terms of highlighting some of the advantages of the DTS technology. The most noticeable ones are the high portability and robustness of the DTS floor platform which allowed the device to be easily moved from one laboratory to another during the days

of experiments, without facing any significant technical issues. The straight forward connectivity of the device with a portable laptop without the need for external power supply demonstrated ease of setting up and comfort during operating with the system. These factors are important for the successful applicability of the DTS technology in clinical and home settings.

4.8 Conclusion

This chapter presented an example of a simple linear approach of the Distributive Tactile Sensing applied to detect the locus of centre of pressure. The development of this application provided the opportunity to contrast the DTS technology with that of a gold standard force platform and highlight some of advantages of the DTS technology over other similar sensing systems. It was shown that DTS floor platform can determine the locus of COP with precision of 1.05mm from that of a gold standard force platform in testing postural steadiness applications. The positive outcome of this investigation suggests that the DTS technology provides real alternative to the expensive and complex force platform systems.

In contrast to the linear approach used in this chapter to identify force parameters, the DTS technology is also able to determine additional motion information by using the inherent non-linear dynamic behaviour of elastic plates in combination with other strategies to interpret the outputted sensing data. In the next chapter the ability of the DTS approach to interpret motion data is demonstrated by discrimination which is the prime interpretation method of this technology.

Chapter 5

DTS approach for discrimination of trunk movement in a reaching task

5.1 Introduction

The aim of this chapter is to extend the clinical applicability of the DTS technology to the area of stroke assessment. This requires development of a clinical application which can address current needs in this field. Reaching performance test which has been used intensively in the evaluation of arm-trunk motor dysfunction after stroke (Nowak, 2008). In this study, performance of functional reaching task during sitting was used to discriminate different levels of trunk bending. This was accomplished by developing a second experimental device in the form of a DTS chair. The nature of contact provoked by a sitting human in performing a reaching task to a target in front of him/her led to developing a device with pronounced sensitivity to the movement of the trunk in comparison with that of the arm. This allowed identifying the level of trunk movement which has shown to be correlated to the level of motor impairments in people with stroke (Cirstea & Levin, 2000).

Discrimination of a reaching task in the present study was accomplished by training two individual pattern recognition neural networks based on real and simulation data. Initially the application was developed based on a neural network which was trained with data collected from three randomly selected healthy volunteers. Then a second neural network was

trained with three sets of simulated data subjected to anthropometric characteristics of the three volunteers. The purpose of introducing the second alternative network was to investigate whether the use of mathematical modelling is suitable for generating reaching motion patterns according to a patient's anthropometric data to train neural networks. Such a model would provide more comprehensive understanding of the behaviour of the DTS system, as well as an opportunity for developing more advanced neural networks that can be applied to a wider range of people. Therefore a 2-link dynamic body model consisting of trunk and arm segments was developed and further integrated with the FDM plate model developed in Chapter 3. The complete model of DTS system was implemented in Matlab and investigated under quasi-static condition. Verification was accomplished by testing the ability of the trained with simulation data neural network to classify reaching motion patterns of the three volunteers. Results have indicated that the model is suitable for generating neural network training data by achieving classification accuracy of 99.3% based on 134 correct classifications out of 135 samples.

The positive outcome of this chapter has provided reasonable enthusiasm for testing the feasibility of the DTS technology in real clinical context. Hence, in Chapter 6 a cross-sectional study has been conducted with groups of healthy and stroke volunteers. This has led to clinically verifying the DTS technology by investigating its suitability to determine the arm-trunk contribution of stroke survivors in performing the reaching task.

5.2 Design and construction of DTS chair for sitting applications

The DTS chair developed in this work was constructed following the mechanical construction of DTS devices described in Chapter 4. A standard office chair, consisting of a rigid metal frame with cushioned bottom seat and back support, was converted to a DTS chair by integrating a sensing system to its seat. Figure 5.1 shows two images of the chair before and after modification where the seat of the chair is transformed to distributive flexible surface with sensing elements positioned beneath.

Figure 5.1 – Standard office chair converted to DTS chair by modifying the seat to distributive surface with distributed underneath sensing elements.

An acrylic distributive surface of dimensions 400 x 360 x 6mm was supported along four edges of the chair seat frame. A flat wooden plate was attached underneath the chair frame and used to hold on the sensing elements, electronic board and DAQ hardware of the system. A large number (sixteen) of the required sensing elements was used in the construction of the device to provide scope to select few for use without relocation during experiments. The sensing elements used were low-cost

IR displacement transducers "Vishay-CNY70" with the same operational principle as the "HOA 1405-2", used in the construction of DTS floor platform. Figure 5.2 illustrates the location of sensing elements under the seat. A greater number applied towards the back of the chair was in response to observations of greater deformation in this region and the possibility of raising sensitivity to the sensing scheme.

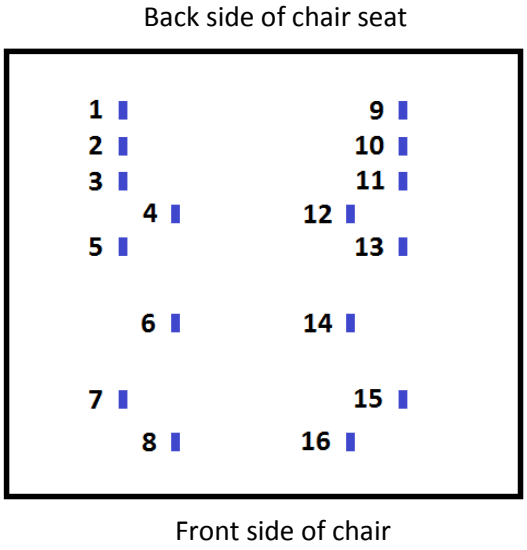

Figure 5.2 – Positions of sensing elements used in DTS chair.

Pieces of white reflective photo paper were attached on the bottom side of the acrylic plate, corresponding with sensing element locations to provide more sensitive outputs. Data acquisition hardware was installed on the back side of the chair through which the DTS chair was power supplied and connected with a control system via a single USB connection. Four adjustable chair lifters were provided to optionally lift up the chair and adjust its height in increments to 5mm. This adjustment enabled compatible seat height to anatomical variation between seated subjects. The aim was to achieve an angle at the knee of 90° during the test. During the conduction of experiments the seat of the DTS chair was covered with a water resistant mat to isolate the sensing system of the chair.

5.3 Discriminating different degrees of trunk bending in the reaching target by the use of neural networks

As described in Section 2.3.2 of the literature review, in healthy individuals reaching to a target placed in front of a person is a task which involves only movement of the arm segments when the target is placed at a distance within the arm reach, and movement of both the arm and trunk segments when the target is placed beyond the arm length. Accordingly, the application for discriminating different degrees of trunk bending was subject to reaching to a target placed at three distinct locations beyond the arm length. Due to the smaller mass of the arm segment compared with that of the trunk, as well as, its indirect contact with the sensing system, the DTS chair was considerably more sensitive to the movement of the trunk compared with that of the arm. In order to unify the performance of reaching task between volunteers, targets were placed at distinct locations defined based on one's arm length. Arm length was measured from the acromion to the third metacarpal head anatomical landmarks. As targets were hit with the tip of the fingers (healthy individuals), the distance from acromion to the finger tips was approximately 115% from the measured arm length. Figure 5.3 illustrates the three discriminative conditions corresponding to reaching to a target placed at distances equal to: 120% of the measured arm length involving minor trunk contribution (Figure 5.3A); 150% of the arm length involving moderate trunk contribution (Figure 5.3B); the maximum reach of the participant involving maximum contribution from the trunk (Figure 5.3C). Maximum reach was defined according to a distance at which each participant could reach the target comfortably without feeling pain and without lifting up the body from the chair.

A **B** **C**

Figure 5.3 – Reaching task conditions involving maximum arm contribution and different contributions from the trunk: A – minor trunk contribution (120% reach); B – moderate trunk contribution (150% reach); maximum trunk contribution ('max. reach').

To develop this application, sensing data was recorded from three healthy volunteers. Patterns corresponding to the three reaching conditions of Figure 5.3 were defined based on features extracted from a sensing transient obtained by interpreting the recorded data. Discrimination was accomplished by training a neural network to recognise the predefined patterns. Matlab code was written to implement the above stated procedures and accomplish an automated discrimination solution.

5.3.1 Volunteers

Participants in this experiment were three volunteers with various anthropometric characteristics. Each volunteer was asked to perform the reaching conditions 15 times, hence neural network training data was presented in 135 samples (45 for each person). The statistics for gender, age, weight, height, arm length, and maximum reach were recorded for each volunteer, shown in Table 5.1.

Volunteer	Gender	Age	Weight (kgf)	Height(cm)	Arm length (cm)	Max. reach (cm)
A	Male	26	68	175	67	124
B	Female	27	52	165	59	115
C	Male	33	81	182	71	130

Table 5.1 – Physical records of the volunteers.

5.3.2 Sensing transients

The most simple and approachable sensing strategy used in this application was based on a single sensing transient derived from averaging the real-time transients of four coupled sensing elements. In order to achieve unification between left and right handed subjects it was important to select sensing elements symmetrically to the left and right side of the chair. The selected sensing elements were 2, 5, 10 and 13, illustrated in Figure 5.2. The selection corresponded with region of larger deflection over the chair seat in an attempt to maximise potential sensitivity.

In order to unify the outputs of the real and further simulated DTS systems, recorded data in the form of voltage measurements was converted to distance via derived Voltage-Distance characteristics of sensing element “Vishay CNY70”, shown in Figure 5.4.

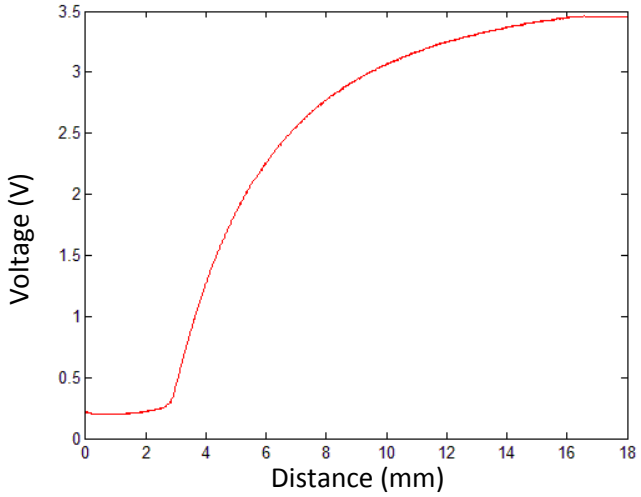

Figure 5.4 – Voltage-Distance characteristics of IR displacement sensor "Vishay CNY70" recorded by the use of Eppendorf Micromanipulator.

A typical coupled sensing transients of the three reaching conditions, i.e. 120% (Condition 1), 150% (Condition 2) and 'max. reach' (Condition 3), are shown in Figure 5.5. The transients represent the overall deflection of the distributive surface, induced by bending trunk during moving forward and backward in an attempt to execute the reaching task and to establish its initial position after completion of the task, respectively. The bigger the trunk bending (flexion), the more pronounced surface deformations, and hence the bigger transient amplitudes. The maximum amplitude of the transients corresponds to the moment at which the target is hit. At this moment the trunk is bent forward to its final position and it is ready to initiate its backward movement in order to bring the body back to its initial position. As reaching to a target placed at 120% of the arm length is associated with minor trunk contribution, the sensing transient of the first reaching condition has a considerably more flat characteristic compared with the transients from the other two conditions. Importantly, this also indicates that the DTS chair lacks sensitivity to the hand movement. Sensing transients of the second and third reaching conditions have shown

specific a down-drift characteristic which has been associated with a "reach initiation stage (RIS)" common to all reaches involving trunk movement. It was found that peak-to-peak amplitude measurement is associated with the level of trunk bending, which has been used as a key indicator for discriminating between the three reaching conditions. Discrimination in this application was accomplished by extracting sensing features which were used to develop discriminative pattern vectors.

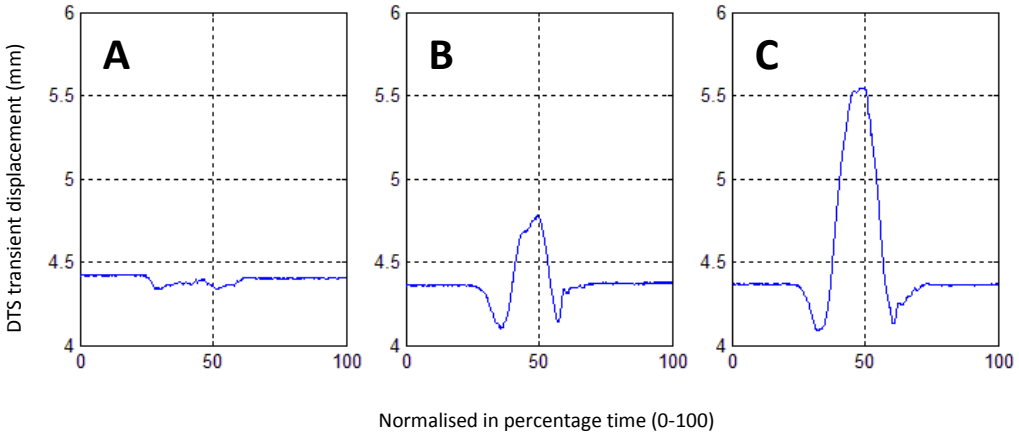

Figure 5.5 – Sensing transient obtained in reaching target task for targets placed at distances corresponding to: A – 120% of the arm length; B – 150% of the arm length; C – maximum reach.

5.3.3 Feature extraction

The development of discriminative patterns requires careful and adequate identification of features which can be associated with specific events and characteristics of the sensing transients. The successful identification of patterns requires selection of features that are repeatable for the type of motion and induced similarity between participants. In this application discriminative patterns were defined as five element vectors where each element represented a certain transient feature.

Figure 5.6 shows a relevant (to this application) sensing transient with selected points (P_1, P_2 and P_3) which are common to all reaching conditions involving trunk participation in performing the reaching task.

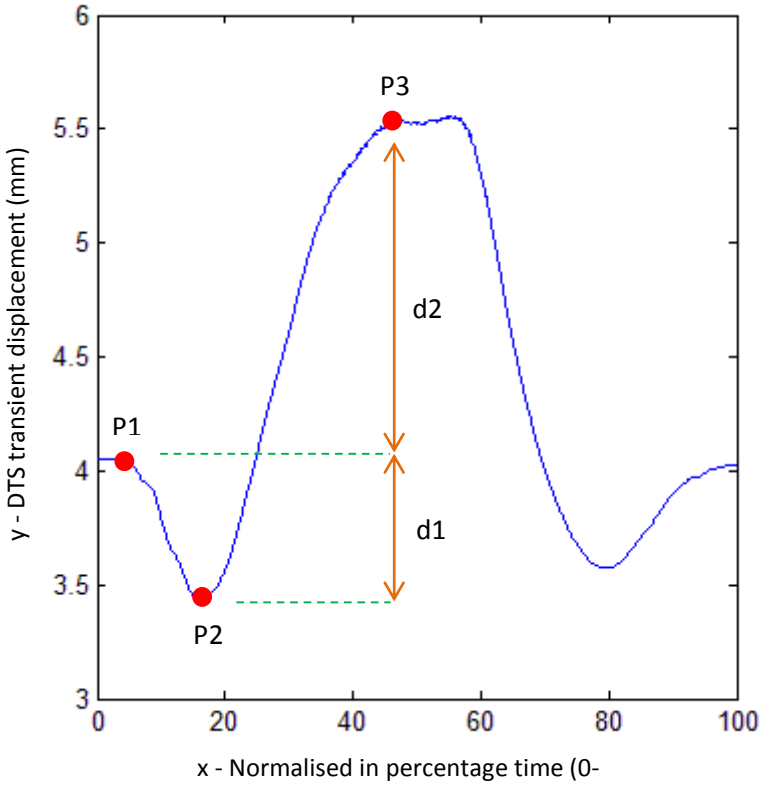

Figure 5.6 – Reaching task DTS transient of 'max. reach' condition with extracted points used in the identification of discriminative features.

These points were used in the identification of features and can be described as follows:

- P_1 – start of the reach initiation stage (RIS) associated with the first downward change of DTS transient from steady state;
- P_2 – end of RIS associated with the first local minima of the DTS transient;
- P_3 – end of forward trunk bending associated with the first local maxima of the DTS transient.

Features were defined based on amplitude differences between P_1, P_2, and P_3 and their absolute values. Therefore discriminative patterns were defined based on the following features:

- Feature 1: $d_1 = P_{1(y)} - P_{2(y)}$
- Feature 2: $d_2 = P_{3(y)} - P_{1(y)}$
- Feature 3: P_1
- Feature 4: P_2
- Feature 5: P_3

resulting in a five element vectors, $v = \{d_1, d_2, P_1, P_2, P_3\}$.

Automatic formation of pattern vectors was accomplished by a Matlab code written for this application. This was applied to each trial capture. Prior to feature extraction, the raw sensing data was filtered by applying the window method used in Chapter 4 in the verification of centre of pressure application (Section 4.5). The filtration was applied to smooth the DTS transients in order to reduce the risk of false feature detection. The appropriate selection of points by the Matlab code was visually verified prior the definition of patterns and neural network training.

5.3.4 Neural Networks for Pattern Recognition

In this work neural networks were used to discriminate between reaching task patterns. An artificial neural network is a mathematical model that tries to replicate the structure and functionalities of biological neural networks (Krenker et al., 2011). This type of modelling has shown to be very useful where input data has found to be highly non-linear (Grossi, 2011). In respect to flexible structures as elastic beams and plates, Tam (2010) has stated that small deflections can be considered as linear, however, when the deformation of such structure is greater, the deformation output becomes non-linear. Other common mathematical

models used in pattern recognition applications include genetic algorithms, fuzzy logic and rough sets (Jagielska et al., 1999). From the vast amount of literature in the field of artificial intelligence, it is arguably which is the best and most reliable technique, however, neural networks has been identified as a key tool in classification and pattern recognition applications in human motion analysis (Schollhorn, 2005). A comprehensive review into the use of neural networks is provided by Schollhorn, who reports on gait classification research. In previous work on the Distributive Tactile Sensing, the use of artificial neural networks has also been identified as a major discrimination method which has shown to be highly successful in variety of industrial and clinical applications (Tam et al., 2010; Elliot, 2007; Tongpadungrod, 2002; Stone et al., 1998).

Artificial neural networks consist of interconnected artificial neurons each of which represents a simple mathematical function (Krenker et al., 2011). Such a function is obtained based on three mathematical operations: multiplication, summation and activation. At the entrance of artificial neuron the inputs are weighted by multiplying every input value with individual weight. In the middle section of artificial neuron is sum function that sums all weighted inputs and bias. At the exit of artificial neuron the result of the sum function is passed through activation function (also called transfer function). This is illustrated in Figure 5.7 through a diagram of artificial neuron.

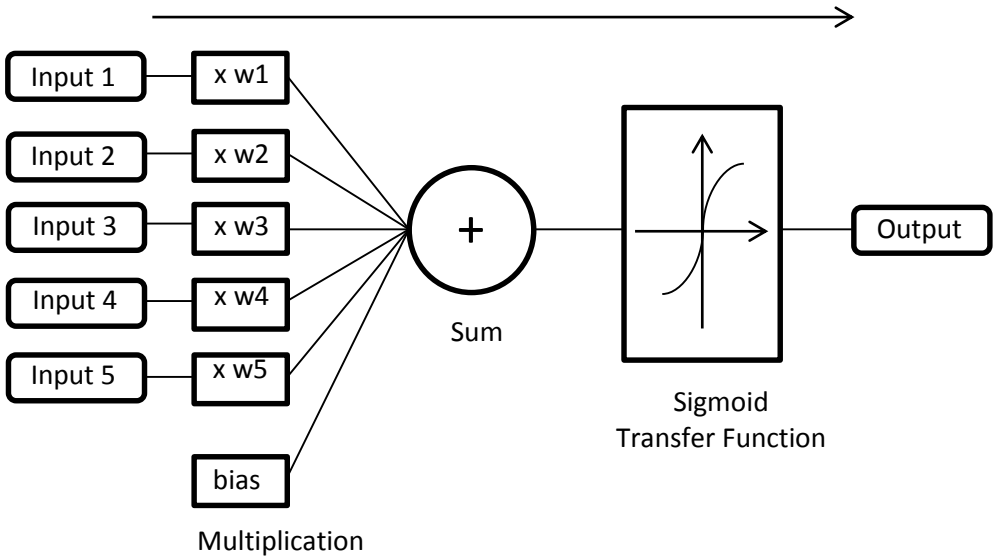

Figure 5.7 – Diagram of artificial neuron.

Different types of neural network architectures have been developed for applications such as pattern recognition, data classification and function fitting.

Similar to people, artificial neural networks learn by example. The learning process involved within neural networks for pattern recognition is based on associating a particular input or set of inputs with a predefined target output. This is accomplished through a specific training process in which weighted neurons are adjusted so that they fit with predefined by the user target outputs. Once the network is trained, it can be used to recognise new patterns of the same type. The power of neural networks comes when a pattern that has no output associated with it, is given as an input. In this case, the network gives the output that corresponds to a taught input pattern that is least different from the given pattern. Various algorithms exist that cause the neuron to adjust its weights. These are known as neural network training algorithms, from which one of the most common is the backward error propagation used in feed-forward and

feedback networks (Stergiou and Siganos, 1996). The back-propagation training is applied in conjunction with an optimization method such as gradient descent. The method calculates the gradient of a loss function with respect to all the weights in the network. Further, the gradient is fed to the optimization method which in turn uses it to update the weights, in an attempt to minimize the loss function moving from layer to layer in a direction opposite to the way activities propagate through the network.

Feed-forward networks allow signals to travel one way only, from input to output. Feedback networks tend to use loops which allow the signals to travel in both directions, from input to output and vice versa. Feedback networks are known as flexible networks which have constantly changing state until they reach an equilibrium point.

A common type of artificial neural networks consists of three layers of artificial neurons. In this network a layer of input neurons is connected to a layer of hidden neurons which is connected to a layer of output neurons. The activity of the input neurons represents the raw information that is fed into the network. The activity of each hidden neurons is determined by the activities of the input neurons and the weights on the connections between the input and hidden neurons. The behaviour of the output neurons depends on the activity of the hidden neurons and the weights between the hidden and the output neurons. Furthermore, the behaviour and performance of a neural network depends on both the weighted neurons and its transfer function, which typically represents a linear, threshold or sigmoid function. From these, the sigmoid function is probably the most common transfer function used to solve non-linear problems in patter recognition.

In this project already established models of neural networks were implemented using Matlab's Neural Network Toolbox. A neural network, NN1, trained with the established in previous section patterns of trunk

bending was defined with three-layer feed-forward architecture with sigmoid hidden and output neurons. The performance of NN1 neural network was tested with 6, 8, 10 and 12 neurons on the hidden layer, using scaled conjugate gradient back-propagation learning algorithm. As the number of neurons had a negligible effect for this application due to the relatively high distinctive discrimination patterns, training was accomplished with a number of 8 hidden neurons. The data used for training was presented in 135 sample vectors (15 samples x 3 conditions x 3 volunteers) from which 70% were assigned for training, 15% for validation, and 15% to test the performance of the generated network.

The performance of the network was evaluated using linear regression. Obtained results from the accomplished network training are presented in Figure 5.8. The illustrated regression plots indicate optimal fit between the network and predefined target outputs. A correlation coefficient of 1 is demonstrated by the 45 degree gradient lines in the four regression plots.

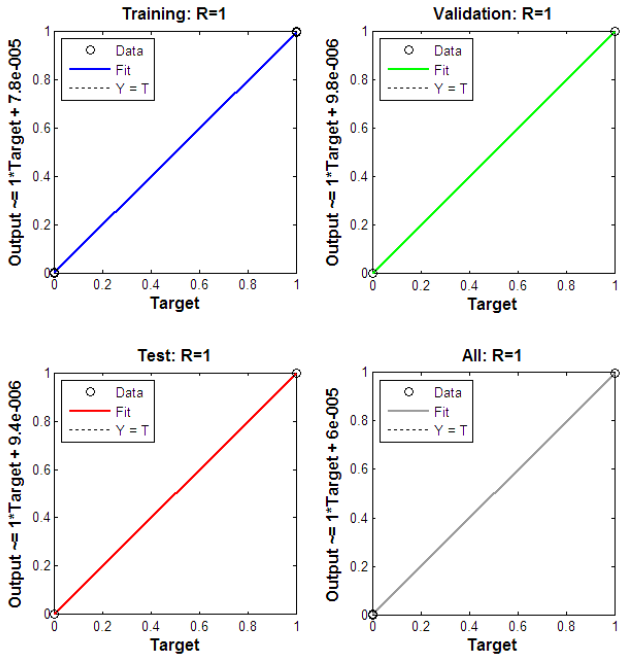

Figure 5.8 – Regression plots of the implemented neural network training.

5.4 Reaching task simulation applied to train Neural Networks

In this section mathematical model of body system consisting of trunk and arm segments has been developed based on a 2-link dynamic manipulator approach described by Lewis et al. (2004). The model was used in combination with the developed in Chapter 3 FDM plate model to simulate the performance of a complete DTS system in performing reaching target task. Hence, reaching task patterns based on simulated data corresponding to the three volunteers used in previous section were generated and used to train second for this chapter neural network. Verification was accomplished by testing the ability of the neural network to discriminate the real reaching task patterns of the three volunteers.

5.4.1 Mathematical model of 2-link dynamic manipulator moving in a vertical plane

In order to obtain the forces generated by the moving human body in performing reaching task, a mathematical model of 2-link dynamic manipulator illustrated in Figure 5.9 was developed based on Lagrange's equations of motion (also known as Euler-Lagrange).

The developed body model consisting of trunk and arm segments represents the dynamics of reaching task defined in a 2-dimensional vertical plane. As the purpose of the developed reaching task application is to investigate how much the trunk bends in a forward direction, but not its rotation and movements in the frontal body plane, the developed in this section body model would provide acceptable and satisfactory for the purposes of this application force outputs. The model was used to calculate dynamic forces acting on the hip joint for the period of executing reaching task. Calculations were subject to Inverse Dynamics (Inverse Kinematics) which means that mathematical equations have been solved

for the forces and moments acting on the joints subject to predefined motion of the two links. Matlab codes were written to implement the model and simulate the complete DTS system.

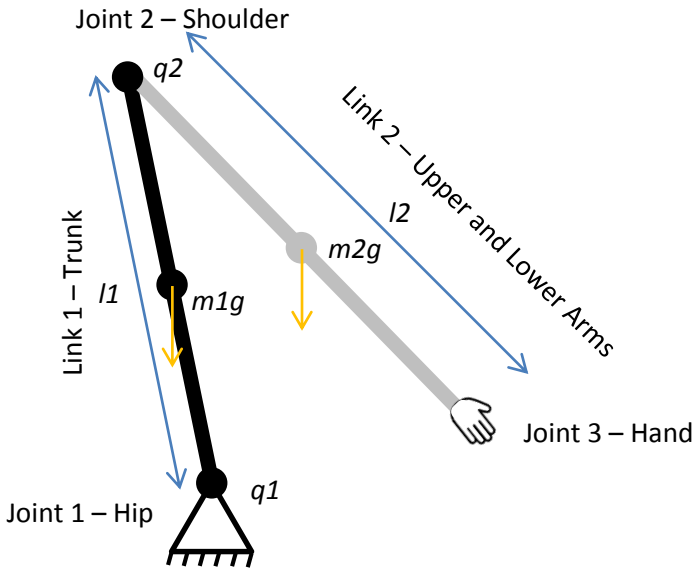

Figure 5.9 – Illustration of 2-link body model consisting of: trunk segment (link 1); upper and lower arm segment (link 2); hip joint (joint 1); shoulder joint (joint 2); and hand joint (joint 3).

In current practice, there are variety of algorithms for modelling dynamic manipulators developed based on two main approaches, the Lagrange and Newton-Euler principles. The model presented in this chapter was developed based on the Lagrange principle, an energy method. In contrast, the dynamic equations of the Newton-Euler approach are derived through a detailed analysis of forces and torques at each rigid body in the mechanism. For this work, the relatively simple Lagrange method is a suitable approach, chosen to derive dynamic equations of reactive forces representing a human subject moving while seated. Derivation of the Lagrangian is central to the approach derived from the entire kinetic and potential energies of the system in generalised coordinates.

The model has been developed assuming that the links representing the mechanism of the body in the motion of the reaching task are homogenous and have lengths l_1 (trunk segment) and l_2 (arm segment). The masses of the rigid links are m_1 and m_2 concentrated at the middle of the trunk and arm links, respectively. Gravitational acceleration is considered to be g = 9.8 m/s^2.

5.4.1.1 Mathematical description of the model

The Lagrange's equation of motion for a conservative dynamic system is given by (Marion, 1965):

$$\frac{d}{dt}\frac{\partial L}{\partial \dot{q}} - \frac{\partial L}{dq} = \tau \tag{5.1}$$

where: q is an n-vector of generalised coordinates q_i

τ is an n-vector of generalised forces τ_i

L is the Lagrangian representing the difference between the kinetic and potential energies:

$$L = K - P \tag{5.2}$$

The joint variable vector q, consisting of joint angles θ_j *(j = 1, 2)* represents the dynamic movement of the model links for period of time T.

$$q = [\theta_1 \quad \theta_2] \tag{5.3}$$

Respectively the generalised force vector is:

$$\tau = [\tau_1 \quad \tau_2] \tag{5.4}$$

The desired motion of the 2-link model is specified for a time interval $0 \le t \le T$. The generalised coordinates are established by:

$$\theta_j(t) = \theta_j(0) + \frac{\theta_j(T)-\theta_j(0)}{T}\left[t - \frac{T}{2\pi} sin\left(\frac{2\pi t}{T}\right)\right], \quad j = 1,2 \tag{5.5}$$

The kinetic and potential energies for the first link are obtained:

$$K_1 = \frac{1}{2} m_1 \frac{l_1^2}{4} \dot{\theta}_1^2 \tag{5.6}$$

$$P_1 = m_1\, g\, \frac{l_1}{2} sin\theta_1 \tag{5.7}$$

where m_1 and l_1 are the mass and length of link1, respectively.

The kinetic and potential energies for the second link are obtained:

$$K_2 = \frac{1}{2} m_2\, \vartheta_2^2 = \frac{1}{2} m_2 \frac{l_1^2}{4} \dot{\theta}_1^2 + \frac{1}{2} m_2 \frac{l_2^2}{4} \left(\dot{\theta}_1 + \dot{\theta}_2\right)^2 + m_2 \frac{l_1 l_2}{2} \left(\dot{\theta}_1^2 + \dot{\theta}_1 \dot{\theta}_2\right) cos\theta_2 \tag{5.8}$$

$$P_2 = m_2 g y_2 = m_2 g [\frac{l_1}{2} sin\theta_1 + \frac{l_2}{2} \sin(\theta_1 + \theta_2)] \tag{5.9}$$

where m_2, l_2 and ϑ_2 are the mass, length and velocity of link2.

$$\vartheta_2 = \sqrt{\dot{x}_2^2 + \dot{y}_2^2} \tag{5.10}$$

$$x_2 = \frac{l_1}{2} cos\, \theta_1 + \frac{l_2}{2} cos(\theta_1 + \theta_2) \tag{5.11}$$

$$y_2 = \frac{l_1}{2} sin\, \theta_1 + \frac{l_2}{2} sin(\theta_1 + \theta_2) \tag{5.12}$$

$$\dot{x}_2 = -\frac{l_1}{2} \dot{\theta}_1\, sin\theta_1 - \frac{l_2}{2} \left(\dot{\theta}_1 + \dot{\theta}_2\right) sin(\theta_1 + \theta_2) \tag{5.13}$$

$$\dot{y}_2 = \frac{l_1}{2} \dot{\theta}_1\, cos\, \theta_1 + \frac{l_2}{2} \left(\dot{\theta}_1 + \dot{\theta}_2\right) cos(\theta_1 + \theta_2) \tag{5.14}$$

$$\vartheta_2^2 = \dot{x}_2^2 + \dot{y}_2^2 = \frac{l_1^2}{4}\dot{\theta}_1^2 + \frac{l_2^2}{4}\left(\dot{\theta}_1 + \dot{\theta}_2\right)^2 + \frac{l_1 l_2}{2}\left(\dot{\theta}_1^2 + \dot{\theta}_1\dot{\theta}_2\right)cos\theta_2 \qquad (5.15)$$

The Lagrangian for the whole system is obtained as:

$$L = K - P = K_1 + K_2 - P_1 - P_2 =$$
$$= \frac{1}{2}(m_1 + m_2)\frac{l_1^2}{4}\theta_1^2 + \frac{1}{2}m_2\frac{l_2}{4}\left(\dot{\theta}_1 + \dot{\theta}_2\right) + m_2\frac{l_1 l_2}{2}\left(\dot{\theta}_1^2 + \dot{\theta}_1\dot{\theta}_2\right)cos\theta_2 -$$
$$- (m_1 + m_2)g\frac{l_1}{2}sin\theta_1 - m_2 g\frac{l_2}{2}\,sin(\theta_1 + \theta_2) \qquad (5.16)$$

The generalised force is derived from the Lagrangian in equation 5.1. For this mechanism we can take derivatives of the Lagrangian. Thus:

$$\frac{\partial L}{\partial \dot{\theta}_1} = (m_1 + m_2)\frac{l_1^2}{4}\dot{\theta}_1 + m_2\frac{l_2}{2}\left(\dot{\theta}_1 + \dot{\theta}_2\right) + m_2\frac{l_1 l_2}{2}\left(2\dot{\theta}_1 + \dot{\theta}_2\right)cos\theta_2 \qquad (5.17)$$

$$\frac{d}{dt}\frac{\partial L}{d\dot{\theta}_1} = (m_1 + m_2)\frac{l_1^2}{4}\ddot{\theta}_1 + m_2\frac{l_2^2}{4}\left(\ddot{\theta}_1 + \ddot{\theta}_2\right) + m_2\frac{l_1 l_2}{2}\left(2\ddot{\theta}_1 + \theta_2\right)cos\theta_2 -$$
$$-m_2\frac{l_1 l_2}{2}\left(2\dot{\theta}_1\dot{\theta}_2 + \dot{\theta}_2^2\right)sin\theta_2 \qquad (5.18)$$

$$\frac{\partial L}{\partial \theta_1} = -(m_1 + m_2)g\frac{l_1}{2}cos\theta_1 - m_2 g\frac{l_2}{2}cos(\theta_1 + \theta_2) \qquad (5.19)$$

$$\frac{\partial L}{\partial \dot{\theta}_2} = m_2\frac{l_2^2}{4}\left(\dot{\theta}_1 + \dot{\theta}_2\right) + m_2\frac{l_1 l_2}{2}\dot{\theta}_1\,cos\theta_2 \qquad (5.20)$$

$$\frac{d}{dt}\frac{\partial L}{d\dot{\theta}_2} = m_2\frac{l_2^2}{4}\left(\ddot{\theta}_1 + \ddot{\theta}_2\right) + m_2\frac{l_1 l_2}{2}\ddot{\theta}_1\,cos\theta_2 - m_2\frac{l_1 l_2}{2}\dot{\theta}_1\dot{\theta}_2\,sin\theta_2 \qquad (5.21)$$

$$\frac{\partial L}{\partial \theta_2} = -m_2\frac{l_1 l_2}{2}\left(\dot{\theta}_1^2 + \dot{\theta}_1\dot{\theta}_2\right)sin\theta_2 - m_2 g\frac{l_1 l_2}{2}cos(\theta_1 + \theta_2) \qquad (5.22)$$

After substituting the derived Lagrangian derivatives into the Lagrangian's equation of motion, the system torques at joint 1 and joint 2 are obtained:

$$\tau_1 = \left[(m_1 + m_2)\frac{l_1^2}{4} + m_2\frac{l_2^2}{4} + 2m_2\frac{l_1 l_2}{2}cos\theta_2\right]\ddot{\theta}_1 + \left[m_2\frac{l_2^2}{4} + m_2\frac{l_1 l_2}{2}cos\theta_2\right]\ddot{\theta}_2 -$$
$$- m_2\frac{l_1 l_2}{2}\left(2\dot{\theta}_1\dot{\theta}_2 + \dot{\theta}_2^2\right)sin\theta_2 + (m_1 + m_2)g\frac{l_1}{2}cos\theta_1 + m_2 g\frac{l}{2}cos(\theta_1 + \theta_2) \quad (5.23)$$

$$\tau_2 = \left[m_2\frac{l_2^2}{4} + m\frac{l_1 l_2}{2}cos\,\theta_2\right]\ddot{\theta}_1 + m_2\frac{l_2^2}{4}\ddot{\theta}_2 + m_2\frac{l_1 l_2}{2}\dot{\theta}_1^2\,sin\theta_2 +$$
$$+ m_2 g\frac{l_2}{2}\,cos(\theta_1 + \theta_2) \quad (5.24)$$

Having derived the torque τ_1 acting on the hip joint, a Matlab code was written to implement the calculations of the 2-link dynamic body model following the above derived mathematical equations. In the next section the model is tested based on the anthropometric characteristics of the three volunteers participated in this experiment.

5.4.2 Simulation Setup

Three different set-ups for simulation have been defined based on the anthropometric characteristics of the three volunteers used in the development of the reaching task application. Each simulation was subject to the three reaching task conditions relevant to this application. The initial positioning of the model links was approximated according to a normal sitting posture with narrow trunk and straight arm pointing the relevant knee as shown in the illustration of Figure 5.10. Motion of the arm segment (link2) for the three reaching conditions was defined by rotation of that segment around joint 2 from its initial position to its forward horizontal positioning. Motion of the trunk segment (link1) was defined according relevant to this application reaching distances based on volunteer's arm length. Therefore the simulated conditions corresponded to reaches involving maximum arm contribution and different levels contribution from the trunk relevant to the ones performed in the real situation. The masses and lengths of the simulated body segments were

calculated via standardised percentage measures (Plagenhoef et al., 1983) relevant to volunteer's weight and height.
Therefore the masses and lengths of the links have been defined as follows:

Mass of Link 1 (trunk segment) – 54% of the total body weight;
Mass of Link 2 (arm segment) – 5.4% of the total body weight;
Length of Link 1 (trunk segment) – 30% of the total body height;
Length of Link 2 (arm segment) – 36% of the total body height.

The dynamic motion simulated by the system has been executed for a period of 1.5 seconds including the return phase which brings the system to its initial position (0.75s for each, forward and backward phases). The setup of FDM plate model was defined according the characteristics of the relevant distributive surface of the DTS chair. Therefore the simulated model was defined as edge supported elastic plate made of acrylic material and with dimensions 400 x 360 x 6mm. The input forces used in the simulations have been defined as sum of two components: 1 – a static force with magnitude of 480N (70% of the total body weight corresponding to approximate measure of the resultant force measured at the seat of a chair while sitting); 2 – generated by the 2-link body model vertical dynamic force, which has been discretized with a sampling rate of 50Hz. The sequence of discretized dynamic force has been applied to the FDM plate model, subject to static uniformly distributed input force, to simulate the behaviour of the system in quasi-static condition. The deformation characteristics of the simulated elastic plate have been approximated with that of the real DTS device by choosing Young's modulus of 1GPa, which is approximated from the range of acrylic materials ("Materials Data Book," 2003; "The Engineering Toolbox," 2015).

5.4.3 Neural Network based verification

Simulated DTS transients obtained by the above described mathematical model were used to train second for this chapter neural network - NN2. Discriminative patterns were generated by applying the feature extraction methodology of NN1 explained in Section 5.3. The network architecture and training algorithm were defined with the same specifications as these used in NN1. Training data was presented in 45 sample vectors (5 samples x 3 conditions x 3 simulated participants) from which 70% were assigned for training, 15% for validation, and 15% to test the performance of the generated network. Similar to NN1 training results has indicated optimal correlation between generated from the network and predefined target outputs by achieving correlation coefficient of 1. The developed with simulation data neural network was tested in recognising the patterns obtained from the three volunteers.

5.4.4 Results

Figure 5.10 shows selected DTS transients of volunteer A (Table 5.1) obtained from the real and simulated DTS systems for the relevant in this application three discriminative conditions of trunk bending (120%, 150%, and 'max. reach' conditions). Due to the time variations in executing reaching task the time periods for all conditions were normalised in the scale of percentage from 0 to 100.

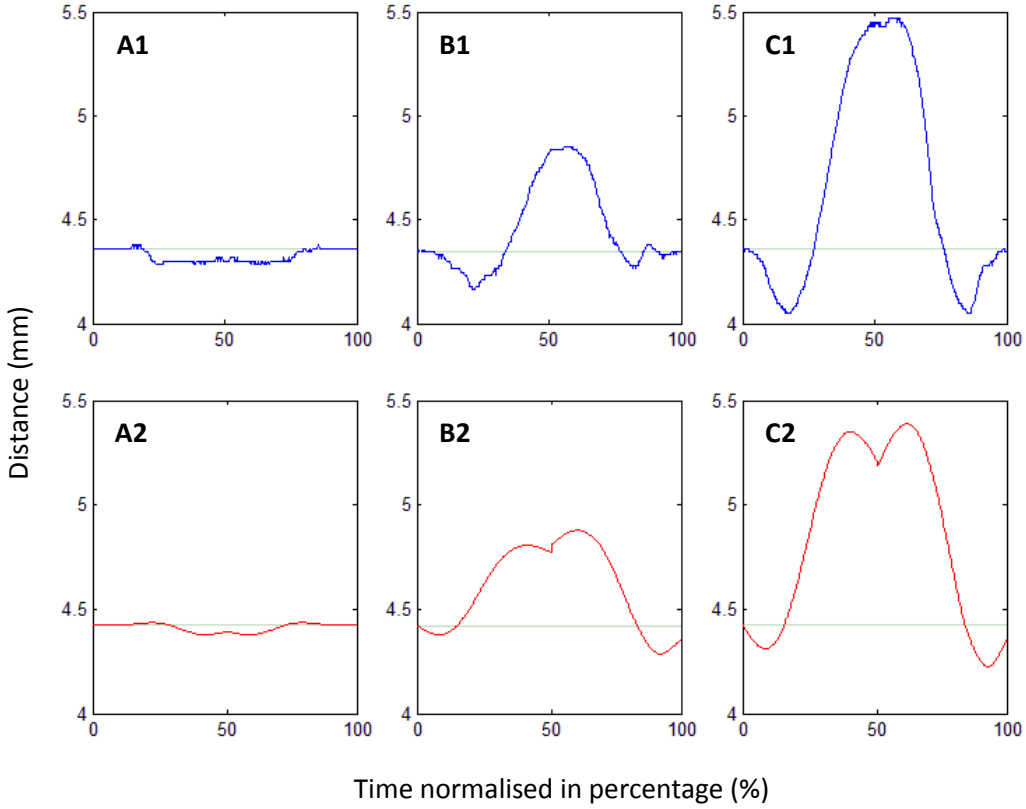

Figure 5.10 – Comparison between DTS transients of Volunteer A obtained based on real and simulated data: $\boldsymbol{A_{(1,2)}}$ *– Condition 1 (120%);* $\boldsymbol{B_{(1,2)}}$ *– Condition 2 (150%);* $\boldsymbol{C_{(1,2)}}$ *– Condition 3 ('Max. Reach');* $\boldsymbol{1_{(A,B,C)}}$ *– Real DTS System;* $\boldsymbol{2_{(A,B,C)}}$ *– Simulated DTS System.*

The illustrated transients provide comparison in the performance of the real and simulated DTS systems for the three reaching conditions. The plots show very similar shapes and amplitudes of the simulated transients (A2, B2 and C2) with the real ones (A1, B1 and C1). This indicates that the generated dynamic model can provide appropriate for the purposes of this project representation of contact forces produced by the moving human body in performing reaching task. Simulation transients of 150% and 'max. reach' conditions, illustrated in Figure 5.11 B2 and C2, show a decrease of the transient at the final stage of forward body movement (associated with normalised time of 50%), and an increase of the transient

at the initial stage when the trunk begins to move backwards in order to bring the body to its initial position. The two stages are associated with deceleration and acceleration of the trunk at the middle stage of the reaching task when the trunk stops to move (normalised time at 50%) and initialises its backward movement. These features are less noticeable in the transients obtained from real people due to the natural way of performing reaching task in which the relevant deceleration and acceleration are less pronounced. Similarly, the decreasing transient drift associated with the reach initiation stage is noticeably less pronounced in the simulation transients compared with the real ones. In real situation this is more noticeable due to the use of chair back support in which the trunk is resting prior executing the task. When the execution of the task begins, the trunk exerts vertical forces affecting the deformations of the distributive surface.

Table 5.2 shows results obtained in testing NN2 to classify reaching task patterns of the three healthy volunteers used in the development of discriminating trunk bending application. Neural network classification was applied to the relevant to this application three discriminative conditions of trunk bending corresponding to minor (120% reach - Condition 1), average (150% reach - Condition 2) and maximum ('max. reach' - Condition 3) trunk bending.

	Number of correct classifications (out of 15)		
Volunteer	**Condition 1 (120% reach)**	**Condition 2 (150% reach)**	**Condition 3 Maximum Reach**
A	15	14	15
B	15	15	15
C	15	15	15
Average Classification Accuracy – 99.3% **(134 correct classifications out of 135)**			

Table 5.2 – Verification results of NN2 tested to classify real reaching task patterns of Volunteers A, B and C.

5.4.5 Discussion

Presented results indicate that the developed model can generate acceptable simulation transients that can be used to artificially investigate the behaviour of the DTS system. The plots of Figure 5.11 show that simulated transients have similar characteristics with that of the real transients in terms of their form and amplitude values, which is essential for the appropriate extraction of sensing features used to generate discriminative patterns of trunk movement. The high classification accuracy obtained for NN2 have confirmed that the model is suited for generating data and can be successfully used to train neural networks with simulation data. This suggests that reasonable correlation was achieved between real and simulated transients for participants with different anthropometric characteristics, which is important for generating valid discriminative patterns.

5.5 Summary and Conclusion

The work presented in this chapter demonstrated that the DTS technology can be successfully applied to seated patients. The configuration of the developed DTS chair has shown to be compatible with the seated reaching task applied in stroke assessment and rehabilitation. It is demonstrated that the DTS chair can discriminate different levels of trunk bending when performing the reaching task and this applied to evaluate the level of motor impairment for people with stroke hemiparesis. Discrimination has been accomplished by using two neural networks derived from real and simulated data. Obtaining correlation coefficients of 1 in training networks NN1 and NN2, indicated optimal correlation between the considered in this application three discriminative conditions of reaching task. The results have been verified by obtaining average classification accuracy of

99.3% in testing the ability of NN2 to discriminate patterns of reaching task.

It was demonstrated that the developed simulation model is suitable for understanding the behaviour of the system for this application, and provides an efficient means to train neural networks. The model provides flexibility to be modified and upgraded with additional components, which in future work can be used to obtain more advanced understanding the dynamics of reaching task (i.e. in 3D space) and develop more advanced neural networks applicable in wider range of people.

The positive outcome of this chapter has led to testing the feasibility of the DTS technology for real. The next chapter presents the conduction of a cross-sectional investigation undertaken to test the ability of the DTS chair to discriminate trunk bending in random groups of healthy and stroke volunteers.

Chapter 6

Clinical Study

6.1 Introduction and Aim

In Chapter 5 it was demonstrated practically and theoretically that the DTS technology can be applied to discriminate different levels of trunk contribution to performing a functional reaching task during sitting. As stated in Chapter 2 (Section 2.3.2), the level of trunk contribution in performing a reaching task has shown to be correlated to the level of motor impairments in people with stroke (Cirstea & Levin, 2000). Applying the DTS technology in discriminating the level of trunk contribution to reaching in stroke survivors will provide a satisfactory indication for the suitability of DTS technology to be applied in the areas of stroke assessment and rehabilitation. To meet this aim, in this chapter the performance of the DTS chair developed in Chapter 5 was evaluated in a cross-sectional study with groups of healthy controls and stroke survivors.

Initially, the robustness of the DTS chair to classify reaching task patterns was tested with a convenience sample of 10 healthy volunteers. The functional reaching task was performed to targets positioned in front of the sitting participants. Figure 6.1 illustrates relevant to the experimental setup of this study target positions corresponding to distances calculated based on participant's arm length. For the healthy participants, trunk movement was induced by targets placed at distances exceeding the length of the arm. Therefore, targets placed at 120%, 150% and 'max. reach' positions were used as three discriminative conditions of trunk

flexion. Targets placed within the reach of the participant (80% and 100%) were used to investigate the performance of the DTS chair in conditions which did not involve trunk movement.

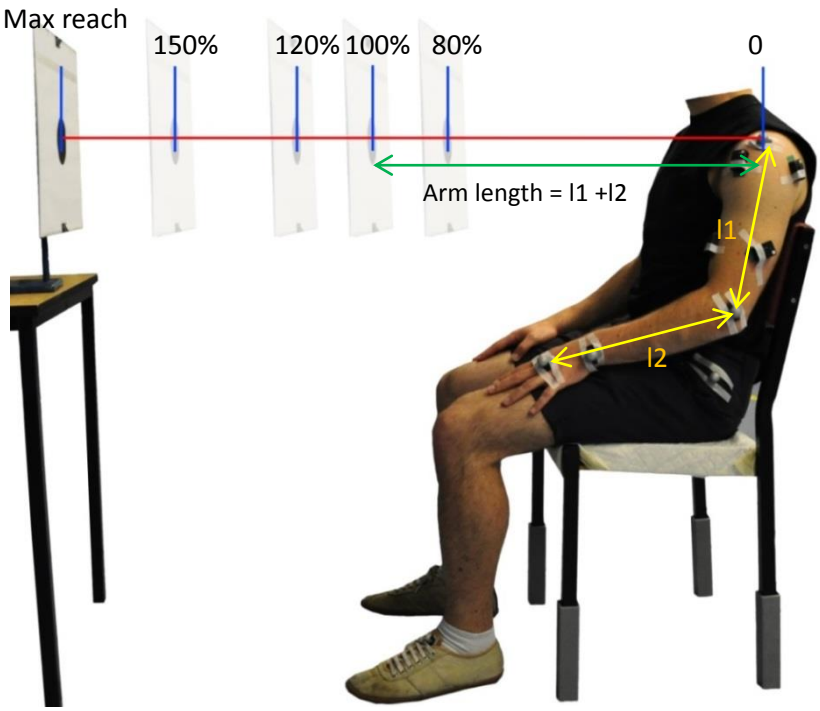

Figure 6.1 – Reaching task experimental setup illustrating a participant sitting on the instrumented DTS chair prior reaching to targets placed at 80%, 100%, 120%, 150% and 'max. reach' locations defined based on the participant's arm length.

The ability of the DTS chair to discriminate conditions of trunk bending was tested based on the developed in Chapter 5 neural networks trained with data from real and simulated DTS systems (NN1 and NN2, respectively). Appropriateness of DTS transients was determined based on arm and trunk movement kinematics obtained using 3D motion capture, and electromyography (EMG) systems. Due to the relatively high level of consistency and low variability of data in healthy individuals, testing with

this group was important to provide the indication of the sensitivity of the DTS chair in the arm-trunk movement of the reaching task. Kinematic data recorded from healthy subjects was used to associate trunk bending (trunk flexion) angles with, the relevant to this application, three discriminative conditions of the reaching task. Later, this information was used to verify the classification results obtained with the stroke group.

In the second part of the study performance of the DTS chair was tested with a group of 5 stroke volunteers. Classification results have been verified by referenced kinematic data obtained from testing with the healthy group. Testing with stroke survivors has provided the opportunity to further investigate behaviour of the system in a real situation and evaluate clinical usage of the DTS technology.

In testing healthy participants, average classification accuracy of 92.4% and 97.3% was achieved for NN1 and NN2, respectively. Results indicated that the DTS chair could successfully discriminate different levels of trunk contribution to reaching tasks when applied to a relatively wide range of healthy individuals. Relevance in classification accuracy of NN1 and NN2 implies that the mathematical model developed in Chapter 5 was suitable for investigating the behaviour of the DTS system and developing more advanced neural networks.

In testing with the stroke group, average classification accuracy of 93.3% and 94.7% has been achieved for NN1 and NN2, respectively. Results have shown that the DTS technology can be successfully applied to determine the level of trunk involvement in a reaching task in people with residual motor deficits after stroke. Further investigation of the behaviour of the DTS transients showed that signal transients had distinctive amplitudes in different reaching conditions associated with small variations in trunk bending. Furthermore DTS transients might contain information which could be associated with the quality of performing the reaching task.

The work presented in this chapter has verified the clinical applicability of the DTS technology in the area of stroke assessment. Working with stroke

survivors has provided valuable knowledge and experience that will be applied in further development of the technology to help stroke survivors (e.g. providing feedback and knowledge of results).

6.2 Assessment of functional recovery after stroke

One of the major clinical tools for the assessment of motor impairment after stroke is Fugl-Meyer test. Reliability and consistency Fugl-Meyer clinical test has been shown previously (Sanford et al., 1993). The Fugl-Meyer test is an impairment measure which has been designed to assess physical recovery, as well as efficacy of treatment after stroke (Gladstone et al., 2002). Motor impairment is measured by scoring test items on a three-point ordinal scale. Assessment with Fugl-Meyer clinical test requires appropriate and comprehensive understanding of the Fugl-Meyer assessment criteria originally developed in early 1975 (Fugl-Meyer et al., 1975). Therefore the use of Fugl-Meyer test allows variation in interpretation based on the ratter's knowledge, assessment experience, as well as personal estimation. It has been reported (Deakin et al., 2003) that although this type of examination provides clinical score that are considerably relevant to the level of motor impairment, its usage is not appropriate for understanding the functionality of the impaired body segments. As for most other assessment scales of this type including Barthel (Mahoney & Barthel, 1965), Bobath (1970), and Brunnstorm (1970) scales, the measurement of recovery for patients with mild motor impairments is limited by a ceiling factor (Gladstone et al., 2002).

Currently, in terms of engineering instrumentation motion capture is widely used in the assessment of upper-limb physical recovery after stroke (Alt Murphy et al., 2011). It has been proposed that these systems are one of the most accurate means of measuring human motion. In

particular, Vicon-Peak (2004, Denver, USA) has been identified as a leading manufacturer of this technology (Gibbs, 2008). Motion capture operates by computerised tracking of markers placed over selected body landmarks. Analysis of motion capture data reveals important kinematic information that cannot be captured by the naked eye. This information is derived from many kinematic variables such as position and velocity of body landmarks, joint angles and angular velocity, etc. Advantage of this technology is that it provides high accuracy in detecting marker positions in space and this information can provide detailed kinematic analysis post examination. Analysis of data recorded with motion capture systems can be applied to investigate existing, as well as identifying new motor impairments. Alongside the advantages however, motion capture systems have some significant limitations. In addition to the high cost and time consuming examination, trained specialists are required to operate the system and perform post-processing of the collected data. Motion capture is generated via attachment of IR reflective markers to the human body which often leads to lack of information of the recorded data due to a problem of disrupted marker visibility, and the restriction of providing quick examination outcome. Other limitations such as the requirement of spacious rooms where the system can be installed, and changing the system setup for different studies make their use not feasible in clinical settings.

The DTS chair can overcome some of the limitations of the traditional motion capture systems. The DTS technology provides a low-cost, easy to use and relatively accurate alternative which can be readily applied in both clinical and home settings as self-assessment and rehabilitation tools.

6.3 Considerations and design of the experiments

6.3.1 Participants

In this study a group of 10 healthy individuals and 6 chronic stroke survivors of both sexes were recruited. All stroke participants were out of NHS care and had completed hospital and outpatient rehabilitation programs. The conduction of the clinical study was approved by Brunel University Research Ethics Committee. A copy of ethics letter of approval for this study is included in Appendix 1.

Severity of stroke (involvement of the upper limb) has been assessed prior to experiments based on the Fugl-Mayer clinical test, conducted by a collaborating physiotherapist from Brunel University. Three stroke participants had mild, two had moderate, and one had severe impairment of the upper limb based on Fugl-Meyer upper extremity test score. Fugl-Meyer score (upper limb) ranges between 1 and 60, where the range between 1 and 18 corresponds to severe, 19-46 corresponds to moderate and 47-60 corresponds to mild degree of impairment. The participant with severe motor impairment was excluded from the study due to inability to complete the task independently. The other five participants were able to perform the reaching task independently. For completing the task, the seated participants were required to point to the target successfully for targets placed at different distances within the maximum reach of each participant.

The physical relevant statistics of the volunteer participants in this study are presented in Table 1.

Volunteer *H - Healthy S - Stroke*	**Gender**	**Age**	**Weight (kgf)**	**Height (cm)**	**Side tested**	**Arm length (cm)**	**Max. reach (cm)**	**Fugl-Meyer score**
H1	Male	28	85	183	Right	71	132	N/A
H2	Male	27	84	170	Right	67	115	N/A
H3	Female	25	48	160	Right	59	111	N/A
H4	Female	26	67	165	Right	65.5	121	N/A
H5	Male	26	66	170	Left	63.5	124	N/A
H6	Male	78	72	176	Right	68.5	118	N/A
H7	Female	53	63	164	Right	70	122	N/A
H8	Male	57	78	187	Right	74	133	N/A
H9	Male	51	83	178	Right	67	125	N/A
H10	Male	39	82	180	Right	71	129	N/A
S1	Female	52	50	160	Right	68	43	20/60
S2	Male	28	80	178	Left	71	127	58/60
S3	Female	56	54	168	Left	65	120	59/60
S4	Female	48	57	155	Left	62	106	59/60
S5	Male	49	83	175	Right	69	98	38/60

Table 6.1 – Physical records of the healthy and stroke volunteers.

6.3.2 Equipment and material

Data collection was completed at the biomechanics laboratory, Centre for Sports Medicine and Human Performance, Brunel University. A DTS chair, a real-time motion analysis system (Motion Analysis, USA), and EMG system (Delsys Trigno, USA) were used simultaneously to provide DTS, kinematic and electromyography data, respectively. Eight IR reflective markers were placed superficially on specific anatomical landmarks on an individual's arm and trunk following a standard procedure to create an upper body model. Surface electromyography (EMG) was recorded with wireless electrodes from muscles responsible for arm and trunk movements. Figure 6.2 shows the positions of motion markers (M1 – M8)

and EMG electrodes (E1 – E6). The anatomical landmarks of the motion markers and EMG electrodes are defined as follows:

M1 – Neck
M2 – Left Acromion process (Shoulder)
M3 – Right Acromion process (Shoulder)
M4 – Lateral Epicondyle of Elbow (Elbow)
M5 – Radial Styloid process (wrist)
M6 – Third Metacarpal (Knockle)
M7 – Left Greater Trochanter (Hip)
M8 – Right Greater Trochanter (Hip)
E1 – Long head of Triceps (TR), shown in cyan colour in the plots of the results section
E2 – Biceps (BI), shown in black colour in the plots of the results section
E3 – Anterior Deltoid (AD), shown in magenta colour in the plots of the results section
E4 – Posterior Deltoid (PD), shown in green colour in the plots of the results section
E5 – Right Erector Spinae (RES), shown in red colour in the plots of the results section
E6 – Left Erector Spinae (LES), shown in blue colour in the plots of the results section

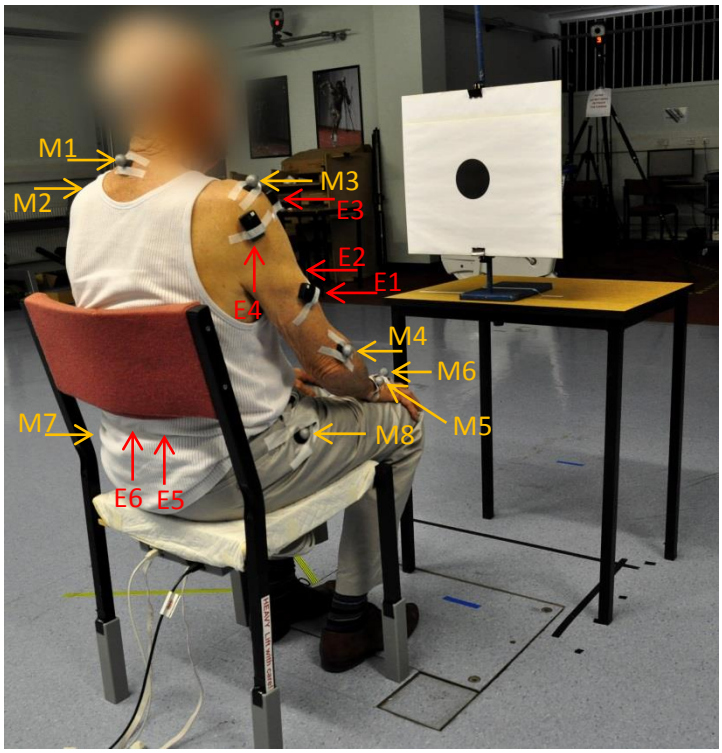

Figure 6.2 – Healthy volunteer with motion markers and EMG electrodes placed on his body prior to data recording.

In order to collect synchronised data from all systems, DTS and EMG data were collected via a DAQ device (NI USB-6255, 16bit resolution) synchronised with the motion system. Kinematic data was collected with sampling rate of 150Hz, while DTS and EMG data was recorded with sampling rate of 1500Hz set by the EMG system requirement.

A target of black circle positioned in the centre of a white background plastic surface was placed at different distances within and beyond the critical boundary (defined based on 90% one's arm length) of the arm reach, and aligned with respect to the horizontal and vertical coordinates of the shoulder. The full arm length of each individual was defined as the sum of upper and lower arm lengths measured between acromion and lateral epicondyle (upper arm), and lateral epicondyle and third metacarpal bone (lower arm).

6.3.3 Procedure

Participants were instructed to sit comfortably in the DTS chair following their natural sitting posture with hands resting on their thighs. The height of the chair was adjusted so that participant's feet were flat on the floor with the knee (the angle between tibia (shank) and femur (thigh) segments) and hip (the angle between femur and trunk) joints at angle of 90 degrees. In healthy participants, a target was placed at different locations of 80%, 100%, 120%, 150% of the length of the arm reach, as well the maximum reach of the participant. Therefore targets at 80% and 100% represented reaches within the critical boundary of arm reach (no trunk movement), and targets at 120%, 150 and maximum reach represented reaches to targets placed beyond the critical boundary (minor, moderate and maximum trunk movement). In stroke participants, a target was placed at different locations according the maximum reach of each participant. Therefore the stroke participants were examined based

on target locations defined as follows: Participant S1 – 50%, 60% 63% ('max. reach' defined at 63%); Participants S2, S3 and S4 – 80%,100%, 120%, 150% and 'max. reach'; Participant S5 – 80%, 100%, 120% and 142% ('max. reach' defined at 142%). Following the considerations defined in Chapter 5, maximum reach was defined according to a distance at which each participant could reach the target comfortably without feeling pain or discomfort and without lifting their bottom from the chair. By giving a 'Go' command, participants were instructed to reach to the target from a start point (when hand was placed on the thigh on the same side of the participant's moving arm) in one continuous motion toward the target without correction. Participants were asked to perform the task using a self-selected pace. Start point was marked on the participant's thigh and used to standardise arm posture before the start of the movement. Target locations were presented in randomised blocks (relevant to each participant target positions) and each block contained fifteen trials. Adequate rest periods were incorporated within and between blocks of trials to avoid fatigue.

6.4 Results

6.4.1 Testing with healthy volunteers

From the large number of recorded trials in this study, two with minimal disruption of the motion data and minimal noise in the EMG signals were selected and included in the results section to provide understanding of the performance of DTS system and verify the obtained results using motion capture and EMG data. Data recorded from DTS, motion capture and EMG systems for two conditions involving reaches without and with trunk movement is shown in Figures 6.3 and 6.4 respectively synchronised showing sensing transients, joint angles and EMG signal

onsets (from top to bottom). The arm and trunk joint angles are defined based on the orientation of the corresponding segment from either a 'zero' horizontal (elbow and wrist angles) or vertical lines (trunk and shoulder angles) in the Cartesian coordinate system.

The flat character of the trunk angle plot in Figure 6.3 indicates no trunk participation when reaching was executed to targets placed within the critical boundary of reach. Respectively, the significant change in shoulder, elbow and wrist angle plots correspond to movement of the entire arm. In confirmation to these findings are also the constant tonic behaviour of LES and RES EMG onsets indicating no trunk movement, and the pronounced activity of AD and BI onsets associated with movement of the hand. It is important to point out that in this case the DTS transient has a constantly flat character (associated with lack of deformation over the DTS chair surface) indicating that the DTS chair is not considerably sensitive to the movement of the arm. In contrast, the DTS and trunk angle plots in Figure 6.4 show pronounced DTS displacement and trunk bending in the reaching conditions involving contribution from the trunk. This indicates that the DTS chair is sensitive to the entire upper body and arm movements and in particular to the movement of the trunk in executing the reaching task.

Time event information of EMG onsets was found to be associated with certain features in the DTS signals. For example activation of LES and RES muscles matched with the end of a reach initiation stage (RIS), during which the trunk prepares for executing the reaching task prior the start of the movement. This can be seen in Figure 6.4 where the activation of LES and RES EMG onsets matches with the first local minima of the DTS transient.

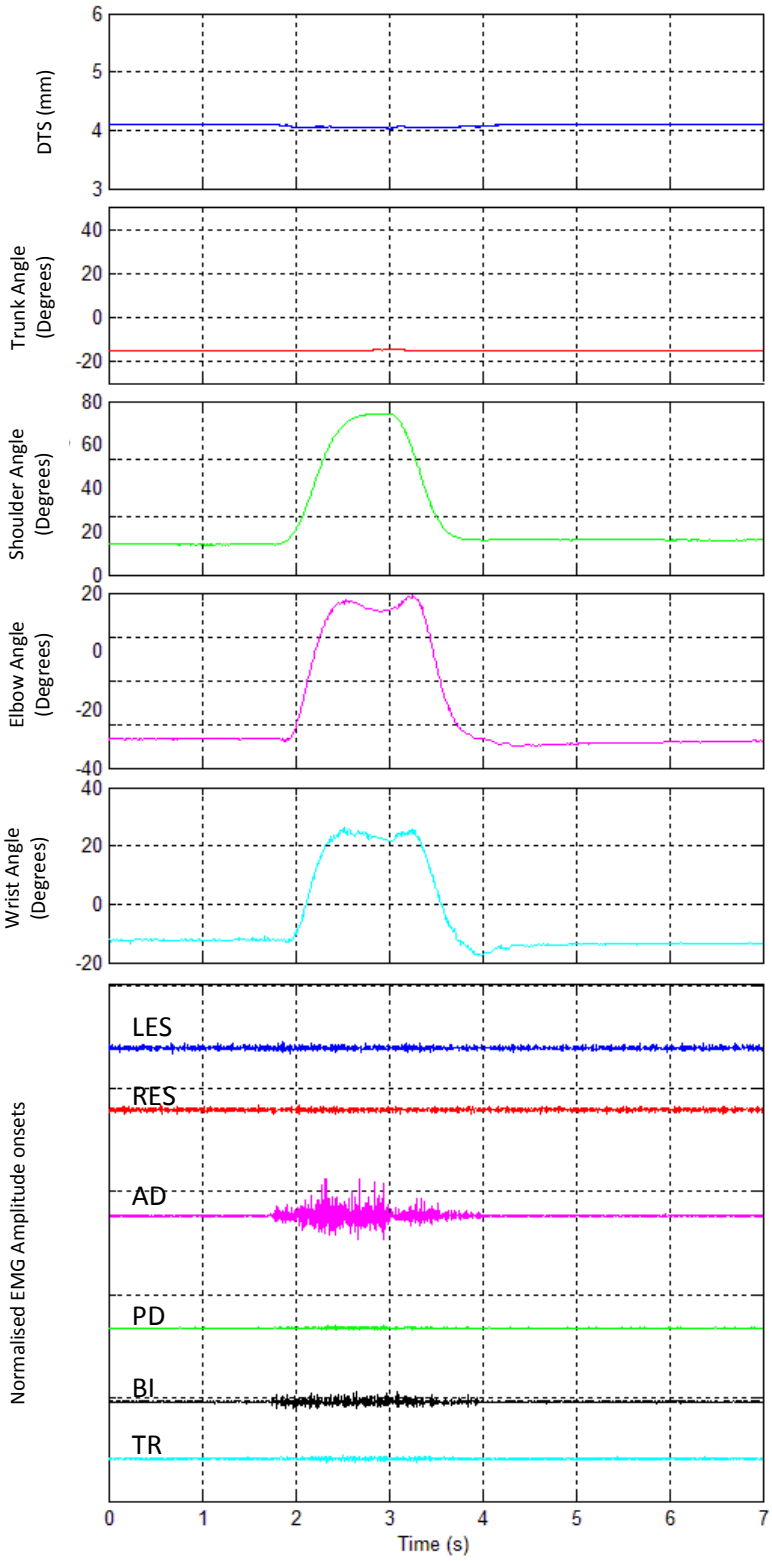

Figure 6.3 – Time normalised DTS transient, body angles and EMG onsets of selected healthy trial corresponding to reaching to a target placed within the critical boundary of arm reach (100% reach).

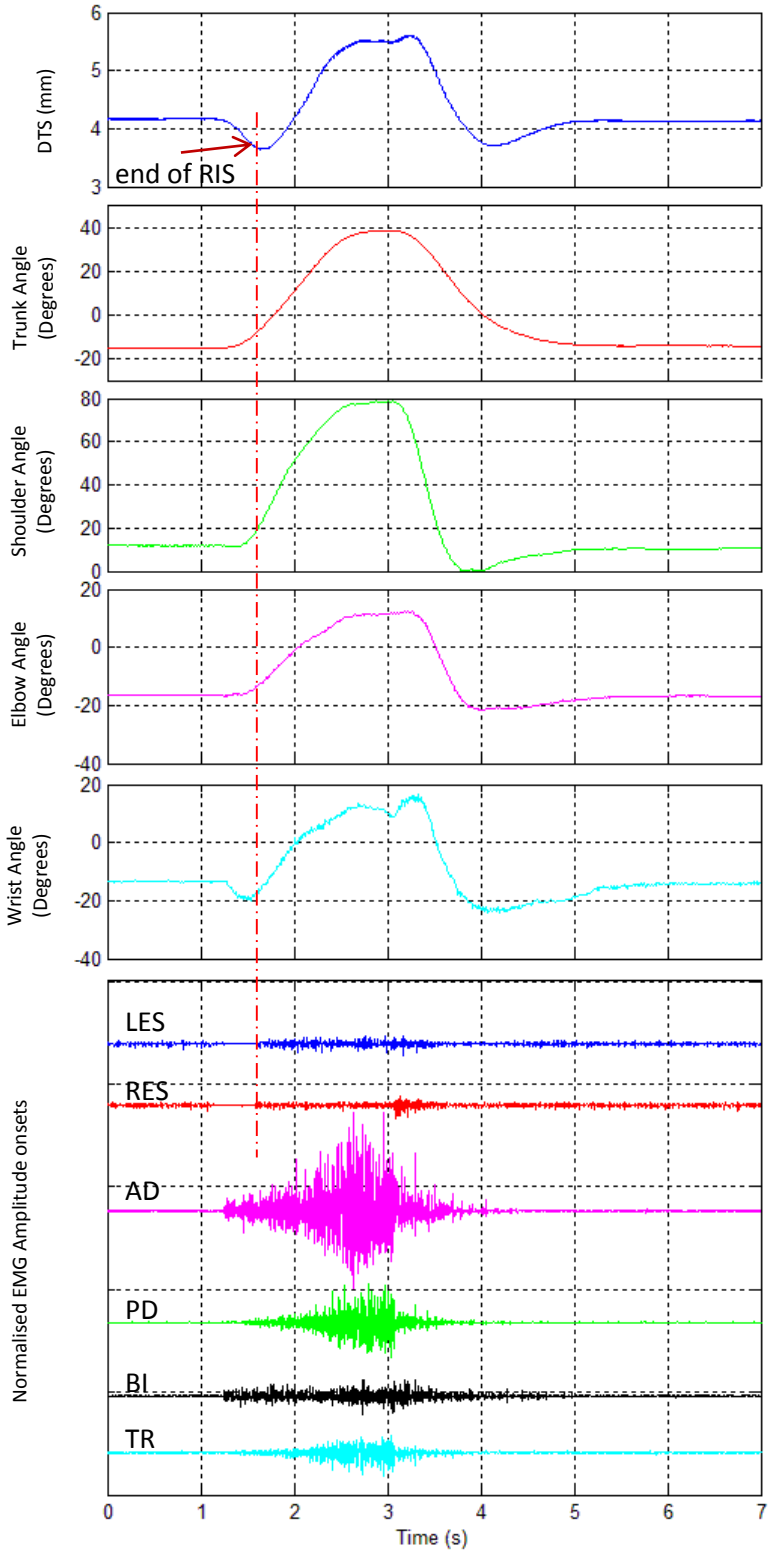

Figure 6.4 – Time normalised DTS transient, body angles and EMG onsets of selected healthy trial corresponding to reaching to a target placed beyond the critical boundary of arm reach ('max. reach').

6.4.1.1 Neural Networks classification accuracy

DTS data collected from healthy subjects was in the form of sensory transients used in combination to generate discriminative reaching task patterns following the feature extraction technique described in Section 5.4.3. Patterns were generated for the three reaching task conditions involving trunk contribution corresponding to targets placed at 120%, 150% and 'max. reach' distances based on the arm length. The ability of the DTS chair to discriminate trunk bending in randomly selected healthy people was tested by obtaining the number of correct classifications for the generated patterns using the generated in Chapter 5 NN1 and NN2 neural networks. Results presented in Table 6.2 contrast the classification accuracy of NN1 and NN2 obtained for the three discriminative conditions in all ten healthy volunteers.

Volunteer	**Number of correct classifications (out of 15)**					
	120%		**150%**		**'Max. reach'**	
	NN1	**NN2**	**NN1**	**NN2**	**NN1**	**NN2**
H1	15	15	15	15	15	15
H2	15	15	12 (3 - max)	11 (4 - max)	15	15
H3	15	15	11 (4 - max)	11 (4 - max)	15	15
H4	15	15	15	12 (3 - max)	15	15
H5	15	15	15	15	15	15
H6	0 (15 - 150)	15	15	15	15	15
H7	15	15	15	14 (1 - max)	15	15
H8	11 (4 - 150)	15	15	15	15	15
H9	15	15	15	15	15	15
H10	15	15	15	15	15	15
	TOTAL					
	131/150	**150/150**	**143/150**	**139/150**	**150/150**	**150/150**
	AVERAGE ACCURACY **NN1 – 92.4% (416 correct classifications out of 450)** **NN2 – 97.6% (439 correct classifications out of 450)**					

Table 6.2 – Classification accuracy of neural networks NN1 and NN2.

6.4.1.2 Trunk angle window of operation for the three discriminative conditions of reaching task

Trunk angle recorded in all healthy participants was used to obtain the range of operation (or the limits) of the bending trunk for the three reaching task conditions. For that purpose trunk angles, presented in Table 6.3, were obtained for each healthy participant based on averaging 10 trials of the relevant reaching condition. The range of operation for each condition, illustrated graphically in Figure 6.5, was defined according the derived min, average and max trunk angles. This information was needed in testing with the stroke group to verify the performance of the DTS chair by associating the trunk angle (obtained with 3D motion capture) and the Fugl-Mayer score with the classification outcome of neural networks NN1 and NN2.

Volunteer	**Averaged of 10 trials Trunk Angle (Degree)**								
	Condition 1 (120%)			**Condition 2 (150%)**			**Condition 3 (Max. reach)**		
H1	0.4			28.4			61.4		
H2	3			34.1			52.5		
H3	1.5			22.3			48		
H4	7.7			31			48.8		
H5	2			20.6			60.4		
H6	2			36.4			54.3		
H7	8.4			34.2			60		
H8	9.9			30.2			50.9		
H9	2.1			26.8			51.8		
H10	4.1			27.6			54.5		
	Min	**Avg**	**Max**	**Min**	**Avg**	**Max**	**Min**	**Avg**	**Max**
	0.4	**4.1**	**9.9**	**20.6**	**29.2**	**36.4**	**48**	**54.3**	**61.4**

Table 6.3 – Trunk angle of all healthy volunteers obtained from kinematic data for the three discriminative conditions of reaching task.

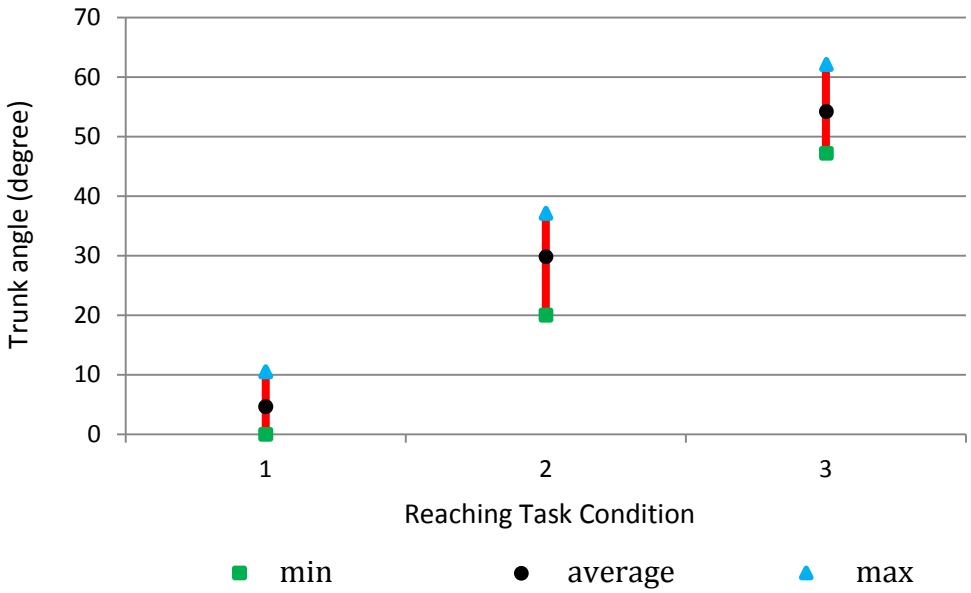

Figure 6.5 – Graphical illustration of the obtained range of operation of the bending trunk for the three conditions of reaching task.

6.4.2 Testing with stroke survivors

Figure 6.6 shows data obtained from a representative stroke participant with moderate impairment severity. In this example of reaching task, the target was placed at locations within the length of the arm (identified as 63% reach). The trunk angle plot indicates significant trunk bending. This is also confirmed by the activation of LES and RES EMG onsets. The wavy shape of arm angle plots illustrates impaired arm movement associated with a hemiplegic pattern of movement. Summarising these findings, Figure 6.6 was used as an example showing that in this study, in contrast to the healthy participants, the participants with moderate stroke did use their trunk in order to reach to targets placed within the arm length.

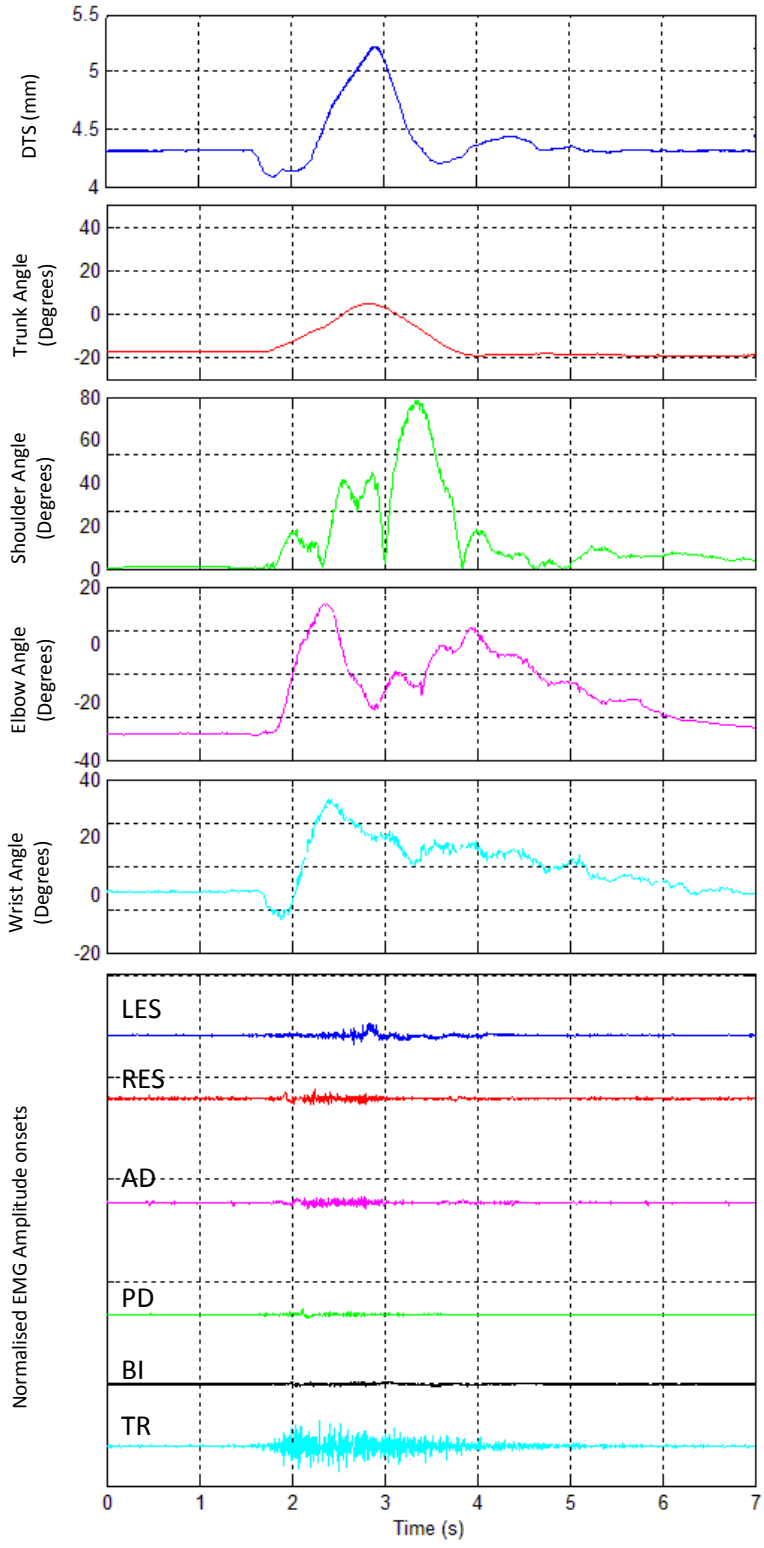

Figure 6.6 – Time normalised DTS transient, body angles and EMG onsets of selected stroke trial (participant S1) corresponding to reaching to a target placed within the arm length ('max. reach' at 63%).

6.4.2.1 Neural Network classification accuracy

The reference table (Table 6.3) developed after testing healthy group was used in order to associate the trunk angles (obtained with the 3D motion capture) of the stroke participants with relevant discrimination conditions (obtained with the DTS chair based on NN1 and NN2). For that purpose the level of motor impairment in the stroke group was tested based on targets placed at the critical boundary of reach (or within it if the maximum reach of the participant was within the critical boundary, i.e. participant S1). Obtained results have been summarised in Table 6.4.

Volunteer	**Level of motor impairment based on Fugl-Meyer test**	**Average trunk bending to the critical boundary** *(degree)*	**Relevant discrimination condition**	**Number of correct classifications (out of 15)** **NN1**	**NN2**
S1	Moderate	21	Condition 2	10	11
S2	Mild	4.3	Condition 1	15	15
S3	Mild	4.3	Condition 1	15	15
S4	Mild	6	Condition 1	15	15
S5	Moderate	30.9	Condition 2	15	15
AVERAGE ACCURACY **NN1 – 93.3% (70 correct classifications out of 75)** **NN2 – 94.7% (71 correct classifications out of 75)**					

Table 6.4 – Classification accuracy of NN1 and NN2.

6.4.2.2 Additional results obtained during data analysis

Examination of the DTS transient amplitudes obtained from one of the stroke participant (S1 in table 6.1) with moderate stroke, showed that DTS transients corresponding to targets placed at small absolute distances from each other (7cm and 2cm) had distinctive amplitudes. This has been

shown in Figure 6.7 which also shows relevant kinematic data that was used to validate this results.

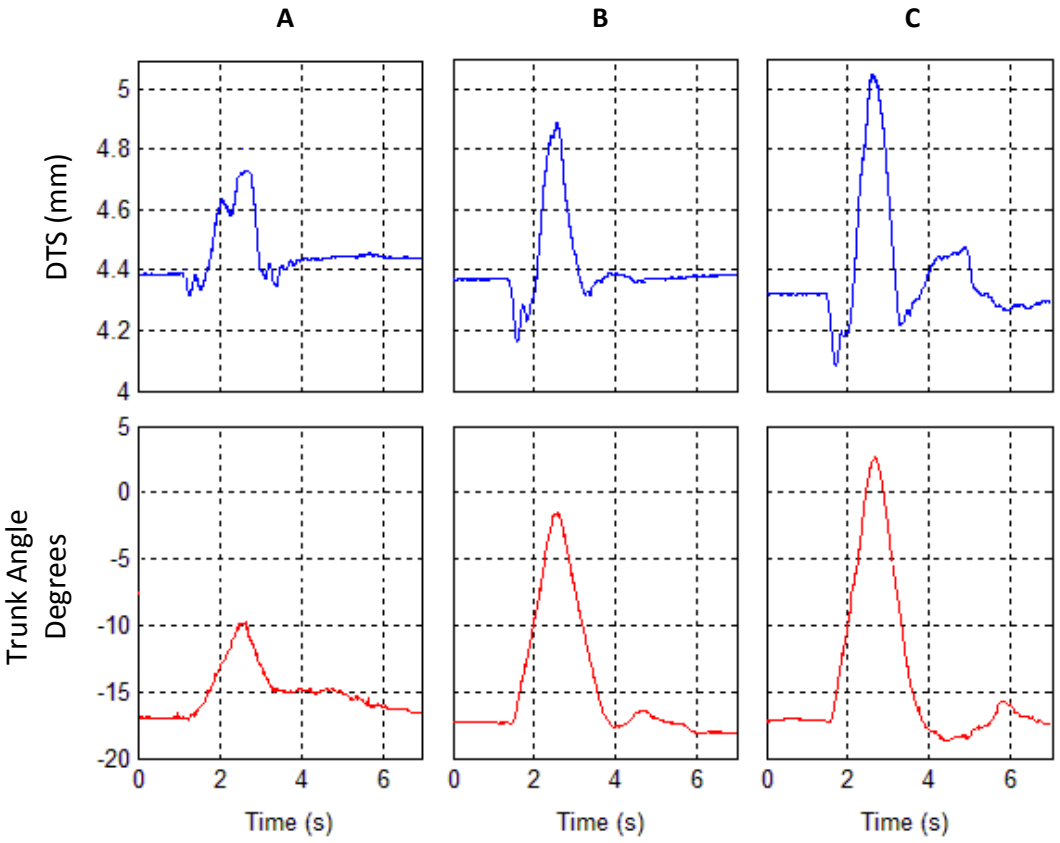

Figure 6.7 – Time normalised DTS transient and trunk angle plots of a stroke participant (S1) subject to performing reaching to targets placed at distances corresponding to 50% (A), 60% (B) and 63% (C) of the arm length.

DTS transients of mild stroke participants with the same motor impairment severity according to Fugl-Meyer test have shown to have different smoothness. This can be seen in Figure 6.8 which shows four DTS transients of a healthy participant (A) and three mild stroke participants (B, C and D). The disrupted smoothness of the transients in plots C and D suggests the presence of features in the sensory transients which can be associated with quality of reaching task movement.

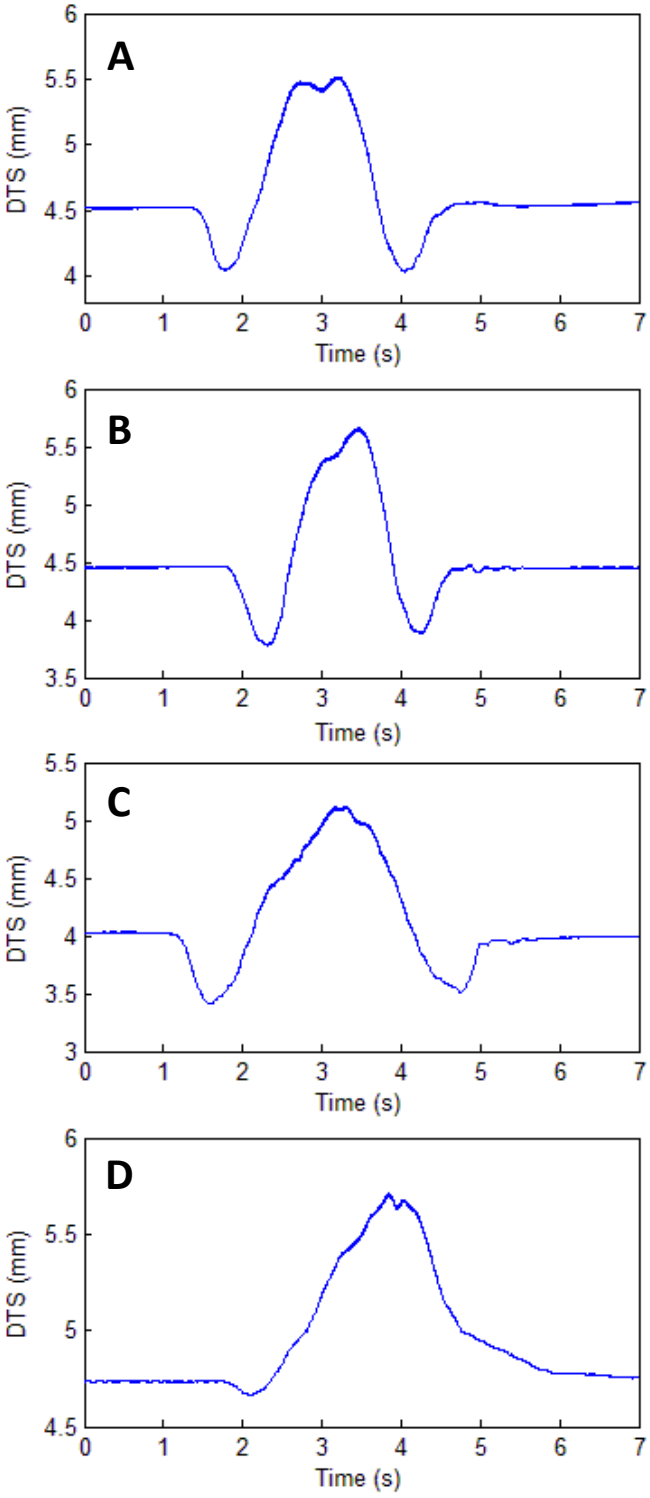

Figure 6.8 – 'Max. reach' DTS transients of 1 healthy subject (A) and 3 mild stroke (B, C and D) participants with Fugl-Meyer clinical scores of 59, 58 and 59 (out of 60), respectively.

6.5 Discussion

The purpose of this study was to test the ability of the DTS chair to discriminate different levels of trunk contribution to performing a functional reaching task with stroke survivors. Average classification accuracy of NN1 and NN2 indicated that the DTS chair could discriminate between movements with different contributions of trunk bending during a reaching task. This was shown in the relatively wide range of healthy people tested. Comparable classification outputs of NN1 and NN2 in the majority of trials suggest that the interpretation techniques used are appropriate and stable. The classification accuracy achieved when using NN2 has confirmed that the mathematical model developed in Chapter 5 is suitable for generating data which can be used to train neural networks.
In Section 6.4.3 kinematic data was used to obtain the angle ranges (min, average and max) of trunk bending for the relevant three discriminative conditions. This information played important role in verifying the classification results obtained in testing with the stroke group by associating the level of trunk bending in stroke participants with the corresponding reaching task condition (based on information presented in Table 6.3).
In this study recorded EMG data provided advanced understanding on the characteristics of DTS transients. It was shown that EMG data can be significantly meaningful in determining time event information during reaching task. Recorded muscle activity confirmed the participation of arm and trunk movement in executing reaching task.

Testing with stroke participants provided the chance to test the behaviour of the DTS system subject to increased movement variability in performing reaching task due to motor impairment after stroke. Obtained classification accuracy of 93.3% and 94.7% for NN1 and NN2, respectively, indicated sufficient discrimination performance of the system.

6.6 Conclusion

In this chapter the clinical feasibility of the DTS technology has been tested in a cross-sectional study with groups of healthy and stroke volunteers. Conduction of a clinical study with stroke survivors has led to a real test of the application where the motor problems were exposed in experimental settings.

The work of this chapter demonstrated that the level of upper-limb motor impairment is successfully identified by discriminating different levels of trunk contribution to performing a functional reaching task while sitting. Using 3D motion capture and EMG systems to verify the results, it was demonstrated that the DTS chair is able to distinguish between small changes in performing the reaching task that may be associated with functional improvement alongside features which are informative in respect to the quality hemiplegic movements. Results obtained in this study showed that the DTS technology has the potential to be developed to advanced applications for monitoring the level of functional improvement during rehabilitation. However further investigation will be needed before the DTS technology can be applied clinically as a final solution for the assessment of upper limb function in stroke survivors. This will need testing for robustness in the task performed.

Chapter 7

Conclusion

The aim of this thesis is to verify the clinical applicability of DTS technology in the assessment of postural steadiness and stroke rehabilitation. For this purpose, two experimental devices were designed, developed and tested using mathematical models and commercially available measuring systems. First, a mechanically and methodologically simple solution to the conventional force plates in the determination of centre of pressure biomechanics parameter was presented. In contrast to previous work of the Distributive Tactile Sensing where the majority of applications were based on discrimination, the COP application of this thesis also demonstrated that the DTS technology is suitable for obtaining information associated with measurement of forces.

The prime application of this thesis was built as a mechanically simple, tactile sensing mechatronic system for discriminating human motion in the process of stroke recovery in reaching task. Such application was intended for use in assessing and monitoring progress in stroke recovery. The outcome of the work over this application showed robustness with respects to variations to real stroke survivors with levels of mild-to-moderate hemiparesis of the upper limbs. The development of the system has followed requirements of design principles for low cost taking into account robustness to variation in motion, build and initial posture of a group of volunteers.

The work conducted in this thesis has demonstrated that the DTS technology provides advantage over other competitive sensing systems

and has a considerable potential to be applied in clinical and home settings for monitoring and rehabilitation purposes. Major advantages of the DTS approach are summarised as follows:

- The DTS approach is mechanically simple, can be implemented at relatively low-cost devices, and without any specific installation, calibration and operational requirements.
- High levels of robustness and portability, as well as low power consumption make the technology applicable in a wide range of setting, both in and outdoor environments including clinics and homes.
- The DTS approach deploys automatic and real-time analysis of the collected sensing data, which leads to providing examination outcome at the time of examination with minimised need for clinician to interpret collected data.
- The technology can be developed for monitoring and feedback applications in conjunction with portable devices such as laptops tablets and smartphones.

Work conducted in this thesis has provided robust confidence in the successful clinical applicability of the DTS technology in the areas of postural control and stroke assessment. Obtained results have proved that the DTS technology can successfully be used to identify motor impairments in stroke population. The development of a complete solution to help assessment of stroke survivors however, requires further investigation of the behaviour of the DTS system. Conduction of a longitudinal study with groups of stroke survivors to test variability of DTS system transients is required to bring the technology a step closer in the development of a final clinical product of a reasonable cost.

7.1 Limitations of the research

In this thesis the applicability of two experimental devices, the DTS floor platform and DTS chair, was verified in postural steadiness and stroke assessment. The DTS floor plate was developed to application for detecting and tracking the locus of centre of pressure which is a major force parameter in the quantification of balance disorders. As the principles of the Distributive Tactile Sensing are supposed to discriminate human motion at the time of examination, a major limitation of this application is that COP or raw sensing data were not used to develop patterns of postural steadiness to discriminate disorders automatically and in real time. This work was not conducted as the project priorities were to demonstrate that the DTS technology provides an alternative to the conventional force platforms in detecting force parameters such as the locus of centre of pressure.

The second of the project experimental devices, the DTS chair, was developed to an application for discriminating levels of motor impairment of hemiparetic stroke survivors. As this was a novel application of the DTS approach, a pilot clinical study was conducted with relatively small group of stroke participants. The relatively high classification accuracy achieved during the experiments in Chapter 6 demonstrated successful discrimination, however it should be noted that resolution between the three discriminative conditions of the reaching task was relatively small. Another limitation of this application is that the determination the level of motor impairment of the upper limps was restricted to a 2-dimensional plane. Investigations in the 3-dimensional space would provide more complete understanding the behaviour of the DTS chair and potentially even greater variation between conditions of reaching task, allowing increasing the resolution of DTS chair and hence more distinguishable reaching patterns.

7.2 Future work

Before the developed DTS floor platform and chair systems can be applied as medical tools in the areas of postural steadiness and stroke rehabilitation, respectively, conduction of the following future work is recommended:

DTS floor platform for the assessment of postural steadiness:

- Conducting a study in which COP data will be collected from representative number of healthy participants and patients with balance or other postural impairments. This will allow for testing the reliability of COP measures obtained with the DTS floor platform.
- Developing pathologic patterns of postural steadiness based on COP data, and raw sensing data to automatically discriminate disorders in real time. This will enable the researcher to apply the DTS technology to a real application test and expose real problems of people with postural deficits.
- Developing a methodology for detecting or estimating other force parameters such as the ground reaction force vector and its 3-dimensional components. This will provide an opportunity the DTS technology to be further compared with commercialised force measuring devices, extensively and in more detail.

DTS Chair for stroke assessment and rehabilitation:

- Investigating the resolution of the DTS chair during reaching tasks. This will show the minimal level of trunk contribution that can be detected, and respectively the real accuracies that can be achieved.
- Conducting two longitudinal studies with groups of mild and moderate stroke hemiparetic individuals. Testing with narrow

groups of stroke patients will enable determining and evaluating variability of DTS data in performing reaching task.

- Developing an algorithm which will provide real time feedback (knowledge of results) to the user.
- Investigating the behaviour of DTS chair considering the upper extremity trunk movement in 3-dimensions. Positive outcome of such investigation leads to developing advanced applications which for example may be informative and knowledgeable for specific types of the motor impairment.

Appendix1 – Copy of Letter of Approval for the conduction of a clinical study with stroke survivors

University Research Ethics Committee

06 May 2014

Letter of Approval

Proposer: **Mr. Nikolay Mikov**

Title: **A distributive tactile sensing (DTS) device for assessment of arm movements during reaching**

Dear Mr. Mikov,
The University Research Ethics Committee has considered the amendments recently submitted by you in response to the Committee's earlier review of the above application.

The Chair, acting under delegated authority, is satisfied that the amendments accord with the decision of the Committee and has agreed that there is no objection on ethical grounds to the proposed study.

Any changes to the protocol contained in your application, and any unforseen ethical issues which arise during the project, must be notified to the Committee.

The Committee would appreciate a report on the project following its completion. This should include some indication of the success of the project, whether any adverse events occurred, and whether any participants withdrew from the research.

Kind regards,

David Anderson-Ford
Chair, Research Ethics Committee
Brunel University

References

Ache Dias, J., Borges, L., Mattos, D. J. D. S., Wentz, M. D., Domenech, S. C., Kauffmann, P., & Borges Junior, N. G. (2011). Validity of a new stabilometric force platform for postural balance evaluation. *Revista Brasileira de Cineantropometria E Desempenho Humano*, *13*(5), 367–372.

Aggarwal, J. K., & Cai, Q. (1999). Human Motion Analysis: A Review. *Computer Vision and Image Understanding*, *73*(3), 428–440.

Alt Murphy, M., Willén, C., & Sunnerhagen, K. S. (2011). Kinematic variables quantifying upper-extremity performance after stroke during reaching and drinking from a glass. *Neurorehabilitation and Neural Repair*, *25*(1), 71–80.

Amato, F., López, A., Peña-Méndez, E. M., Vaňhara, P., Hampl, A., & Havel, J. (2013). Artificial neural networks in medical diagnosis. *Journal of Applied Biomedicine*, *11*, 47–58.

Aoki, M., Tokita, T., Kuze, B., Mizuta, K., & Ito, Y. (2014). A characteristic pattern in the postural sway of unilateral vestibular impaired patients. *Gait & Posture*, *40*(3), 435–40.

Ardestani, M. M., Chen, Z., Wang, L., Lian, Q., Liu, Y., He, J., … Jin, Z. (2014). Feed forward artificial neural network to predict contact force at medial knee joint: Application to gait modification. *Neurocomputing*, *139*, 114–129.

Bobath, B. (1970). Adult Hemiplegia: Evaluation and treatment. *London: William Heinemann Medical Books*.

Brett, P. N. (1997). A techhnique for measuring contact force distribution in minimally invasive surgical procedures. *Institution of Mechanical Engineers*, *Part H*(211), 309–316.

Brunnstorm, S. (1970). Movement therapy in hemiplegia. *New York: Harper & Row*.

Cavanaugh, J. T., Guskiewicz, K. M., & Stergiou, N. (2005). A Nonlinear Dynamic Approach for Evaluating Postural Control New Directions for the Management of Sport-Related Cerebral Concussion, *35*(11), 935–950.

Chen, S., Lewthwaite, R., Schweighofer, N., & Winstein, C. J. (2013). Discriminant validity of a new measure of self-efficacy for reaching movements after stroke-induced hemiparesis. *Journal of Hand Therapy : Official Journal of the American Society of Hand Therapists*, *26*(2), 116–22.

Cheung, Y. K. (1968). The Finite Strip Method in the Analysis of Elastic Plates with Two Opposite - Simply Supported Ends. *Proc. Inst. Civ. Eng.*, *40*, 1–7.

Cirstea, M. C., & Levin, M. F. (2000). Compensatory strategies for reaching in stroke. *Brain*, *123*, 940–953.

Cirstea, M. C., & Levin, M. F. (2007). Improvement of arm movement patterns and endpoint control depends on type of feedback during practice in stroke survivors. *Neurorehabilitation and Neural Repair*, *21*(5), 398–411.

Deakin, A., Hill, H., & Pomeroy, V. (2003). Rough Guide to the Fugl-Meyer Assessment Upper limb section. *Physiotherapy*, *89*(12), 751–763.

Delignières, D., Torre, K., & Bernard, P.-L. (2011). Transition from persistent to anti-persistent correlations in postural sway indicates velocity-based control. *PLoS Computational Biology*, *7*(2).

Deschamps, T., Beauchet, O., Annweiler, C., Cornu, C., & Mignardot, J.-B. (2014). Postural control and cognitive decline in older adults: position versus velocity implicit motor strategy. *Gait & Posture*, *39*(1), 628–30.

Dolicanin, C., Nikolic, V., & Dolicanin, D. (2010). Application of Finite Difference Method to Study of the Phenomenon in the Theory of Thin Plates. *Journal of Applied Mathematics and Mechanics*, *1*, 29–43.

Elliott, M. T., Ma, X., & Brett, P. N. (2009). Discriminating Ambulation Using a Smart Sensing Plate.

Elliott, M. T., Petra, I., Ma, X.-H., Brett, P. N., & Holding, D. J. (2009). Quantifying sway through surface deflection patterns: a novel approach using distributive tactile sensing. *Proceedings of the*

Institution of Mechanical Engineers, Part H: Journal of Engineering in Medicine, *223*(7), 903–911.

Favre, J., Hayoz, M., Erhart-Hledik, J.C., Andriacchi, T.P. (2012). A neural network model to predict knee adduction moment during walking based on ground reaction force and anthropometric measurements. *Journal of Biomechanics* 45, 692–698.

Fugl-Meyer, A. R., Jaasko, L., Leyman, I., Olsson, S., & Steglind, S. (1975). THE POST-STROKE HEMIPLEGIC PATIENT. *Scand J Rehab Med*, *7*, 13–31.

Ganesan, M., Lee, Y.-J., & Aruin, A. S. (2014). The effect of lateral or medial wedges on control of postural sway in standing. *Gait & Posture*, *39*(3), 899–903.

Gibbs, S. (2008). *Clinical applications of motion analysis*. *Clinical Nursing & Patient Care* (pp. 0–2). Dundee.

Gladstone, D. J., Danells, C. J., & Black, S. E. (2002). The Fugl-Meyer Assessment of Motor Recovery after Stroke: A Critical Review of Its Measurement Properties. *Neurorehabilitation and Neural Repair*, *16*(3), 232–240.

Goldie, P. A., Bach, T. M., & Evans, O. M. (1989). Force platform measures for evaluating postural control: Reliability and validity. *Archives of Physical Medicine and Rehabilitation*, *70*(510-517).

Gresham, G., Duncan, P., Stason, W., Adams, H., Adelman, A., Alexander, D., … Trombly, C. (1995). *Post-Stroke Rehabilitation, Clinical Practice Guideline* (Number 16., p. 248). Rockville, Maryland: AHCPR Publication No. 95-0662.

Grossi, E. (2011). Artificial Neural Networks and Predictive Medicine : a Revolutionary Paradigm Shift. *InTech*. Retrieved from: http://www.intechopen.com/books/artificial-neural-networksmethodological- advances-and-biomedical-applications/artificial-neural-networks-and-predictive-medicine-arevolutionary- paradigm-shift

Ho, D., Tham, L. (1992). Analysis of plates by finite strip method. *Computers & Structures 52*, 6, 1283-1291, 1994.

Hrennikoff (1941). Solution of Problems of Elasticity by the Frame-Work Method. *ASME J. Appl. Mech*. 8, A619–A715.

Hufschmidt, a., Dichgans, J., Mauritz, K.-H., & Hufschmidt, M. (1980). Some methods and parameters of body sway quantification and their neurological applications. *Arch. Psychiat. Nervenkr.*, *228*(2), 135–150.

Jagielska, I., Matthews, C., & Whitfort, T. (1999). An investigation into the application of neural networks, fuzzy logic, genetic algorithms, and rough sets to automated knowledge acquisition for classification problems. *Neurocomputing*, *24*(1-3), 37–54.

James, G. A., Lu, Z., VanMeter, J., Sathian, K., Hu, X., & Butler, A. (2009). NIH Public Access. *Top Stroke Rehabilitation*, *16*(4), 270–281.

Joo, S.-B., Oh, S. E., Sim, T., Kim, H., Choi, C. H., Koo, H., & Mun, J. H. (2014). Prediction of gait speed from plantar pressure using artificial neural networks. *Expert Systems with Applications*, *41*(16), 7398–7405.

Kaczmarczyk, K., Wit, A., Krawczyk, M., & Zaborski, J. (2009). Gait classification in post-stroke patients using artificial neural networks. *Gait & Posture*, *30*(2), 207–10.

Kameswara Rao, N. S. V. (2011). Numerical and Finite Difference Methods. In *FOUNDATION DESIGN, Theory and Practice* (p. 634). Sabah, Malaysia: John Wiley & Sons (Asia) Pte Ltd.

Kapteyn, T. S., Bles, W., Njiokiktjien, C. J., Kodde, L., Massen, C. H., & Mol, J. M. F. (1983). Standardization in platform stabilometry being part of posturography. *Agressologie*, *24*, 321–326.

"Kistler" FP - Type 92600AA, product datasheet. (n.d.). Retrieved from http://www.kistler.com/fileadmin/files/divisions/automotive-research-test/engines-marine-and-stationary/600-350e-03.11.pdf

Krenker, A., Bešter, J., & Kos, A. (2011). Introduction to the Artificial Neural Networks. In *Artificial Neural Networks - Methodological Advances and Biomedical Applications*. Rijeka, Croatia: InTech. Retrieved from: http://www.intechopen.com/books/artificial-neural-networksmethodological- advances-and-biomedical-applications/introduction-to-the-artificial-neural-networks

Lafond, D., Corriveau, H., Hébert, R., & Prince, F. (2004). Intrasession reliability of center of pressure measures of postural steadiness in healthy elderly people. *Archives of Physical Medicine and Rehabilitation*, *85*(6), 896–901.

Langhorne, P., Coupar, F., & Pollock, A. (2009). Motor recovery after stroke: a systematic review. *The Lancet. Neurology*, *8*(8), 741–54.

Lee, M. ., & Nicholls, H. . (1999). Review Article Tactile sensing for mechatronics—a state of the art survey. *Mechatronics*, *9*(1), 1–31.

Levin, M. F., Michaelsen, S. M., Cirstea, C. M., & Roby-Brami, A. (2002). Use of the trunk for reaching targets placed within and beyond the reach in adult hemiparesis. *Experimental Brain Research*, *143*(2), 171–80.

Lewis, F., Dawson, D., & Abdallah, C. (2004). Robot Dynamics. In N. Munro (Ed.), *Robot Manipulator Control, Theory and Practice* (p. 607). Marcel Dekker, Inc.

Lim, C. H., Vats, E., & Chan, C. S. (2014). Fuzzy human motion analysis: A review. *Pattern Recognition*, *48*(5), 1773–1796.

Linthorne, N. P. (2001). Analysis of standing vertical jumps using a force platform. *American Journal of Physics*, *69*(11), 1198–1204.

Lisboa, P. J., & Taktak, A. F. G. (2006). The use of artificial neural networks in decision support in cancer: A systematic review. *Neural Networks*, *19*(4), 408–415.

Liu, Y., Shih, S.M., Tian, S.L., Zhong, Y.J., Li,L., (2009). Lower extremity joint torque predicted by using artificial neural network during vertical jump. *Journal of Biomechanics* 42, 906–911.

Lord, S., Sherrington, C., Menz, H., & Close, J. (2007). *Falls in Older People, Risk Factors and Strategies for Prevention* (Second Edi., p. 408). Cambridge: Cambridge University Press.

Lu, T.-W., & Chang, C.-F. (2012). Biomechanics of human movement and its clinical applications. *The Kaohsiung Journal of Medical Sciences*, *28*(2 Suppl), S13–25.

Luo JF, Liu Yijun, Berger EJ. (1998). Analysis of two-dimensional thin structures (from micro- to nano-scales) using the boundary element method. *Comput Mech*. 22, 402–12.

Mahoney, F. I., & Barthel, D. W. (1965). Functional evaluation: The Barthel Index. *Maryland State Medical Journal*, *April*, 61–65.

Maki, B. E., Holliday, P. J., & Fernie, G. R. (1987). Test for the of Relative Postural Stability Model and Balance. *IEEE Transactions on Biomedical Engineering*, *BME-34*(10), 797–810.

Mancini, M., & Horak, F. (2010). The relevance of clinical balance assessment tools to differentiate balance deficits. *Eur J Phys Rehabil Med*, *46*(2), 239–248.

Mane, S. M., Kambli, R. a., Kazi, F. S., & Singh, N. M. (2015). Hand Motion Recognition from Single Channel Surface EMG Using Wavelet & Artificial Neural Network. *Procedia Computer Science*, *49*, 58–65.

Marion, J. B. (1965). Classical Dynamics of Particles and Rigid Bodies. *Academic*, *New York*.

Mark, L. S., Nemeth, K., Gardner, D., Dainoff, M. J., Paasche, J., Duffy, M., & Grandt, K. (1997). Postural dynamics and the preferred critical boundary for visually guided reaching. *Journal of Experimental Psychology.Human Perception and Performance*, *23(5)*, 1365–1379.

Materials Data Book. (2003). Cambridge University Engineering Department.

McLachlan GJ. (1992). Cluster analysis and related techniques in medical research. *Stat Methods Med Res* 1:27–48.

Merdler, T., Liebermann, D. G., Levin, M. F., & Berman, S. (2013). Arm-plane representation of shoulder compensation during pointing movements in patients with stroke. *Journal of Electromyography and Kinesiology : Official Journal of the International Society of Electrophysiological Kinesiology*, *23*(4), 938–47.

Mizrahi, J., Solzi, P., Ring, H., & Nisell, R. (1989). Postural Stability in stroke patients: Vectorial expression of asymmetry, sway activity and relative sequence of reactive forces. *Medical & Biological Engineering & Computing*, *27*(181-190).

Molloy, A. J. (2006). *Force Sensing for Measuring Human Body Movement*. Aston University.

Murray, M. P., Seireg, A. A., & Sepic, S. B. (1975). Normal postural stability and steadiness: Quantitative assessment. *J. Bone Joint Surg.*, *57A*, 510–516.

Nakayama, H., Jorgensen, H. S., Raaschou, H. O., & Olsen, T. S. (1994). Recovery of Upper Extremity Function in Stroke Patients: The Copenhagen Stroke Study, *75*(April).

Navier, C. L. M. H. (1823).Extrait des recherchessurla flexion des plans elastiques. B*ull. Sci. Soc. Philomarhique de Paris*, 5, pp. 95–102.

Nowak, D. a. (2008). The impact of stroke on the performance of grasping: usefulness of kinetic and kinematic motion analysis. *Neuroscience and Biobehavioral Reviews*, *32*(8), 1439–50.

Oh, S. E., Choi, A., & Mun, J. H. (2013). Prediction of ground reaction forces during gait based on kinematics and a neural network model. *Journal of Biomechanics*, *46*(14), 2372–80.

Parker, V. M., Wade, D. T., & Langton Hewer, R. (1986). Loss of arm function after stroke: measurement, frequency, and recovery. *International Rehabilitation Medicine*, *8*(2), 69–73.

Pasma, J. H., Engelhart, D., Schouten, A. C., Kooij, H. V. A. N. D. E. R., Maier, A. B., & Meskers, C. G. M. (2014). REVIEW IMPAIRED STANDING BALANCE : THE CLINICAL NEED FOR CLOSING THE LOOP, *267*, 157–165.

Piirtola, M., & Era, P. (2006). Force platform measurements as predictors of falls among older people - a review. *Gerontology*, *52*(1), 1–16.

Plagenhoef, S., Evans, F. G., & Abdelnour, T. (1983). Anatomical data for analysing human motion. *Research Quarterly for Excercise and Sport*, *54*, 169–178.

Prieto, T. E., Myklebust, J. B., Hoffmann, R. G., Lovett, E. G., Member, S., & Myklebust, B. M. (1996). Measures of Postural Steadiness : Differences Between Healthy Young and Elderly Adults, *43*(9), 956–966.

Qatu, M. S., Asadi, E., & Wang, W. (2012). Review of Recent Literature on Static Analyses of Composite Shells : 2000-2010. *Open Journal of Composite Materials*, *2* (July 2012), 61–86.

Razak, A. H. A., Zayegh, A., Begg, R. K., & Wahab, Y. (2012). Foot plantar pressure measurement system: a review. *Sensors (Basel, Switzerland)*, *12*(7), 9884–9912.

Rhea, C. K., Kiefer, A. W., Haran, F. J., Glass, S. M., & Warren, W. H. (2014). Medical Engineering & Physics A new measure of the CoP trajectory in postural sway : Dynamics of heading change, *36*, 1473–1479.

Rossi, E., Mitnitski, A., & Feldman, A. G. (2002). Sequential control signals determine arm and trunk contributions to hand transport during reaching in humans, 659–671.

Rumelhart, D. E., Hinton, G. E., & McClelland, J. L. (1986). A general framework for parallel distributed processing. Parallel distributed

processing: Explorations in the microstructure of cognition. Vol 1. Foundations (pp. 45–76). Cambridge, MA:MIT Press

Sanford, J., Moreland, J., Swanson, L. R., & Paul, W. (1993). Reliability of the Fugl-Meyer Assessment for Testing Motor Performance in Patients Following Stroke, 447–454.

Sawada, Y., Ohtomo, N., Tanaka, Y., Tanaka, G., Yamakoshi, K., Terachi, S., … Limura, O. (1997). New technique for time series analysis combining the maximum entropy method and non-linear least squares method: its value in heart rate variability analysis. *Medical & Biological Engineering & Computing*, *Jul,35*(4), 318–322.

Schollhorn (2004). Applications of artificial neural nets in clinical biomechanics. *Clinical Biomechanics 19* 876–898.

Schumann, J., Gupta, P., & Liu, Y. (2010). Applications of Neural Networks in High Assurance Systems, *268*.

Soare, M. (1967). *Application of Finite Difference Equations to Shell Analysis* (p. 438). Bucharest: Pergamon Press.

Soutas-Little, R. W., Hillmer, K. M., Hwang, J. C., & Dhaher, Y. Y. (1992). Role of ground reaction torque and other dynamic measures in postural stability. *IEEE Engineering in Medicine and Biology Society Magazine*, *11*(4), 28–31.

Stergiou and Siganos (1996). Neural Networks. Retrieved January 2015. http://www.doc.ic.ac.uk/~nd/surprise_96/journal/vol4/cs11/report.html

Stergiou, N., & Decker, L. M. (2011). Human movement variability, nonlinear dynamics, and pathology: is there a connection? *Human Movement Science*, *30*(5), 869–88.

Stewart, J. (2010). *Planning of unconstrained reach actions after unilateral sensorimotor stroke*. University of Southern California.

Stone, R. S., Brett, P. N., & Evans, B. S. (1998). An automated handling system for soft compact shaped non-rigid products. *Mechatronics*, *8*(2), 85–102.

Stroke Association, UK. (2015), (January). Retrieved from www.stroke.org.uk

Sutherland, D. H. (2001). The evolution of clinical gait analysis part l: kinesiological EMG. *Gait & Posture*, *14*(1), 61–70.

Szilard, R. (2004a). Elastic Plate Theories and Their Governing Differential Equations. In *THEORIES AND APPLICATIONS OF PLATE ANALYSIS, Numerical and Engineering Methods* (pp. 23–61).

Szilard, R. (2004b). Finite Difference Methods. In *THEORIES AND APPLICATIONS OF PLATE ANALYSIS, Numerical and Engineering Methods* (pp. 247–316).

Szilard, R. (2004c). *THEORIES AND APPLICATIONS OF PLATE ANALYSIS. Classical, Numerical and Engineering Methods*. Hoboken, New Jersey: John Wiley & Sons, Inc.

Tam, B., Ma, X., Webb, D. J., Holding, D. J., & Brett, P. N. (2010). Discriminating contact in lumen with a moving flexible digit using fibre Bragg grating sensing elements. *Proceedings of the Institution of Mechanical Engineers, Part H: Journal of Engineering in Medicine*, *224*(6), 765–774.

Terekhov, Y. (1976). Stabilometry and some aspects of its applications - A review. *Biomedical Engineering*, *11*, 12–15.

Thai, H.-T., & Kim, S.-E. (2015). A review of theories for the modeling and analysis of functionally graded plates and shells. *Composite Structures*, *128*, 70–86.

The Engineering Toolbox. (n.d.). Retrieved from: www.engineeringtoolbox.com

Tiwana, M. I., Redmond, S. J., & Lovell, N. H. (2012). A review of tactile sensing technologies with applications in biomedical engineering. *Sensors and Actuators A: Physical*, *179*, 17–31.

Tongpadungrod, P., Rhys, T. D. L., & Brett, P. N. (2003). An approach to optimise the critical sensor locations in one-dimensional novel distributive tactile surface to maximise performance. *Sensors and Actuators A: Physical*, *105*(1), 47–54.

Van der Kooij, H., van Asseldonk, E., & van der Helm, F. C. T. (2005). Comparison of different methods to identify and quantify balance control. *Journal of Neuroscience Methods*, *145*(1-2), 175–203.

Van Kordelaar, J., van Wegen, E. E. H., & Kwakkel, G. (2012). Unraveling the interaction between pathological upper limb synergies and

compensatory trunk movements during reach-to-grasp after stroke: a cross-sectional study. *Experimental Brain Research*, *221*(3), 251–62.

Vicon-Peak. (2004). Retrieved January 2015. www.vicon.com

Wang, Z., & Newell, K. M. (2014). Neuroscience and Biobehavioral Reviews Inter-foot coordination dynamics of quiet standing postures, *47*, 194–202.

Zhang, G. P. (2000). Neural Networks for Classification : A Survey. *IEEE TRANSACTIONS ON SYSTEMS*, *30*(4), 451–462.

Zhang, T. (2011). Adaptive forward-backward greedy algorithm for learning sparse representations. *IEEE Transactions on Information Theory*, 57(7), 4689–4708.